Accelerated Characterization of Full-Scale Flexible Pavements Using a Vibroseis

Principal and Co- Principal Investigators:

Dr. Brady R. Cox

Dr. John S. McCartney

Christina N. Trowler

Project Number: MBTC 3013

Date: March 2010

Table of Contents

List of Tables

List of Figures

Chapter 1

1.0 Introduction

1.1 Overview

Geosynthetic basal reinforcement has been used in flexible pavements and unbound roads to limit the occurrence of rutting, fatigue, and environmental-related cracking, and to permit reduction in base course thickness. However, the lack of a representative, cost-efficient test that can be used to evaluate the behavior of full-scale pavement test sections has prevented parametric analyses of variables that may affect the performance of basally-reinforced flexible pavements (base thickness, subgrade and base soil properties, geosynthetic properties, depth of geosynthetic placement, stress state, and load magnitude and frequency). Current accelerated tests involve either small-scale, laboratory cyclic plate load tests, which often have scale effects, or heavy vehicle simulators, which require significant space, high construction costs, and long durations. Accordingly, the research objective of this study was to develop and validate new accelerated testing approaches using a Vibroseis (shaker truck) to characterize large-scale, geosynthetic reinforced pavement models.

This report includes a description of the methodology and results from two different types of dynamic tests using a Vibroseis truck as the loading mechanism: (1) relatively small-strain tests (shear strains less than 0.2%) where embedded geophones allowed for measurement of shear and normal strain distribution within the geosynthetic reinforced test sections as a function of depth, and (2) relatively large-strain tests (surface deflections on the order of 1 inch) where significant numbers of ESAL's (30,000 plus) were applied to the geosynthetic reinforced test sections while permanent surface deflection basins were monitored with LVDT's as a function of number of loading cycles. These two dynamic tests were conducted on large-scale

unreinforced, geogrid reinforced, and geotextile reinforced test sections constructed in a 4-ft deep by 12-ft wide by 12-ft long pit at the Engineering Research Center (ERC) of the University of Arkansas. The small-strain tests were performed on test sections constructed completely out of poorly-graded sand. This simple, uniform material was chosen so as to evaluate how geosynthetic reinforcement influenced subsurface strain distribution without interference from other complicating factors that would make relative comparison of strain distribution difficult (i.e. different soil layer interfaces, varying negative pore water pressures in soils with significant fines content, etc.) The large-strain tests were performed on test sections constructed out of 10 inches of Class 7 base course overlying 30-plus inches of poorly-graded sand. Both sets of tests were performed so as to determine the contribution of geosynthetic reinforcement to structural pavement performance (i.e. relative strain distribution and surface deflection only). No attempts were made to evaluate the other potentially beneficial mechanisms of geosynthetic reinforcement.

This report is separated into five chapters. Chapter 1 consists of an introduction. Chapter 2 is a literature review related to geosynthetic reinforcement of the base layer in flexible pavements. Specifically, this review will focus on studies involving construction and evaluation of pavement test sections with and without geosynthetic reinforcement. Chapter 3 summarizes the testing approach used to evaluate the impact of geosynthetic reinforcement on the in-situ strain distribution during dynamic surface loading. Chapter 4 presents a description of the accelerated dynamic deflectometer (ADD) testing approach and results from this large-strain surface loading test. Chapter 5 presents conclusions developed from the current research.

Chapter 2

2.0 Literature Review

2.1 Overview

This chapter summarizes findings from the technical literature related to geosynthetic reinforcement of the base layer in flexible pavements. Specifically, this review will focus on studies involving construction and evaluation of pavement test sections with and without geosynthetic reinforcement. A goal of this review is to outline experience from these tests which may help identify the ideal conditions in which geosynthetic reinforcement is and isn't beneficial, geosynthetic properties that contribute to the performance of the test sections, possible mechanisms of geosynthetic reinforcement in pavement base layers, and inconsistencies between the observations from the different studies.

2.2 Introduction

The design of flexible pavements consists of selecting materials that will distribute the stresses applied from traffic to a wider area of subgrade. By doing so, the pavement is expected to support an expected amount of traffic over anticipated desired design life. Most premature pavement failures are structural in nature, meaning that one or more of the materials in the system have reached a mechanical failure state. Structural failures happen in practice before the desired design life due to unexpected loadings, environmental interaction, drainage problems, and other factors such as cyclic degradation, frost heave, and subgrade settlement which change pavement materials. In order to extend the lifetime of flexible pavements to help counter some of these adverse effects, pavement engineers have incorporated thicker layers of base material into flexible pavements. However, this strategy has led to excessive cost in some situations. Accordingly, alternatives such as geosynthetic reinforcement of the base course have been

introduced into flexible pavements (Haliburton 1970, Steward *et al.* 1977, and Barenberg *et al.* 1975). Geosynthetic materials, which had been shown to be effective as reinforcing materials in slopes and retaining walls, were expected to lead to an improvement in pavement performance. In slopes and retaining walls, the soil transfers shear stresses to the geosynthetic reinforcements, which resist these imposed stresses by mobilizing tension. Field studies have indicated that geosynthetic reinforcement of pavement base course layers can lead to reduced differential settlement, reduced base course thickness, prolonged service life, and improved stress distribution (Hufenus *et al.* 2005).

2.3 Geosynthetic Material Types

A geosynthetic material is a synthetic material manufactured from polymers such as polyethylene, polypropylene, or polyester. Although geosynthetics have many forms and uses (Koerner 2005), the two forms of geosynthetics that are specifically used for basal reinforcement are woven geotextiles and geogrids. Although both of these reinforcements may contribute to pavement performance, Al-Qadi *et al.* (1994) and (1997) found that the mechanisms by which the two geosynthetic types reinforced the pavement are different.

2.3.1 Geogrid

A geogrid is a geosynthetic material consisting of connected intersecting ribs with opening sizes into which soil particles can enter, enhancing interlocking between the soil and geogrids (Koerner 2005). The interlocking aspect of geogrids makes them ideal for use in granular soils such as the pavement base course. If the surface of a pavement having geogrid basal reinforcement is loaded vertically, the dense soil particles will at first want to expand laterally due to the Poisson effect under elastic strain levels, and then dilate and expand under higher strain levels. Perkins and Ismeik (1997) and Giroud and Han (2004) observed that

geogrids may restrict this lateral movement through interlocking. This mechanism may indicate that stiffer geogrid polymers may yield improved lateral confinement. In this mechanism, the geogrid does not likely go into tension unless higher strains are observed in the system (Giroud and Noiray 1980).

2.3.2 Geotextile

The geotextiles typically used for reinforcement applications are woven filament sheets (Koerner 2005). The main reinforcement mechanism of woven geotextiles is separation. Woven geotextiles are used to separate two dissimilar materials, preventing intermixing (Fannin and Sigurdsson 1996, Perkins and Ismeik 1997, and Al-Qadi *et al.* 1997). For this reason, most geotextiles are placed between the subgrade and base layer. Separation allows a stiff material placed on a soft subgrade to maintain its full thickness throughout the life of the pavement. Similar to geogrids, in order to mobilize tension, the soil and geosynthetic material must deform a certain amount to mobilize the tensile strength of the geosynthetic. Cuelho *et al.* (2009) suggested that the puncture resistance of the geotextile should be taken into account, as penetration of particles through the geotextile will reduce its strength and stiffness (Cuelho *et al.* 2009).

2.4 Testing Methods

Even though geosynthetics have been used in pavements for over 30 years, there are still discrepancies in the results between the testing methods used to quantify the contribution of the geosynthetics on pavement performance (Perkins and Lapeyre 2005). The current testing methods available to detect the contribution of geosynthetics in pavements included small scale laboratory tests, large scale laboratory tests, controlled-traffic track tests, and full-scale pavement field tests. The majority of these tests quantify the performance of the geosynthetic

reinforcement of the base layer by surface deflection measurements. However, a few researchers have instrumented pavements and geosynthetics to determine geosynthetic reinforced pavement performance. The instrumented full scale pavement tests are expected to be the most representative of the actual field conditions because they are loaded in the same manner as actually present in the field. However, the environmental conditions (temperature, subgrade and base water contents) can change over time in full-scale field tests, so they have less control than in laboratory tests.

2.4.1 Laboratory Testing

Laboratory testing is typically used because test sections can be constructed and tested relatively quickly, permitting multiple alternatives to be evaluated. The two most common laboratory tests are track testing with heavy vehicle simulators (HVS), as shown in Figure 2.1 (Barksdale *et al.* 1989, Perkins and Cortez 2005, and Cancelli *et al.* 1996), and cyclic plate load testing on pavement models in laboratory tanks, as shown in Figure 2.3 (Haas *et al.* 1988, Al-Qadi *et al.* 1994, and Ling *et al.* 2001). The use of HVS systems are more representative of actual pavement loading if a large test section is used; however, the construction and testing of these test sections are often time consuming and expensive. This is especially the case if site-specific soils need to be transported to the HVS location. These test tracks are normally constructed indoors in long rectangular boxes (Perkins and Cortez 2005 and Collin *et al.* 1996) or outdoor test tracks (Barker 1987, Halliday and Potter 1984, and Webster 1993) and loaded using a load frame with a wheel attached. The typical variable measured in a HVS tests is a two dimensional rutting profile obtained after different numbers of passes, such as that shown in Figure 2.2.

Figure 2.1: Heavy Vehicle Simulator (Perkins *et al.* 2005).

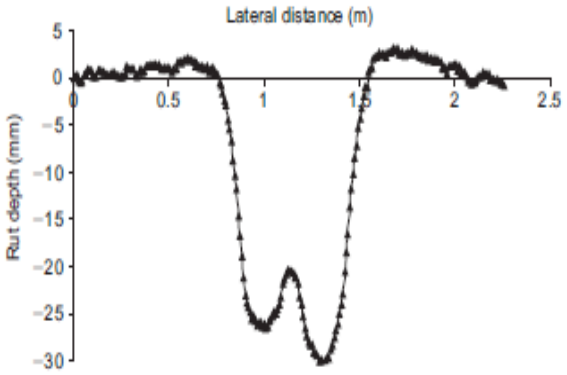

Figure 2.2: Rut profile for 10,000 passes obtained from HVS loading (Perkins *et al.* 2005).

Other studies have involved laboratory tank tests (Tingle and Jersey 2005, Al-Qadi et al. 1994, Perkins 1999, Haas *et al.* 1988, and Ling *et al.* 2001). The pavement models tested in laboratory tanks (refer to Figure 2.3) are not completely representative of full-scale pavements due to boundary and scaling effects. Specifically, the size of the test section and layer thicknesses are reduced; however, the soil is not sieved or reduced in size and the geosynthetic properties are also not reduced. In the case of dynamic surface loading, these tests may be influenced by boundary effects as stress waves will bounce off the sides of the tank and back into the pavement structure. Leng and Gabr (2002), Jersey and Tingle (2005) and Perkins (1999) performed cyclic plate load test on geogrid reinforced sections. These tests were performed by cycling a load on a circular plate until a certain rut depth is accomplished. The outcome of these tests is typically a profile of surface deformation as a function of the number of cycles of load applied to the test section, as shown in Figure 2.4. Figure 2.4 shows deformation as a function of the number of cycles of load applied for two different types of geogrid reinforcement, BX1 and BX2, along with an unreinforced test section (Leng and Gabr 2002).

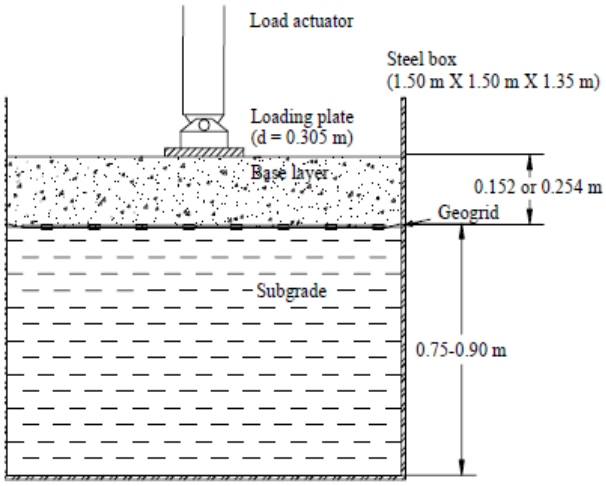

Figure 2.3: Cyclic plate load test in laboratory tanks (Leng and Gabr 2002).

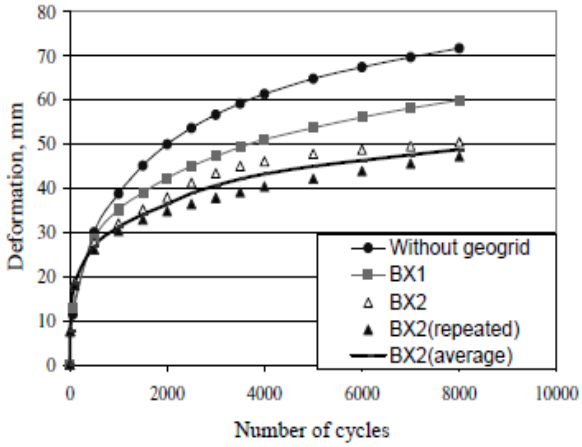

Figure 2.4: Cyclic plate load test results (Leng and Gabr 2002).

2.4.2 Full Scale Field Testing

Full-scale testing is typically performed to evaluate pavements under the actual traffic and environmental conditions present in a given area, as shown in Figure 2.5. However, this can be inconvenient as it is difficult to understand the design conditions that will lead to meaningful results. Another issue is that field sites often have natural variations in the subgrade profile. For this reason, uniform site conditions are harder to verify than soil that is brought in for testing. Therefore, to be able to understand the contribution of the geosynthetic material in the pavement design, a uniform testing material must be used and often times a geosynthetic liner is used to eliminate migration of the natural subgrade into the test section during testing. These test sections must be built from the sides of the test section so that the test section is not trafficked in any way before traffic loads are applied. The outcome of these test are typically rut profiles, as shown in Figure 2.6, measured by surveying the surface of the test section (Cuelho and Perkins 2009 and Tingle 2008).

Figure 2.5: Full-scale field testing (Cuelho and Perkins 2009).

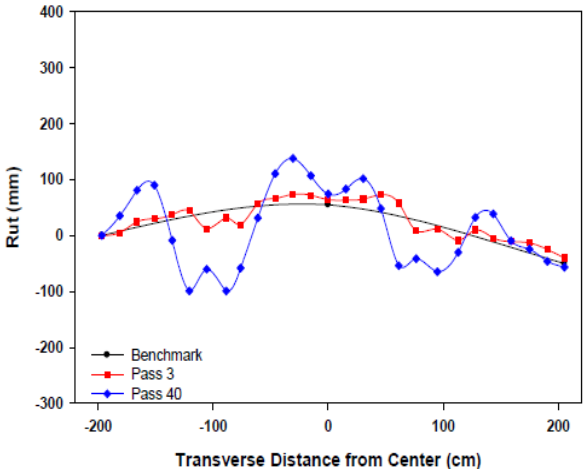

Figure 2.6: Full-scale field testing surface deformation results (Cuelho and Perkins 2009).

2.4.3 Instrumented Test Sections

Both the laboratory and full scale field test normally only measure what is going on at the surface of the test section. When fatigue of the pavement begins, often times the surface of the pavement is not where the true issue is. When moisture builds up in the pavement base and subgrade layer, the shear strength in these layers begins to decrease and weaken. Repeated loading on these weakened layers causes fatigue. Therefore, a testing method that measures strain within the test section is needed to determine what is happening as a function of depth during loading. Several studies have been done on instrumented test sections, but only with limited results (Perkins *et al.* 2009, Perkins *et al.* 1997, Al-Qadi *et al.* 1999, Howard 2006, Warren and Howard 2005). The limited results obtained from previous instrumented pavements are associated with a lack of information pertaining to instrument selection and installation. Therefore, the instrumentation in geosynthetic reinforced roadways historically does not last long enough to obtained valuable information (Al-Qadi *et al.* 1999 and Brandon *et al.* 1996). Weak spots are also created in the pavement layers due to poor compaction around the instrumentation.

2.5 Previous Research

A number of previous studies which conducted research on geogrid and geotextile performance in pavements will be discussed in this section. The research presented in Table 2.1, Table 2.2, and Table 2.3 are laboratory and full scale field test that quantify the contribution of the geosynthetics on pavement performance by surface deflection measurements. This information is presented similar to the information found in Berg *et al.* 2000; however, additional information has been added. Table 2.1 summarizes the details of each researcher's experimental setup and the details of the construction of each test section. Table 2.2 summarizes the properties of the geosynthetic reinforcement and the location of the geosynthetic reinforcement in each test section. Table 2.3 summarizes the loading of each test section, the California Bearing Ratio (CBR) of the subgrade, the deformation of each test section, and the benefit of the geosynthetic reinforcement in terms of the traffic benefit ratio (TBR). The TBR is the ratio of the number of loading cycles on the geosynthetic reinforced test section to reach a certain rut depth to the number of loading cycles to reach the same rut depth on the non-reinforced test section. These studies are presented in an attempt to show how many different variables impact geosynthetic reinforced pavement performance. These variables are often times very difficult to measure independently. Each of these variables are very difficult to assess individually because they are all interrelated, but many of these variables have similar behaviors over a large range of different configurations. Therefore, trends in these variables are developed from the previous research data summarized in Table 2.1, Table 2.2, and Table 2.3. The optimum values obtained from previous research for subgrade strength, geosynthetic placement, base course layer thickness, and geosynthetic properties will be discussed further in this section.

Table 2.1: Summary of previous research test section properties

			Layer Thickness (in)		Layer Classification	
Author	**Testing Facility**	**Facility Dimension (ft)**	**AC**	**Base**	**Base**	**Subgrade**
Al-Qadi (1994)	Soil Tank	10.2 L x 5.9 W x 6.9 D	2.7	5.9 7.8	GW-GM	SM
Al-Qadi (1997)	Pubilc Road	443 L x 49 W	3.5	3.9 5.9	GW	ML
Barker (1987)	Test Track	68.8 L x 15 W x 3.6 D	2.9	5.9	GP	Sandy Silt
Barksdale (1989)	Test Track	16 L x 7.8 W x 4.9 D	1.5	7.8	GP-GM	CL
Brown (1982)	Test Track	17 L x 7.8 W x 4.9 D	1.9	5.9	GW	CL
Cancelli (1996)	Soil Tank	2.9 L x 2.9 W x 2.9 D	2.9	11.8	GW	SP
Cancelli (1999)	Test Track	689 L x 13.1 W x 3.9 D	2.9	11.8 15.7 19.6	Gravel	CL
Collin (1996)	Test Track	47.9 L x 14.4 W x 3.9 D	1.9	7.1 11.8	GW	CL
Cuelho (2009)	Full-Scale	49.2 L x 13.1 W	None	7.8 7.8	GW-GM	SC
Haas (1988)	Soil Tank	14.7 L x 5.9 W x 2.9 D	2.9 2.9 2.9	7.8 11.8 7.8	GW	SP
Perkins (1997)	Soil Tank	6.6 L x 6.6 W x 4.9 D	2.9	11.8 14.7	GW	SM
Tingle (2005)	Soil Tank	6 L x 6 W x 4.5 D	None	13.8 13.3	SW-SM	CH
Webster (1993)	Test Track	144.4 L x 12.5 W x 2.3 D	1.9	5.9 9.8 11.8 13.7 17.7	SM-SC	CH

Table 2.2: Summary of previous research loading properties

Author	Loading Type	Applied Load (lb)	Load Frequency or Speed
Al-Qadi (1994)	11.8 " circular plate	8768	0.5 Hz
Al-Qadi (1997)	Traffic	Traffic	Traffic
Barker (1987)	Moving wheel	26,978	Unknown
Barksdale (1989)	Moving wheel	1484	2.9 mph
Cancelli (1996)	11.8 " circular plate	8992	5 Hz, 10 Hz
Cancelli (1999)	Single wheel front anxle,	5058 per wheel	12.5 mph

Table 2.2 continued: Summary of previous research loading properties

Author	Loading Type	Applied Load (lb)	Load Frequency or Speed
Collin (1996)	Moving wheel	4496	2.7 mph
Cuelho (2009)	Three Axle Dump Truck	45,988	9.32 mph
Haas (1988)	11.8 " circular plate	8992	8 Hz
Perkins (1997)	11.8 " circular plate	8992	0.67 Hz
Tingle (2005)	12" circular plate	8,992	1 Hz
Webster (1993)	Moving wheel	29,225	Unknown

Table 2.3: Summary of previous research geosynthetic properties and test results

Author	Geosynthetic Reinforcement	Secant Modulus in Machine Direction at 5% Strain (lb/ft)	Reinforcement Location	Subbase Thickness (in)	Subgrade CBR	Rut Depth (in)	TBR
Al-Qadi (1994)	Woven Geotextile	13700	Interface	5.9	2	1	1.7
	Woven Geotextile	15600	Interface	7.8	4	1	3
Al-Qadi (1997)	Woven Geotextile	13700	Interface	3.9	7	0.7	1.6
	Punched Geogrid	13700	Interface	3.9	7	0.8	1.4
Barker (1987)	Punched Geogrid	15100	Middle of Base Course	5.9	27	1	1.2
Barksdale (1989)	Woven Geotextile	Unknown	Middle of Base Course	7.8	2.7	0.5	4.7
	Woven Geotextile	Unknown	Interface	7.8	2.7	0.5	1
	Punched Geogrid	8200	Middle of Base Course	7.8	3.2	0.5	2.8
	Punched Geogrid	8200	Interface	7.8	2.5	0.5	1
Cancelli (1996)	Woven Geotextile	13400	Interface	11.8	3	1	1.7
	Punched Geogrid	8200	Interface	11.8	3	1	17
	PVC Coated Polyester Geogrid	16900	Interface	11.8	3	1	1.7
	Multilayer Biaxial Geogrid	12300	Interface	11.8	1	0.5	15
	Multilayer Biaxial Geogrid	12300	Interface	11.8	3	1	5.2
	Multilayer Biaxial Geogrid	12300	Interface	11.8	8	1	3.2
	Biaxial Geogrid	13700	Interface	11.8	1	1	70
	Biaxial Geogrid	13700	Interface	11.8	3	1	7.1

Table 2.3 continued: Summary of previous research geosynthetic properties and test results

Author	Geosynthetic Reinforcement	Secant Modulus in Machine Direction at 5% Strain (lb/ft)	Reinforcement Location	Subbase Thickness (in)	Subgrade CBR	Rut Depth (in)	TBR
Cancelli (1999)	Woven Geotextile	13400	Interface	15.7	3	0.4	220
	Punched Geogrid	8200	Interface	11.8	3	0.8	220
	Punched Geogrid	8200	Interface	15.7	3	0.3	340
	Punched Geogrid	8200	Interface	19.6	3	0.5	8.4
	Punched Geogrid	8200	Interface	11.8	8	0.3	1.2
	Multilayer Biaxial Geogrid	12300	Interface	11.8	3	0.6	300
	Multilayer Biaxial Geogrid	12300	Interface	15.7	3	0.3	330
	Multilayer Biaxial Geogrid	12300	Interface	19.6	3	0.4	13
	Multilayer Biaxial Geogrid	12300	Interface	11.8	8	0.3	1.6
Collin (1996)	Punched Geogrid	8200	Interface	7.1	1.9	1	2
	Punched Geogrid	15100	Interface	11.8	1.9	1	3.3
Cuelho (2009)	Woven Geotextile	1100	Interface	7.2	1.75	1	1.7
	PVC Coated Polyester Geogrid	400	Interface	6.7	2	1	2.6
Haas (1988)	Punched Geogrid	13700	Middle of Base Course	7.8	8	0.8	3.3
	Punched Geogrid	13700	Interface	7.8	8	0.8	3.1
Perkins (1997)	Woven Geotextile	13700	Interface	11.8	1.5	0.9	-
	Punched Geogrid	8200	Interface	11.8	1.5	0.9	17
	Punched Geogrid	8200	Interface	14.7	1.5	0.7	17
Tingle (2005)	Non-woven Geotextile	Unknown	Interface	13.8	22	1	28.9
	Punched Geogrid	800	Interface	13.3	13.7	1	1.5
Webster (1993)	Punched Geogrid	13700	Interface	13.7	3	1	2.7
	Punched Geogrid	15100	Interface	5.9	8	1	22
	Punched Geogrid	15100	Interface	9.8	8	1	6.7
	Punched Geogrid	15100	Interface	11.8	3	1	3.1
	Punched Geogrid	15100	Interface	13.7	3	1	4.7
	Punched Geogrid	15100	Middle of Base Course 13.7		3	1	2.2
	Punched Geogrid	15100	Interface	17.7	3	1	1.3
	Woven Geogrid	15600	Interface	13.7	3	1	0.9
	Knitted Geogrid	14900	Interface	13.7	3	1	1.6

2.5.1 Evaluation of the Impact of Subgrade Strength

The relevance of the different reinforcement mechanisms may depend on the subgrade soil atop which the pavement rests. With softer subgrades the pavement system is able to deform, this deformation is required to mobilize the geosynthetic. However, stiff subgrades will not deform as much and the geosynthetic will not be fully mobilized in these subgrades. The suitability of the subgrade to resist loading is typically quantified in pavement engineering using the California Bearing Ratio (CBR) is a measure of the mechanical strength of a subgrade. As the CBR value increases, the strength of the subgrade also increases. Subgrades with CBR values less than 8 see the most benefit from geosynthetic reinforcement.

2.5.2 Evaluation of the Impact of Base Course Layer Thickness

Numerous studies suggest that geosynthetic reinforcement can be used to increase the structural performance of the pavement; therefore, reducing the thickness of the base course layer. Pavements reinforced with geosynthetics on weaker subgrades, CBR=1, cannot reduce the base course layer (Haas *et al.* 1988). However, on subgrades that are stronger, CBR=8, the base course layer can be reduced by as much as 50 % (Webster 1993). Other studies have shown that geosynthetic reinforcement should not be used to replace base course thickness.

2.5.3 Evaluation of Geosynthetic Location

The ideal location of the geosynthetic material within the pavement layer is dependent on the magnitude of the applied load and the quality and thickness of the soil being reinforced (Berg *et al.* 2000, Barksdale et al. 1989, Jenner and Paul 2000, Haas et al. 1988, Cancellli and Montanelli 1999, Barker 1987, and Webster 1993). Even though each parameter in the pavement, such as thickness of the base course, geosynthetic type, subgrade strength, and loading conditions, all effect the placement of the geosynthetic material within the pavement

system; the most effective placement of the geotextile is always at a layer interface to separate one soil type from another. On the other hand, the most effective location of the geogrid has been shown to be somewhere in the base layer, not at the layer interface (Barksdale *et al.* 1989). However, the thickness of the base course layer does effect the position of the geogrid. The geogrid can be more effective when placed at the bottom of thin bases, but for base thicknesses greater than 9 inches the geogrid performs better closer to the midpoint of the layer (Hass *et al.* 1988). With this being said, the geogrid should not be placed too high in the pavement or it will not be able to prevent lateral spread of the base course soil and a significant rut will develop before the geogrid is mobilized.

2.5.4 Evaluation of Geosynthetic Properties

The properties of the geosynthetic material play a huge role in whether the geosynthetic material will be successful in reinforcing and prolonging the life of the pavement. A stiff geosynthetic material will have very small elongations in the material, allowing small deformations in the pavement. Stiff geosynthetic materials work well on soft subgrades, but the influence of the stiff geosynthetic material decreases with an increase in the bearing capacity of the subgrade. However, forces do not develop in the geosynthetic material until elongation of the material has occurred; therefore, the pavement must develop trafficking and a certain amount of rutting before the geosynthetic is mobilized. As a result, the benefit of geosynthetic reinforcement will increase as the pavement begins to show signs of significant rutting, which means that the bearing capacity of the subgrade is deteriorating. Research done by Barksdale *et al.* (1989) suggest that geotextile requires significantly more deformation of the pavement to mobilized the same amount of reinforcement in the geogrid due to the interlocking ability of the geogrid. Nevertheless, significant rutting and decreased bearing capacity of the subgrade

normally constitutes failure in pavements. For that reason, it is important to develop just enough rutting to mobilize the geosynthetic to prolong the service life of the pavement without failing the pavement (Hufenus *et al.* 2006). Several research studies test the performance of the geosynthetic to pavement deformations that are not reasonable, over an inch (Cuelho *et al.* 2009, Fannin *et al.* 1996, Collin *et al.* 1996, and Montanelli 1997). With an inch of deformation, a flexible pavement will have functional issues, meaning the pavement will discomfort drivers due to its roughness. It is important to review research projects at reasonable deformations for flexible pavements.

2.6 Evaluation of Reinforcement Mechanisms

The reinforcement mechanisms discussed in this section are the factors that affect the performance of geosynthetic reinforced pavements. This section will describe the means in which these mechanisms of geosynthetic reinforcements are able to improve pavement performance.

2.6.1 Lateral Restraint

When vertical loads are applied to the pavement, forces below the pavement spread the aggregate particles apart. Due to the nature of a tire rolling across the pavement, the aggregate particles spread laterally away from the tire creating ruts. It has been shown in several studies that placing geosynthetics between the subgrade and the aggregate base confines the aggregate particles at the interface. Figure 2.7 shows the reinforcement mechanisms achieved by laterally restraining soil particles. When these aggregate particles are confined, vertical shear stresses that cause rutting will be resisted. The aggregate base course and the geosynthetic material interlock due to frictional interaction allowing the geosynthetic material to absorb the vertical shear stresses at the interface that are normally applied to the subgrade below. The shear stresses place

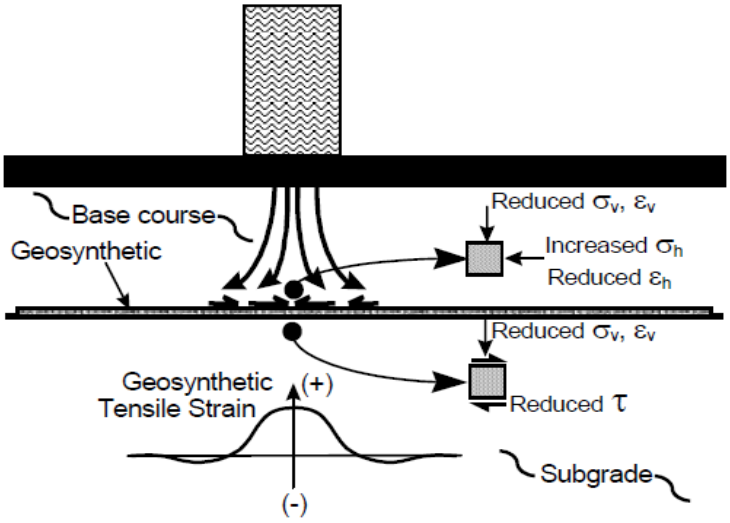

Figure 2.7: Mechanisms achieved by lateral restraint due to geosynthetic reinforcement (Perkins 1999).

the geosynthetic material in tension and the stiffness of the geosynthetic material slows down the development of lateral tensile strain in the base near the geosynthetic (Berg *et al.* 2000). Large deformation is not needed to achieve the confinement mechanism that the geosynthetic material provides for an increase in pavement performance (Hufenus *et al.* 2006).

2.6.2 Separation

When two different materials are placed on top of one another and loaded, the intermixing of the materials tend to occur. Normally in roadways, a stiff material is placed over a soft material and when these two materials intermix, the stiff material layer may decrease in thickness, creating a larger layer of weak soil beneath a thin layer of stiff soil, as shown in Figure 2.8. This mixing of layers is often referred to as migration of fines. When this condition is present, separation is the most important mechanism of the geosynthetic material. Studies performed on pavement reinforcement with geotextiles tend to show that separation and filtration are most important for thin base course aggregate thicknesses and weak subgrade conditions which are susceptible of the migration of fines (Fannin and Sigurdsson 1996). Geotextiles are

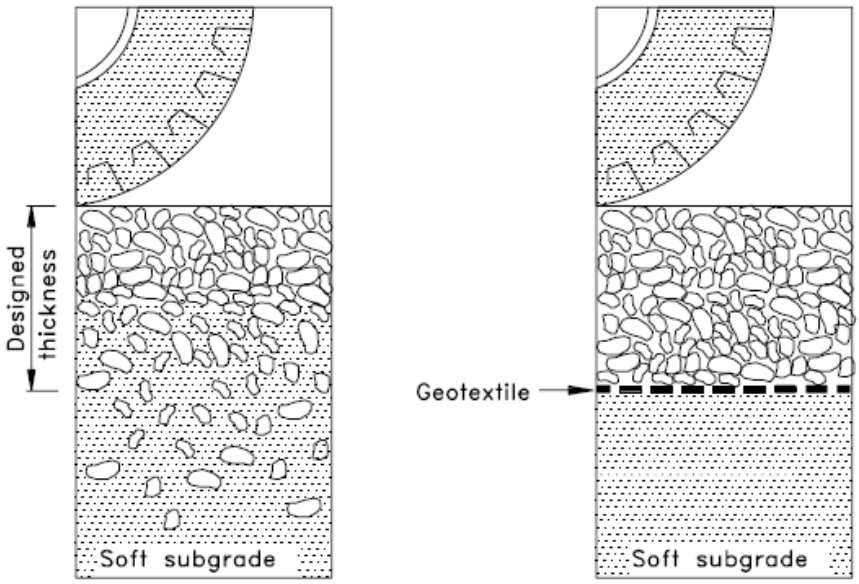

Figure 2.8: Contribution of geotextile separation in pavements to prevent intermixing of layers (Berg *et al.* 2000).

traditionally more effective in providing separation than geogrids (Perkins and Ismeik 1997). The conclusion of research done by Al-Qadi *et al.* (1997) was that the separation mechanism of the geotextile was more important than the reinforcement mechanism of the geogrid.

2.6.3 Tensioned-Membrane Effect

When geosynthetics are placed in heavily trafficked roadways, predominantly unpaved roadways, the soil along the geosynthetic reinforcement is able to deform enough to transfer enough stress to the geosynthetic to mobilize tension (Giroud and Noiray 1980). In this situation, the soil-geosynthetic system behaves as a thin, tensioned membrane, as shown in Figure 2.9. Specifically, the reinforced soil layer is curved downward; therefore, exerting an upwards force which better supports the wheel load and spreads the load out over a larger area leading to increased bearing capacity of the pavement. However, large pavement ruts along with high stiffness geosynthetic materials are needed to mobilize the tensioned-membrane effect.

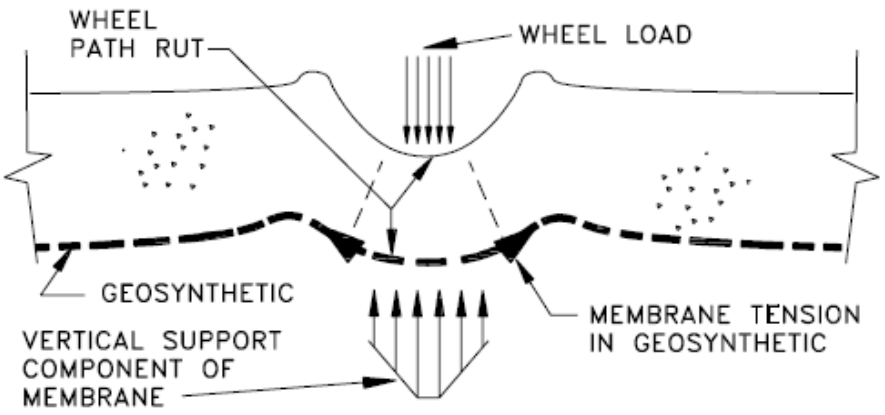

Figure 2.9: Tension membrane effect caused by geosynthetic reinforcement (Berg *et al.* 2000 and Haliburton *et al.* 1981).

Therefore, this type of reinforcement mechanism is not useful to explain the role of basal reinforcement in flexible pavements. With this being said, this mechanism is used extensively in unpaved or temporary roads during construction when the soils are too weak to support heavy equipment (Haliburton *et al.* 1981, Steward et al. 1977, and Hufenus *et al.* 2006).

2.6.4 Stress and Strain Redistribution

When geosynthetic reinforcement is present, the stress and strain distribution in the pavement is changed. This in part is caused by the friction between the soil and the geosynthetic material. The vertical stresses should decrease and become more widely distributed on the subgrade layer when geosynthetic material is present in the pavement. This is caused by the geosynthetic reinforcement of the base course layer which essentially increases the modulus of the base allowing less deformation and rutting in the pavement (Berg *et al.* 2000). Very few studies have been done to measure the impact of geosynthetic reinforcement layer on strain distribution (Perkins *et al.* 1999). This is due to the lack of information regarding instrumentation selection and installation.

2.7 Design Methods

Design methods have been developed, but lack some of the many variables that impact pavement performance. For example, empirical design methods are limited to the circumstances of the configuration studied (Penner *et al*. 1985, Montanelli *et al.* 1997, and Webster 1993). These methods are unable to account for variations in the pavement configuration and geosynthetic type and placement. Due to the variations in the input parameters in flexible pavements, finite element design methods have been created (Perkins 2001, Kwon *et al*. 2005, Leng and Babr 2002, and Perkins 2004). Even though these methods can allow for variations in the different variables, it is difficult to model the behavior of different soil types, geosynthetic behavior, and the interaction between the two (Perkins and Ismeik 1997). These models are also limited to a response of the pavement under a single load. However, the design method should predict pavement response over a number of repeated load cycles. Although, geosynthetic materials have been used to reinforce pavements for decades, the lack of an acceptable design method currently limits the use of geosynthetic reinforcement in pavements.

2.8 Conclusion from the Evaluation of the Literature

Many studies have been performed to infer the contribution that the geosynthetic material has on pavement design. A number of researchers found that the geosynthetic placement in the pavement cross section is most important (Berg *et al.* 2000, Haas *et al.* 1988, and Barksdale *et al.* 1989). Others conclude that separation of two dissimilar materials is the main benefit seen from geosynthetics in pavements (Fannin and Sigurdsson 1996, Al-Qadi *et al.* 1997, and Perkins and Ismeik 1997). Still others have shown that geosynthetics provide little reinforcement benefit (Brown *et al.* 1982, Barker 1987, Halliday and Potter 1984, Cox *et al.* 2010, and Collin *et al.* 1996). These studies show uncertainty in many of the variables and reinforcement mechanisms

due to geosynthetic reinforcement and the fact that the benefits of these reinforcement mechanisms have not yet been quantified.

Chapter 3

3.0 In-Situ Strain Testing Approach and Results

This chapter summarizes the testing approach used to evaluate the impact of geosynthetic reinforcement on the in-situ strain distribution during dynamic surface loading. During this project, the testing approach evolved over time. First, unreinforced, geogrid-reinforced, and geotextile-reinforced soil test sections were constructed in August 2008 at the Engineering Research Center (ERC) at the University of Arkansas. Three test sections were constructed on native subgrade silt and consisted of 8 inches of compacted red dirt (clayey sand) overlain by 12 inches of compacted Class 7 aggregate base (SB2). However, due to the sensitivity of the compaction moisture content of the red clay and Class 7 aggregate base, and the relatively low CBR of the underlying ERC subgrade (< 1), it was extremely difficult to achieve consistent layer densities in the three test sections. Because the sections did not have identical conditions after construction, these test sections were found to be inadequate to draw conclusions as to the relative influence of the geosynthetic reinforcement on the sub-surface strain distribution and surface deformation. Furthermore, constructability issues were encountered in these test sections because the compacted Class 7 aggregate and compacted red clay were so stiff that removal of the embedded dynamic sensors was extremely difficult. As a result, many of the sensors and sensor cables were damaged during excavation of each test section. These problems led to a modified testing plan involving a single, thick layer of compacted sand that was implemented in a second round of tests performed in the May of 2009. This chapter will only include a discussion of the in-situ strain distribution testing approach, procedures, and results from the second series of tests performed in May of 2009.

3.1 Material Properties

3.1.1 Sand

Due to the problems noted above, a poorly-graded sand (SP) was chosen as the test soil. The SP classifies as an A-1-b soil in the American Association of State Highway and Transportation Officials (AASHTO) soil classification system, which is an excellent subgrade material. According to the Unified Soil Classification System (USCS), a sand is classified as well-graded when the coefficient of uniformity (C_u) is greater than six and the coefficient of curvature (C_c) is between one and three. The C_u and C_c for the sand used in this project is 4 and 0.75, respectively. Therefore, this sand is classified as poorly-graded. The grain-size distribution data is presented in Table 3.1 and the grain-size distribution curve is shown in Figure 3.1.

The sand was used as it was observed to lead to consistent density and stiffness values from test section to test section. While not necessarily representative of typical pavement subgrade or base course material, the SP was chosen because of its relative insensitivity to compaction effort and compaction moisture content, and because it was still suitable to identify the mechanisms of geosynthetic reinforcement during dynamic surface loading. The use of SP was desirable for the in-situ strain tests so that the relative sub-surface dynamic strain distributions could be evaluated for each reinforcement type via direct comparison. The use of SP was found to simplify and eliminate construction differences, permitting a more straightforward evaluation of the geosynthetics impact on sub-surface strain distribution.

3.1.2 Geosynthetics

As mentioned in Chapter 2, different geosynthetic reinforcement types have different mechanisms of reinforcement in soils during dynamic surface loading. Two geosynthetics, a geogrid and geotextile manufactured by TenCate-Mirafi, Inc. of Pendergrass, Georgia, were

Table 3.1: Grain-size distribution data for the poorly-graded sand used in this project

Sieve No.	Sieve Size (mm)	Percent Passed (%)
4	4.750	97.12
10	2.000	84.59
40	0.425	21.92
60	0.250	3.95
100	0.150	0.89
200	0.075	0.28

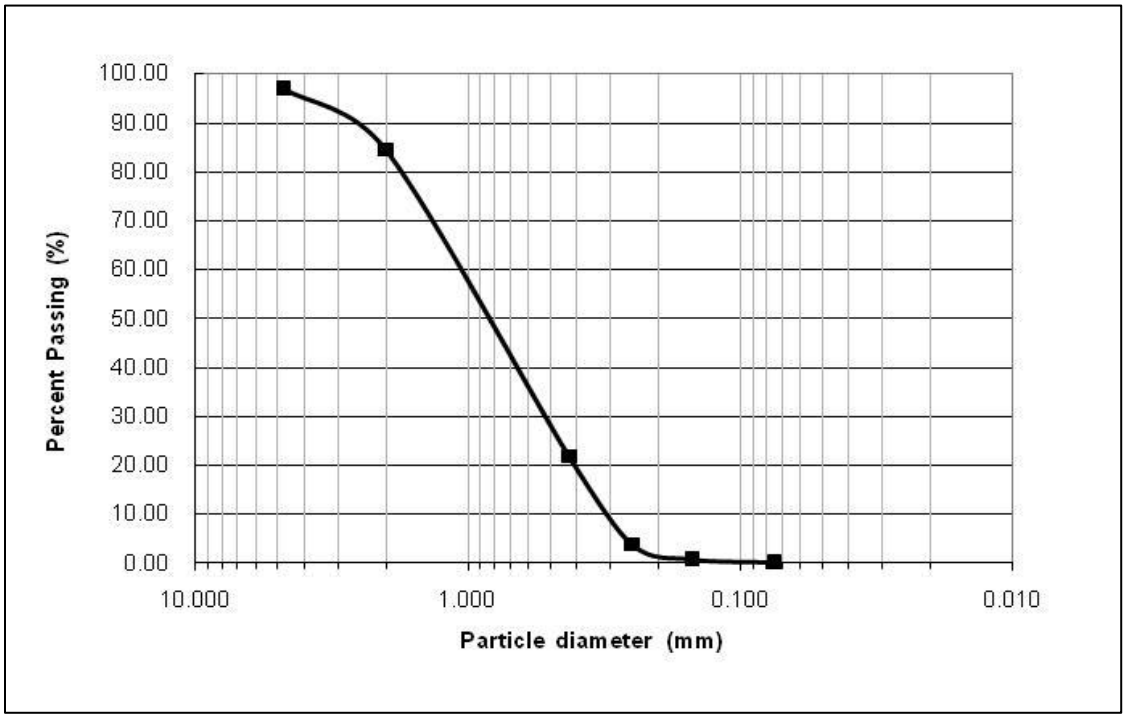

Figure 3.1: Grain-size distribution curve for the poorly-graded sand used in this project**.**

evaluated in this project. The geogrid, shown in Figure 3.2, is a Mirafi® BXG12 and is made of high tenacity polyester multifilament yarns which are woven in tension and finished with a polyvinyl chloride (PVC) coating. The manufacturer indicates that this geogrid is intended to be used for confinement and reinforcement of soil in biaxial loading conditions such as roads. The geotextile, shown in Figure 3.3, is a Mirafi® HP570 and is made from high-tenacity polypropylene yarns which are woven into a network so that they hold their relative position. The manufacturer indicates that the possible uses of this geotextile are separation, filtration,

Figure 3.2: Geogrid used in this project (Mirafi® BXG12) (www.tencate.com).

Figure 3.3: Geotextile used in this project (Mirafi® HP570) (www.tencate.com).

confinement, and reinforcement of soil. The general properties of each geosynthetic are listed in Table 3.2 and the tensile strengths of each geosynthetic are listed in Table 3.3.

3.2 Instrumentation

3.2.1 Geophone Packages

Geophone packages were used in this study to assess the in-situ strain distribution in the test sections. A geophone is a device which converts ground movement (particle velocity) into voltage. Geophones consist of a spring mounted magnetic mass that generates electrical signal proportional to its velocity with respect to a surrounding wire coil. Geophones can only detect movement in the direction that the magnetic mass is oriented. Therefore, to detect movement in the vertical and horizontal direction, two 28-Hz geophones were paired together to form 2-D geophone package. Specifically, the geophones were oriented perpendicular to one another in order to measure velocity (and eventually displacement) in both the vertical and horizontal direction. The geophones were housed within a machined acrylic case with dimension of one inch in height and two inches in width, as shown in Figure 3.4. The geophones were connected by a shielded and grounded electric cable to the data acquisition system in order to analyze the signals during surface loading. After the electric cables were connected to the geophones within the acrylic casing, the geophones were covered with an epoxy to form a waterproof sensor which

Table 3.2: Properties of the geosynthetics provided by the manufacturer

Geosynthetic Type	Structure	Polymer	Roll Dimensions	Mass/Unit Area	Aperture Size
Mirafi® HP570	Woven	Polypropylene	15 ft x 300 ft	14 oz/yd^2	# 30 U.S. Sieve
Mirafi® BXG12	PVC coated Woven	Polyester, PVC	13.1 ft x 164 ft	11.4 oz/yd^2	1 in.

Table 3.3: Geosynthetic tensile strength properties provided by manufacturer

	Minimum Average Roll Value					
	Tensile Strength at 2% Strain		Tensile Strength at 5% Strain		Ultimate Tensile Strength	
Geosynthetic Type	Machine Direction	Cross Machine Direction	Machine Direction	Cross Machine Direction	Machine Direction	Cross Machine Direction
Mirafi® HP570	960 lbs/ft	1320 lbs/ft	2400 lbs/ft	2700 lbs/ft	4800 lbs/ft	4800 lbs/ft
Mirafi® BXG12	625 lbs/ft	840 lbs/ft	1000 lbs/ft	1350 lbs/ft	2500 lbs/ft	4500 lbs/ft

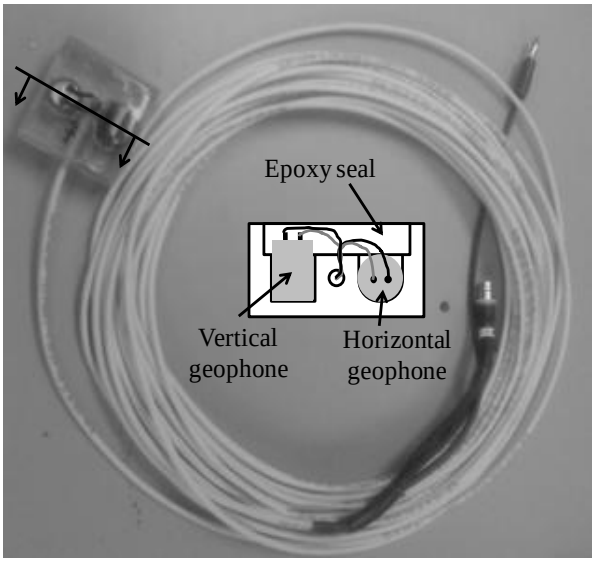

Figure 3.4: Picture and schematic for one of the dynamic geophone packages used in this project. (Cox et al. 2009b)

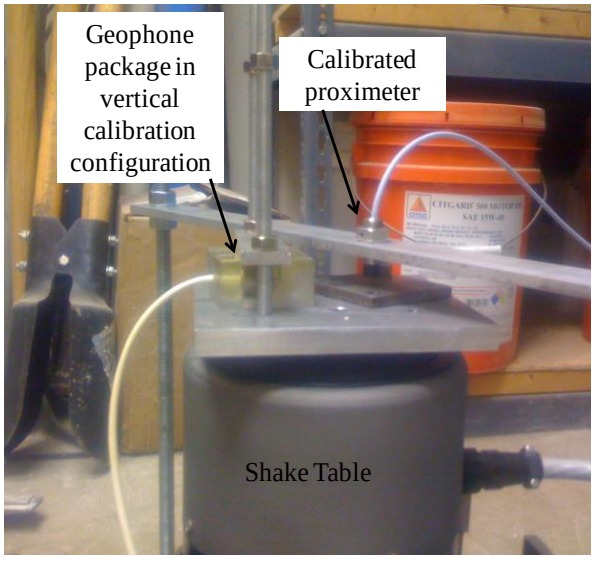

Figure 3.5: 2-D geophone package calibration setup. (Cox et al. 2009b)

could be embedded safely in the test sections. Eight geophone packages were constructed for this project. Each geophone package was calibrated in each direction by applying a sinusoidal motion with constant amplitude to the sensors mounted on a shake table (shown in Figure 3.5), sweeping through frequencies from 5 to 100 Hz. A calibrated proximeter (displacement transducer) was used to determine each geophone's amplitude and phase response as a function of frequency. In Equation 3.1, S is a calibration factor, f is the frequency (5-100 Hz), D is the damping ratio, and f_n is the natural frequency of the geophone (approximately 28 Hz). To obtain the calibration curves, values of S, f_n, and D were selected so that the calculated and measured

$$Amplitude = \frac{Sf^2}{\sqrt{(f_n^2 - f^2) + (2Df_n f)^2}} \quad (3.1)$$

curves match, as shown in Figure 3.6. Calibration was performed in the two orthogonal orientations in order to calibrate both of the geophones in the 2-D geophone package. The calibration factors for the horizontal and vertical geophones in the eight geophone packages used on this project are listed in Table 3.4.

3.3 Test Section Construction

3.3.1 Test Pit Preparation

A site behind the Engineering Research Center (ERC) at the University of Arkansas was cleared. The subgrade soil was excavated to create a pit 4-ft deep by 12-ft wide by 12-ft long. The soil at the bottom of the pit was water-saturated and could not be effectively compacted to form a stable base for the test sections. Therefore, a hole was dug at the front of the pit and a sump pump placed into the pit to pump out excess water during construction of the test sections. The excavated pit and sump pump are shown in Figure 3.7. The pit was then lined with

Table 3.4: Calibration factors for the horizontal and vertical geophones in each of the eight sensors

	Sensor 1		Sensor 2		Sensor 3		Sensor 4	
	Horizontal	Vertical	Horizontal	Vertical	Horizontal	Vertical	Horizontal	Vertical
S (V/in/sec)	0.2797	0.2886	0.2948	0.3001	0.2915	0.295	0.2954	0.3024
fn (Hz)	27.1775	28.0206	25.9438	26.9384	27.0538	28.2187	26.3517	26.3595
D	0.1829	0.1839	0.2058	0.2024	0.1927	0.1929	0.2052	0.2083

	Sensor 5		Sensor 6		Sensor 7		Sensor 8	
	Horizontal	Vertical	Horizontal	Vertical	Horizontal	Vertical	Horizontal	Vertical
S (V/in/sec)	0.2942	0.2833	0.2867	0.2914	0.2932	0.2996	0.2952	0.2818
fn (Hz)	26.9776	26.5736	27.0016	26.3622	26.2513	26.7238	28.0025	26.1570
D	0.2003	0.1899	0.1873	0.2026	0.2047	0.2067	0.1916	0.1932

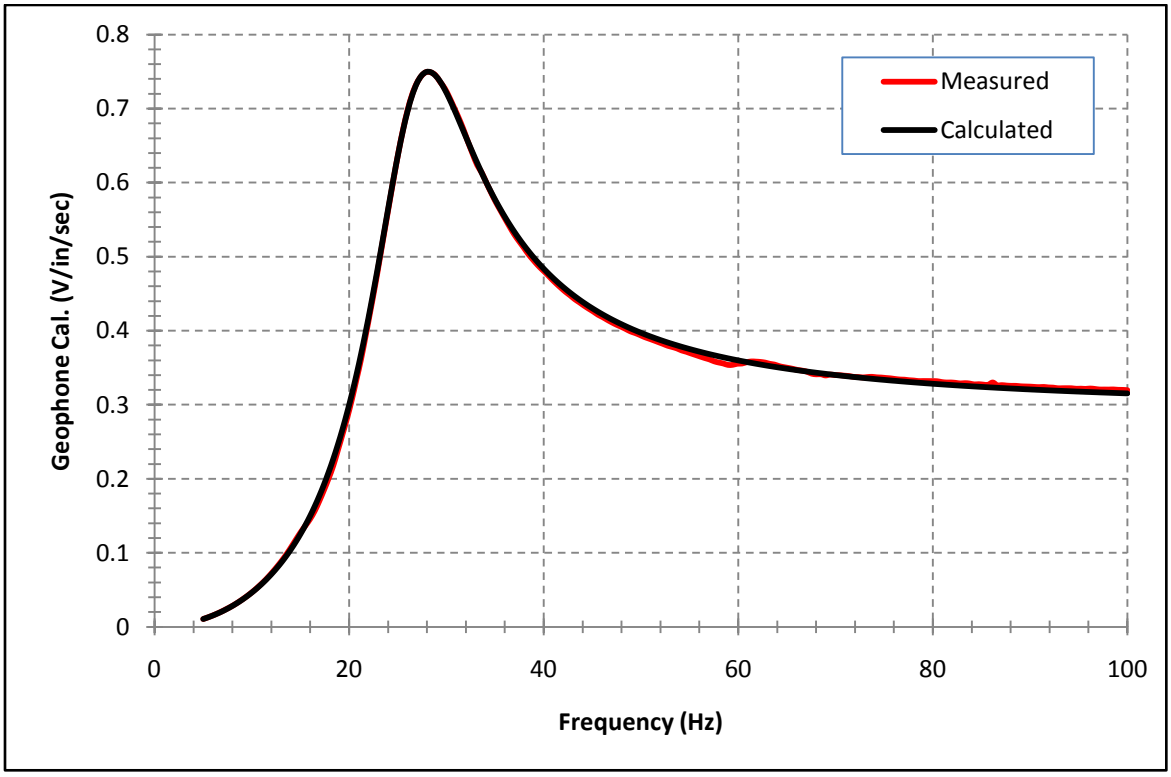

Figure 3.6: Measured and calculated calibration curve for a geophone.

geotextile to create a base to build the test section and to eliminate the intermixing of the ERC subgrade material within the test section materials during testing, as shown in Figure 3.8. Then, eight inches of pea gravel was placed in the bottom of the pit to provide a stable drainage base for the sand layers. The compaction of the gravel layer using a vibratory plate compactor is shown in Figure 3.9. The SP was then compacted in lifts atop the gravel layer. After initial placement, this gravel layer was left intact, but re-compacted during the construction of subsequent sections.

3.3.2 Test Section Construction

All three test sections (unreinforced, geogrid-reinforced, and geotextile-reinforced) were constructed using the same approach. As mentioned, after compaction of the gravel layer, six sand layers were placed in six-inch lifts, as shown in Figure 3.10, and also compacted with the vibratory plate compactor, as shown in Figure 3.11. Sensors and geosynthetics were placed in pre-determined locations within the six sand layers, and will be discussed in Sections 3.3.3 and 3.3.4, respectively. Compaction quality control was performed during construction to ensure that each test section was constructed in a consistent manner. A Troxler nuclear density gauge was used to measure the density (unit weight) and water content of the fourth sand layer in each test section, as shown in Figure 3.12. The average dry unit weight for all three sections was 109.4 pcf with a standard deviation of 1.5 pcf and an average water content of 2.7% with a standard deviation of 0.6% (refer to Table 3.5). This confirms that the constructed test sections are uniform relative to one another (i.e. dry unit weight varies by less than 2% between all sections), which is critical for the comparison of each test section to determine the influence of the geosynthetic reinforcement. Even though the Standard Proctor test was not ideal for SP, seven different moisture contents ranging from 2% to 14% were tested and the range of dry unit weight

Figure 3.7: Construction of the test pit.

Figure 3.8: Geotextile lined test pit.

Figure 3.9: Compaction of 8” gravel layer.

Figure 3.10: Placement of 6” sand layer.

Figure 3.11: Compacted sand layer.

Figure 3.12: Nuclear density gauge reading.

Table 3.5: Nuclear density gauge readings for all three test sections

	Sand (Sp)	
Test Section	**Dry Density (pcf)**	**Water Content (%)**
Geogrid	107.8	2.3
Geotextile	110.7	3.4
Unreinforced	109.6	2.4
Average	109.4	2.7
Standard Deviation	1.5	0.6

was 104 pcf to 109 pcf. As expected, the SP density was insensitive to moisture content. The dry unit weight values recorded in Standard Proctor are consistent with the values recorded in the field.

3.3.3 Geophone Package Placement

After compaction of different lifts, a stiff aluminum bar with a length of 14 ft was placed over the test section. This bar provided a level reference point to measure the proper locations of each sand lift and geophone package. The geophone package placement within the test section is shown in Figure 3.13. The 2-D geophone packages were placed in the middle of each test section and one foot apart. The centerline of the test section was marked on the metal bar and six inches on either side of the centerline were also marked. These marks and a plumb-bob were used to carefully place each geophone package at the proper distance as the test section was being built, as shown in Figure 3.14. The second, third, and fourth row of geophone packages were placed in the same manner, but nine inches higher than the previously placed geophone packages. For the second and fourth row of sensors, it was necessary to dig down three inches into the sand layer to place the sensors at the correct depth, as shown in Figure 3.15. Sand was then compacted by hand around these sensors to ensure movement would not occur and also to establish uniform compaction throughout the test section.

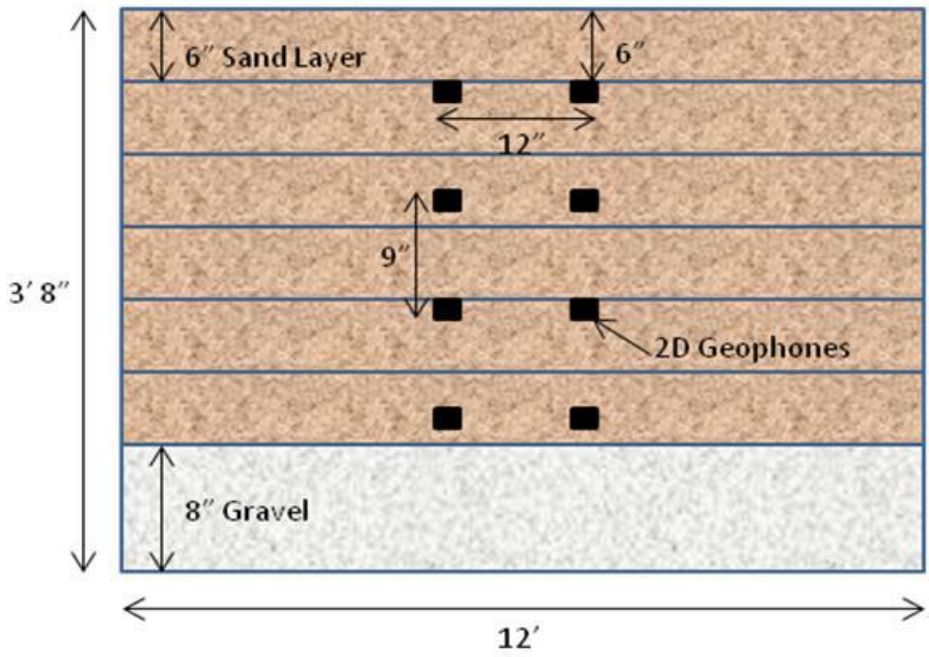

Figure 3.13: Schematic of the geophone package placement within the test sections.

Figure 3.14: Geophone package placement measurements.

Figure 3.15: Geophone package placement three inches deep in sand lift.

3.3.4 Geosynthetic Placement

The reinforced sections were constructed in the same manner as the unreinforced test section, but geosynthetic reinforcement was placed 12 inches down from the top of the test section. The location of the geosynthetic reinforcement was selected based on research that

observed that the optimum embedment depth for geosynthetics is 0.3 D, where D is the loading footprint diameter (Yetimoglu et al. 1994 and Chen et al. 2007). The loading footprint used in this portion of the study is three feet in diameter. Therefore, the optimum geosynthetic placement depth is approximately 12 inches, as shown in Figure 3.16. Both geosynthetic materials, geogrid and geotextile, were placed at the same embedment depth for consistency. Figure 3.17 and Figure 3.18 show the geogrid and geotextile being placed in the test sections, respectively. During installation, care was taken to guarantee that no wrinkles were present in the geosynthetic material.

3.4 Experimental Setup

3.4.1 Loading Mechanism (Vibroseis Truck)

After the test sections were constructed, The University of Arkansas Vibroseis truck (the Hawg), shown in Figure 3.19, was used to apply dynamic surface loads to the test sections. This mobile, servo-controlled hydraulic loading system can apply static hold-down forces up to 14,000 lbs, and a superimposed peak-to-peak dynamic load of up to 12,000 lbs over a wide range of frequencies. The Vibroseis truck applies dynamic loads using a hydraulic servo-motor to drive a 311 lb mass along a low friction shaft. The low friction shaft can be oriented in both the horizontal or vertical direction to apply dynamic shear or compressive loads, respectively, to the ground surface. Both horizontal and vertical orientations were used during evaluation of the test sections to evaluate the distribution in strain with depth during surface loading with shear and compression waves. The Vibroseis truck with the mass in the horizontal (shear) orientation is shown in Figure 3.20, while the vertical (compressive) orientation is shown in Figure 3.21. The flexibility and mobility of the Vibroseis truck was an essential asset to this project.

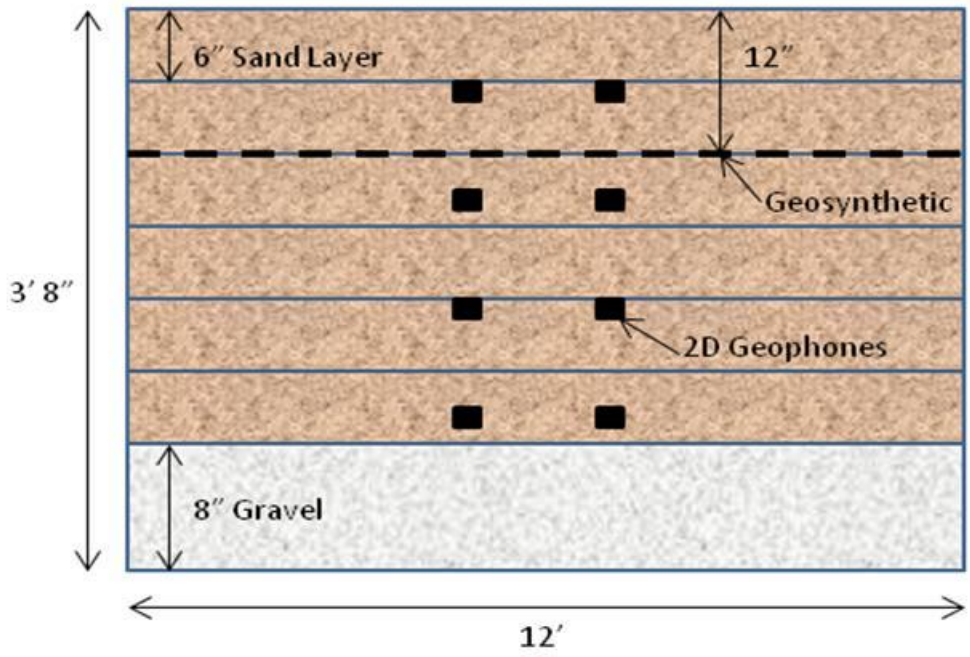

Figure 3.16: Schematic of the geosynthetic placement within the test sections.

Figure 3.17: Geogrid placement.

Figure 3.18: Geotextile placement.

Figure 3.19: University of Arkansas' Vibroseis truck.

Figure 3.20: Shear loading configuration.

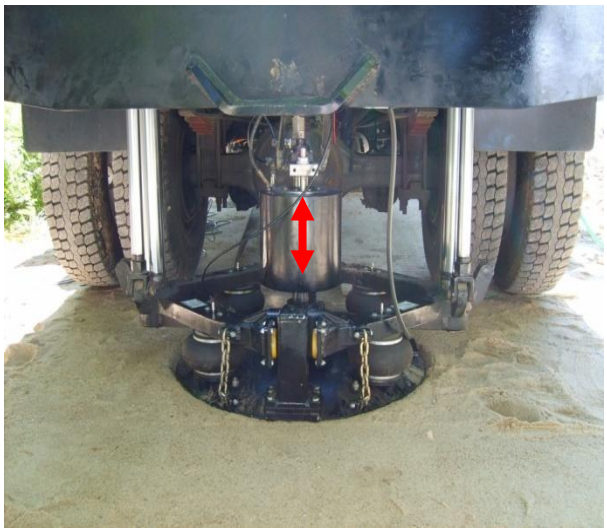

Figure 3.21: Compression loading configuration.

3.4.2 Test Section Loading

The loading of each test section was done directly over the centerline of the geophone array, as shown in Figure 3.22. First, the Vibroseis truck was used to apply a static hold down force of 9,000 lbs (approximately half an ESAL). The full 3-ft diameter base plate was used to apply the load to the ground surface. Next, five dynamic load increments with increasing amplitude were superimposed atop this hold-down force at a frequency of 50 Hz for one second each (i.e. 50 total loading cycles for each force level). The staged dynamic loading sequences for shear and compression loading are represented schematically in Figures 3.23 and 3.24, respectively. This loading was conducted in stages from lowest to highest force level, starting from 550 lbs up to 6000 lbs. The response of the soil system was determined to range from near linear elastic for the lower load range, up to non-linear inelastic for the upper load range (based on measured strain levels induced in the sections). This conclusion was made from observation of G/G_{max} curves for similar types of sand (Menq 2005). Approximately one minute passed between the application of each successive dynamic load. Note that the peak dynamic force levels are approximations as the force levels in each test section varied slightly (i.e. +/- a few hundred pounds). One shortcoming of this approach is that when the Vibroseis is driven in short bursts, it cannot be operated in a force-controlled manner. Therefore, identical drive voltage levels were used in the testing sequences for each of the test sections, but the force levels varied slightly from test section to test section. The effects of this shortcoming are discussed in Section 3.6.

A loading frequency of 50 Hz was used for several reasons. First, the 28-Hz geophones used in the sensors have a 180 degree phase shift near 28 Hz, with reduced dynamic output below this frequency. At 50 Hz, the phase and amplitude responses of the geophones are

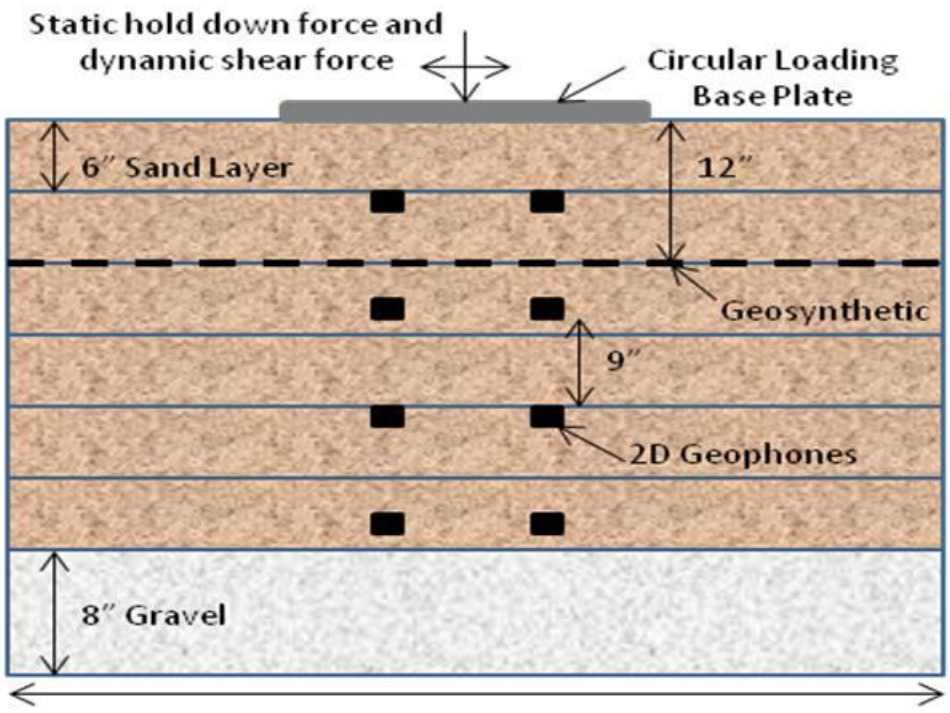

Figure 3.22: Schematic of the location that each test section was loaded.

generally flat, making the data analysis more straightforward. Another reason for using a load application frequency of 50 Hz is that several traffic studies have observed that the predominant frequency content of traffic is in the range of 10 Hz to 60 Hz (Henwood 2002) or 10 Hz to 30 Hz (Zhang 1996).

3.4.3 Data Acquisition

A 32-channel Data Physics dynamic signal analyzer, shown in Figure 3.25, was used to record the 16 output signals from the geophone packages, as well as the Vibroseis drive signal and the input ground force signals from the two accelerometers attached to the base plate and mass on the Vibroseis truck. A four channel Data Physics dynamic signal analyzer (Quattro) was used to drive the Vibroseis truck independently of the data acquisition system. The sampling duration selected for each load increment was 1.2 seconds, 0.2 seconds longer than the 1.0

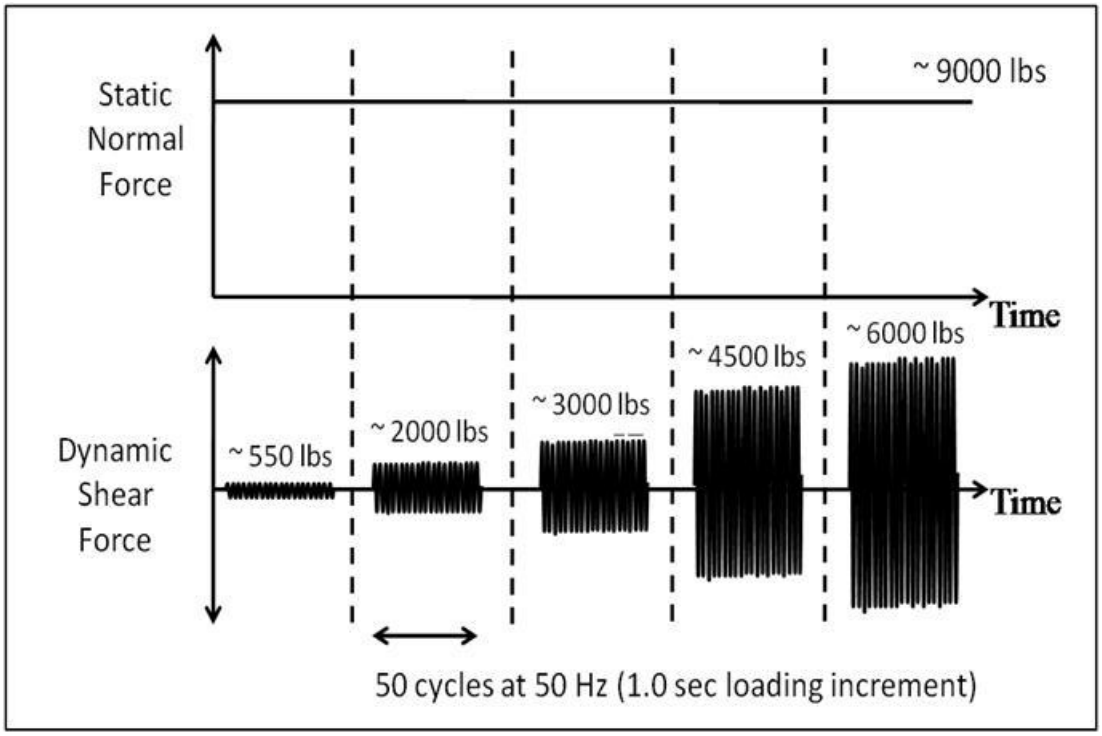

Figure 3.23: Staged dynamic loading sequence applied to each test section to determine in-situ shear strain.

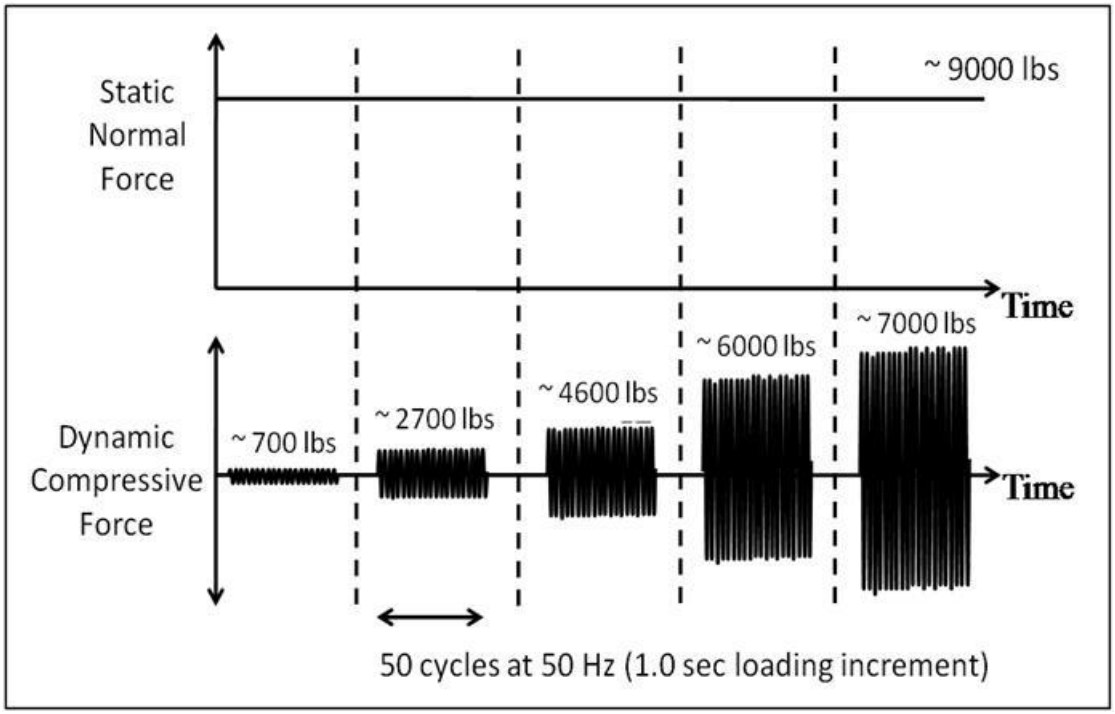

Figure 3.24: Staged dynamic loading sequence applied to each test section to determine in-situ vertical normal strain.

Figure 3.25: Data Acquisition System.

Figure 3.26: Real time monitoring of each output signal.

second loading period. This longer sampling duration ensured that the full signal was collected. The drive signal was used as a trigger to initiate the sampling period, and a 0.1 second buffer was used to collect readings before the trigger as well. A sampling rate of 107,520 samples per second (~108 kHz) was used in order to resolve the relatively small time lags between closely spaced vertical sensors. The signals were monitored with the signal analyzers inside the Vibroseis truck, as shown in Figure 3.26, in real time so that testing could be repeated should a problem occur during testing.

3.5 Data Analysis

The 2-D geophone packages were strategically placed in the test section to create three, four-node rectangular arrays (finite elements) in order to create in-situ strain measurement points at different depths within the test sections. The locations of the geophone packages are shown in Figure 3.27. Each four node rectangular array was defined, as shown in Figure 3.28, with the

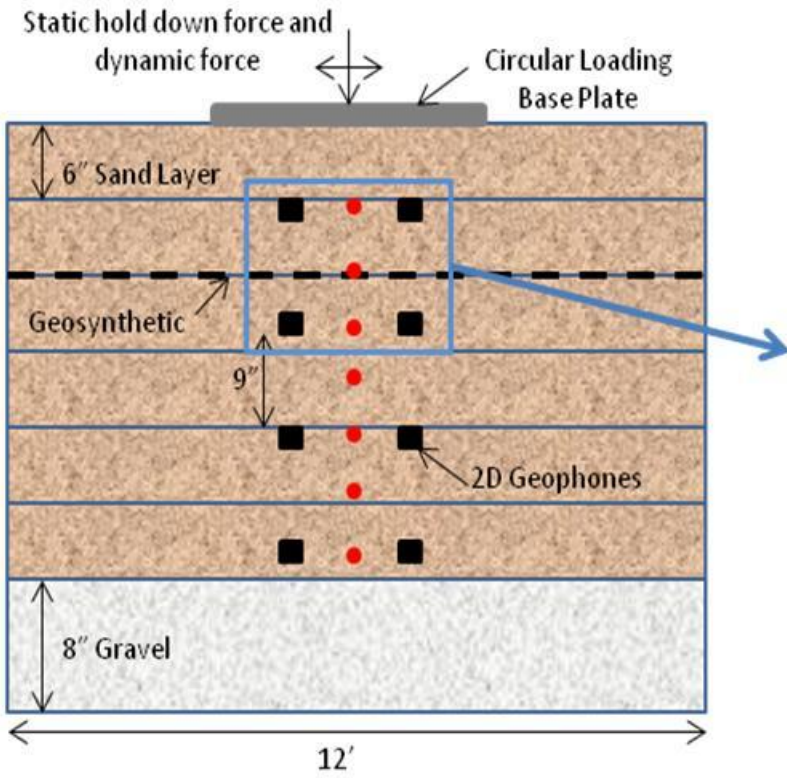

Figure 3.27: In-situ strain measurement points.

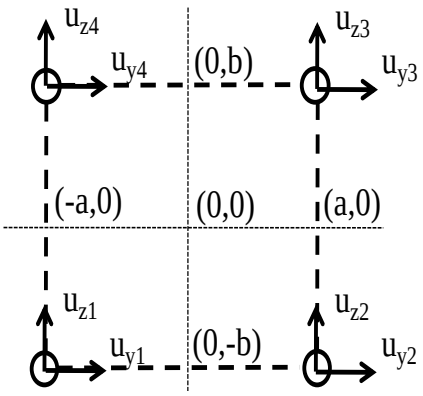

Figure 3.28: Typical four node element. (Cox et al. 2009b)

horizontal direction denoted as y, the vertical direction denoted as z, and the displacements measured in each direction denoted as u_y and u_z, respectively. The lengths of the sides of the rectangular array were denoted as 2a in the y direction and 2b in the z direction, following the coordinate system commonly used to map global coordinates to natural coordinates in the four-node, isoparametric finite element formulation.

In each four-node array, 2a represents the natural distance between the sensors in the horizontal direction (12 inches), and 2b represents the natural distance between the sensors in the vertical direction (9 inches). The horizontal and vertical voltage time histories recorded at each sensor location were converted to velocity time histories by applying the calibration factors to the recorded geophone signals. The displacements u_y and u_z at each node were calculated by

numerically integrating the velocity records for each geophone. An example displacement time record is shown in Figure 3.29. Using the vertical and horizontal displacement records at each node, and implementing the coordinate system shown in Figure 3.28, the normal horizontal strain, ε_y, normal vertical strain, ε_z, and shear strain, τ_{yz}, may be calculated using the four-node, isoparametric finite element equations provided in Equations 3.2, 3.3, and 3.4 (Cook et al. 1989, Cox et al. 2009a, Cox et al. 2009b).

$$\varepsilon_y(y,z) = \frac{1}{4a}\left[-u_{y1}(1-z/b) + u_{y2}(1-z/b) + u_{y3}(1+z/b) - u_{y4}(1+z/b)\right] \tag{3.2}$$

$$\varepsilon_z(y,z) = \frac{1}{4b}\left[-u_{z1}(1-y/a) - u_{z2}(1+y/a) + u_{z3}(1+y/a) + u_{z4}(1+y/a)\right] \tag{3.3}$$

$$\begin{aligned}\tau_{yz}(y,z) = \frac{1}{4}\Big[&-\frac{u_{y1}}{b}(1-y/a) - \frac{u_{z1}}{a}(1-z/b) - \frac{u_{y2}}{b}(1+y/a) + \frac{u_{z2}}{a}(1-z/b) \\ &+ \frac{u_{y3}}{b}(1+y/a) + \frac{u_{z3}}{a}(1+z/b) + \frac{u_{y4}}{b}(1-y/a) - \frac{u_{z4}}{a}(1+z/b)\Big]\end{aligned} \tag{3.4}$$

The locations within the test section where in-situ strains were calculated using these three equations are represented by the red circles shown in Figure 3.27. An example shear strain time history is shown in Figure 3.30, and the method used to define the average shear strain level over the one second loading increment is shown in Figure 3.30. The average maximum shear strain and the absolute value of the average minimum shear strain are compared and the higher of these two values is taken as the shear strain amplitude induced at that depth under the given dynamic load. For the example data in Figure 3.30, the average maximum shear strain is 0.17% and the average minimum shear strain is the absolute value of -0.165% (i.e. 0.165%). Therefore, the average shear strain for this particular location is 0.17%. The normal strains were also calculated using the same approach.

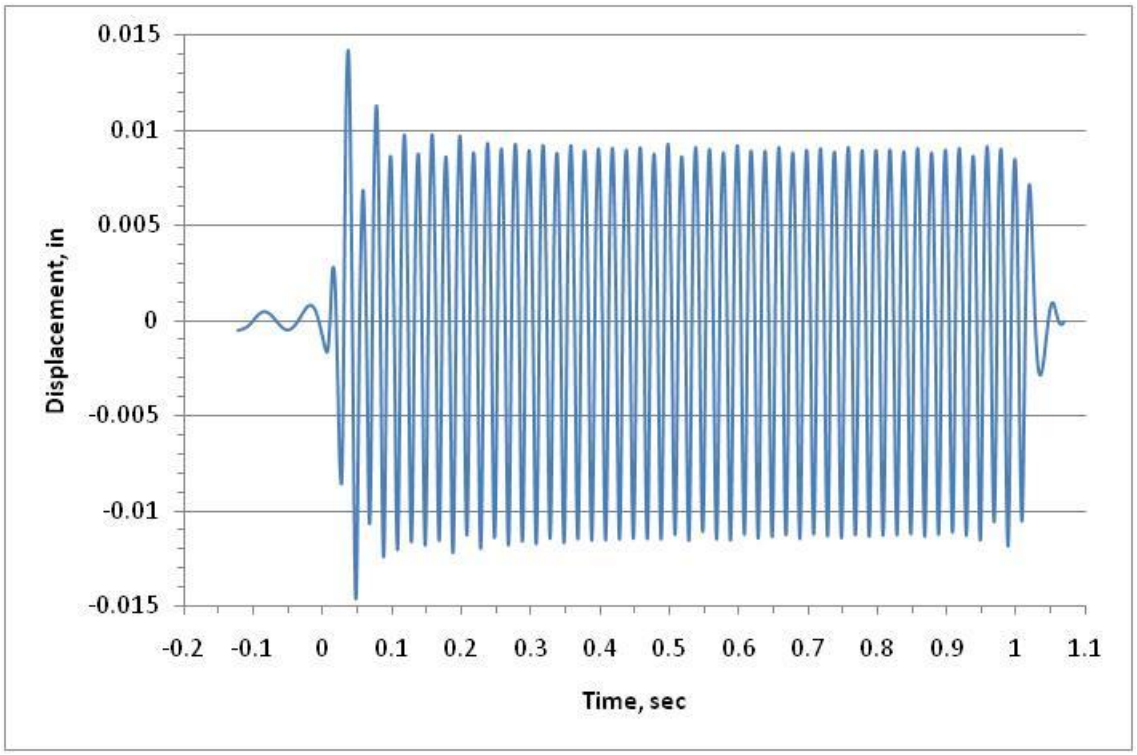

Figure 3.29: Example displacement time history recorded at a sensor location.

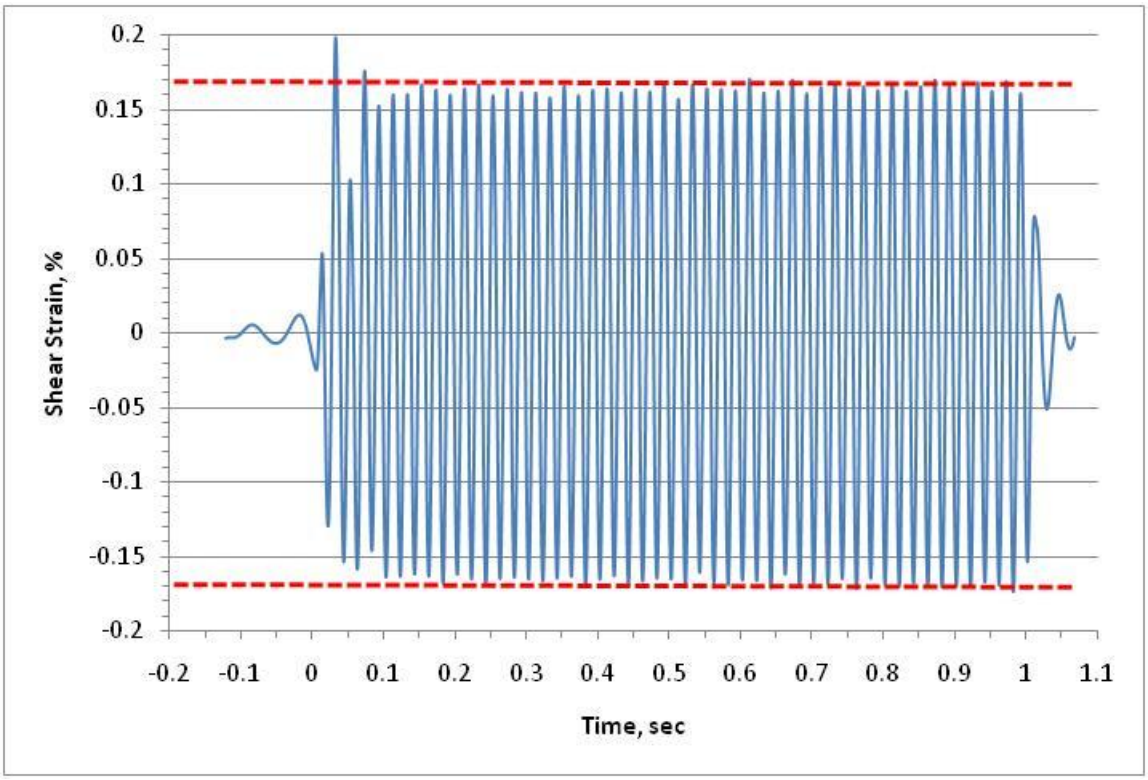

Figure 3.30: Example shear strain time history and method for determining the average shear strain.

The normal horizontal strain, normal vertical strain, and shear strain were calculated at the top, middle, and bottom of each rectangular array of geophone packages (i.e. at the locations marked by red circles in Figure 3.27). At the interface between two elements, the strains obtained from each element were averaged to determine the strain associated with that depth. In order to perform these calculations, it was assumed that the vertical and horizontal distance between each geophone package remained constant throughout testing. In other words, this approach assumes that there was no permanent displacement of the geophone packages during dynamic loading.

3.6 Results

3.6.1 Shear Strain Response

The locations of the calculated in-situ shear strain values as a function of depth are shown in Figure 3.31. The depths of the calculated values were consistent for each of the three test sections. Shear strain versus depth measurements for each loading increment imposed on the unreinforced test section are tabulated in Table 3.6 and shown in Figure 3.32. A reduction in shear strain with depth was expected, as this is consistent with stress distribution theories, such as that developed by Bousinesq. The geogrid and geotextile reinforced test section in-situ shear strain measurements with depth are tabulated in Table 3.7 and Table 3.8, respectively. The shear strain versus depth curves for the geogrid and geotextile reinforced test sections are shown in Figure 3.33 and Figure 3.34, respectively. An interesting observation is that the geosynthetic-reinforced test sections show very similar results for in-situ shear strain versus depth when compared to the unreinforced section. This indicates that for small-strain loading (i.e. less than 0.2%), the geosynthetic reinforcements do not alter the strain distribution behavior of the soil layer.

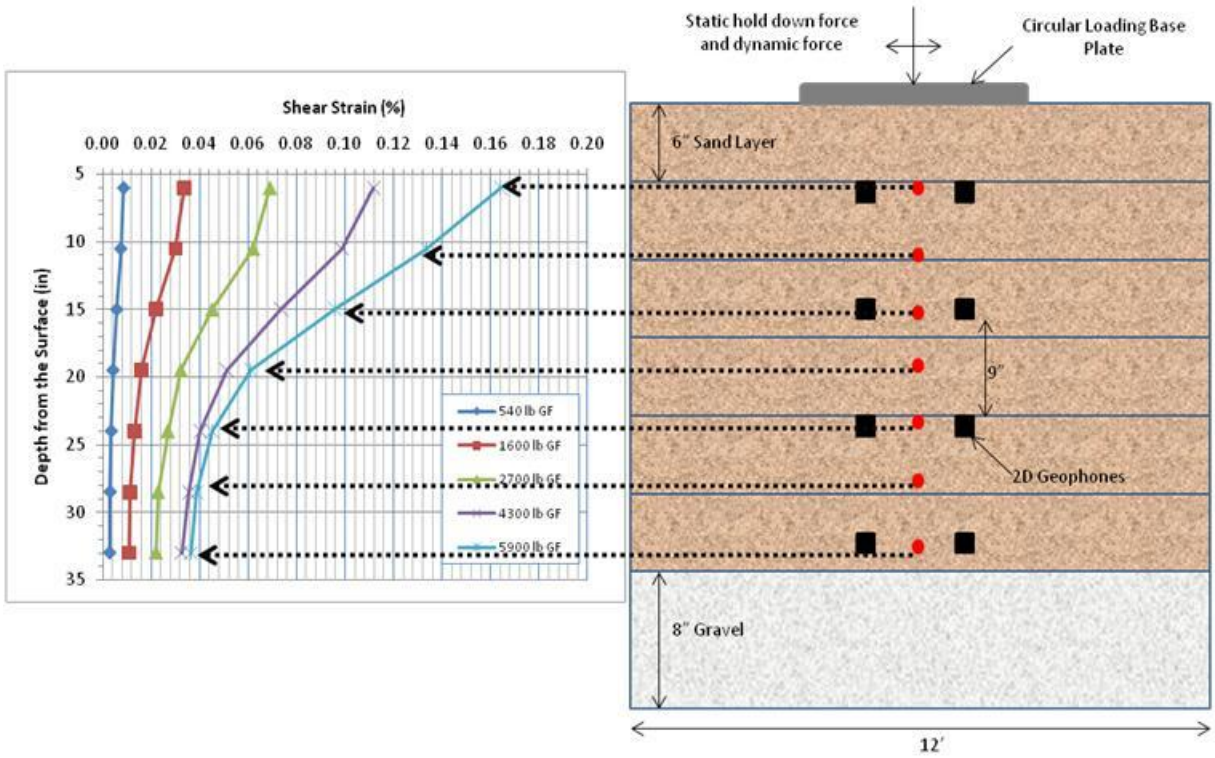

Figure 3.31: In-situ strain measurement locations for the unreinforced test section.

The shear strain versus depth information for the maximum force applied to all three test sections is compared in Figure 3.35. Surprisingly, the largest magnitude of strains was actually observed in the geogrid reinforced section, while similar magnitudes of strain were measured in the unreinforced and geotextile reinforced sections. However, the differences in the measured shear strains are relatively small, considering that the maximum magnitude of strain measured in all of the test sections is less than 0.2%. Furthermore, as mentioned in Section 3.4.2, the loads on each test section varied somewhat due to the inability to operate the Vibroseis with a force feedback loop under such short loading bursts. The maximum forces applied to the unreinforced, geogrid reinforced, and geotextile reinforced test sections were 5900 lbs, 6000 lbs, and 5800 lbs, respectively, So, the force applied to the geogrid section was approximately 100 lbs (1.7%) greater than the unreinforced section. This fact partially explains the larger strains observed in

Table 3.6: Shear strain versus depth measurements for each staged load applied to the unreinforced test section

	Unreinforced Test Section				
	Shear Strain (%)				
Depth from Surface (in)	GF=540 lb	GF=1600 lb	GF=2700 lb	GF=4300 lb	GF=5900 lb
6	0.0081	0.0319	0.0646	0.104	0.1596
10.5	0.0073	0.0286	0.0586	0.0902	0.1265
15	0.00565	0.021	0.0434	0.0684	0.0868
19.5	0.0043	0.0152	0.0307	0.0481	0.0591
24	0.0035	0.01265	0.02565	0.03875	0.044
28.5	0.0029	0.0108	0.0219	0.0334	0.038
33	0.0028	0.0103	0.0211	0.0318	0.0352

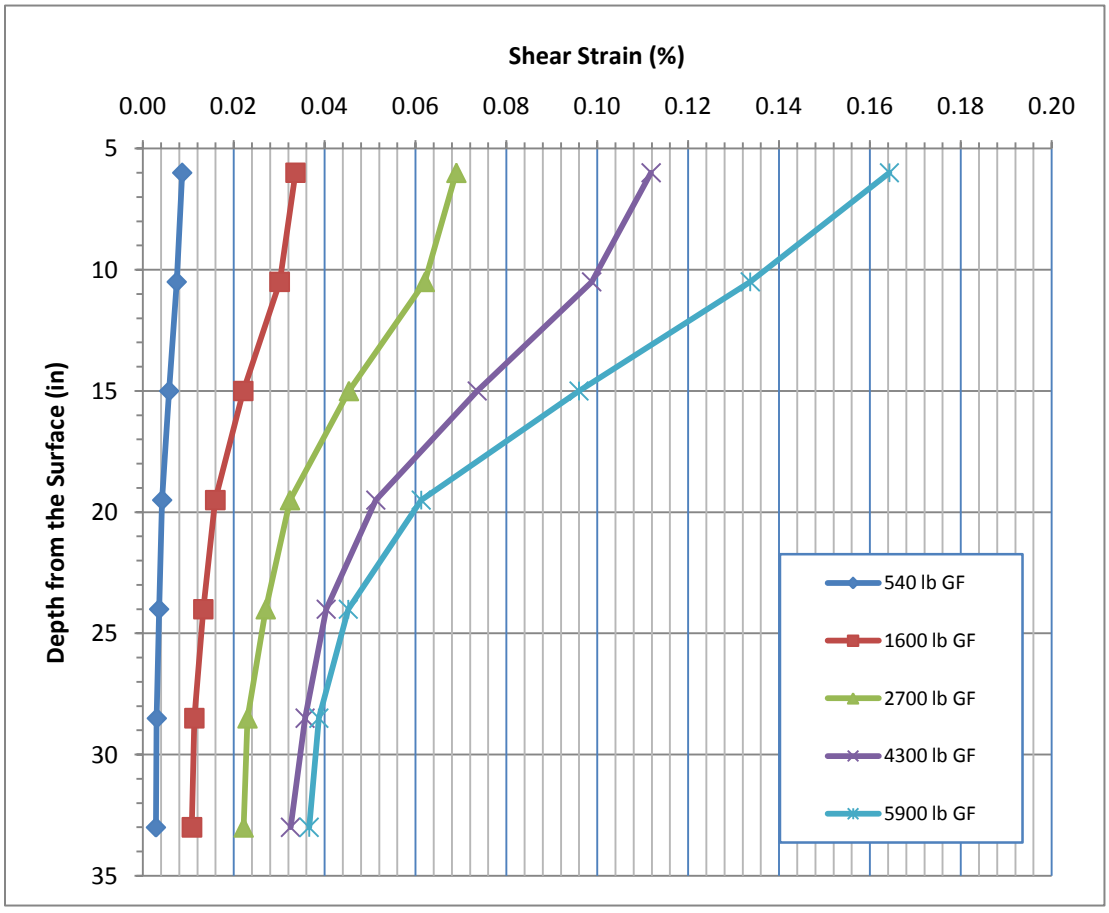

Figure 3.32: Shear strain versus depth for the unreinforced test section at each staged load.

Table 3.7: Shear strain versus depth measurements for each staged load applied to the geogrid reinforced test section

	Geogrid Reinforced Test Section				
	Shear Strain (%)				
Depth from Surface (in)	GF=590 lb	GF=2000 lb	GF=3100 lb	GF=4700 lb	GF=6000 lb
6	0.0056	0.0285	0.064	0.112	0.1677
10.5	0.0055	0.0279	0.0607	0.1027	0.1419
15	0.00505	0.0241	0.05045	0.0832	0.1057
19.5	0.0043	0.0195	0.0396	0.0623	0.0766
24	0.00365	0.0168	0.03375	0.0513	0.06
28.5	0.0032	0.0148	0.0295	0.0443	0.0511
33	0.0029	0.0141	0.0283	0.0422	0.0478

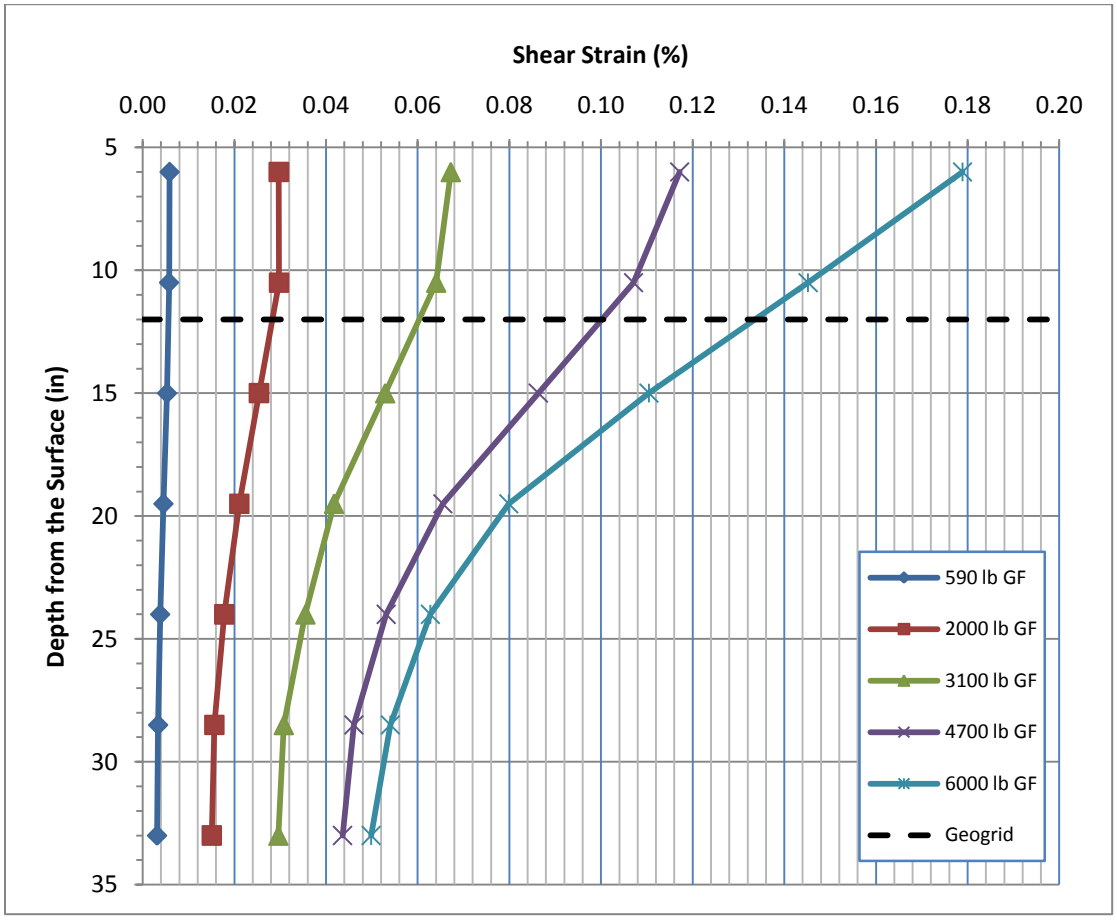

Figure 3.33: Shear strain versus depth for the geogrid test section at each staged load.

Table 3.8: Shear strain versus depth measurements for each staged load applied to the geotextile reinforced test sections

	Geotextile Reinforced Test Section				
	Shear Strain (%)				
Depth from Surface (in)	GF=540 lb	GF=2000 lb	GF=3100 lb	GF=4500 lb	GF=5800 lb
6	0.0056	0.0301	0.0692	0.1127	0.1593
10.5	0.0054	0.0294	0.0658	0.1017	0.127
15	0.0045	0.0236	0.0505	0.0755	0.0889
19.5	0.0036	0.0177	0.0358	0.051	0.0599
24	0.0032	0.0156	0.0311	0.0431	0.0490
28.5	0.0027	0.0136	0.0270	0.0376	0.0433
33	0.0026	0.0131	0.0261	0.0359	0.0408

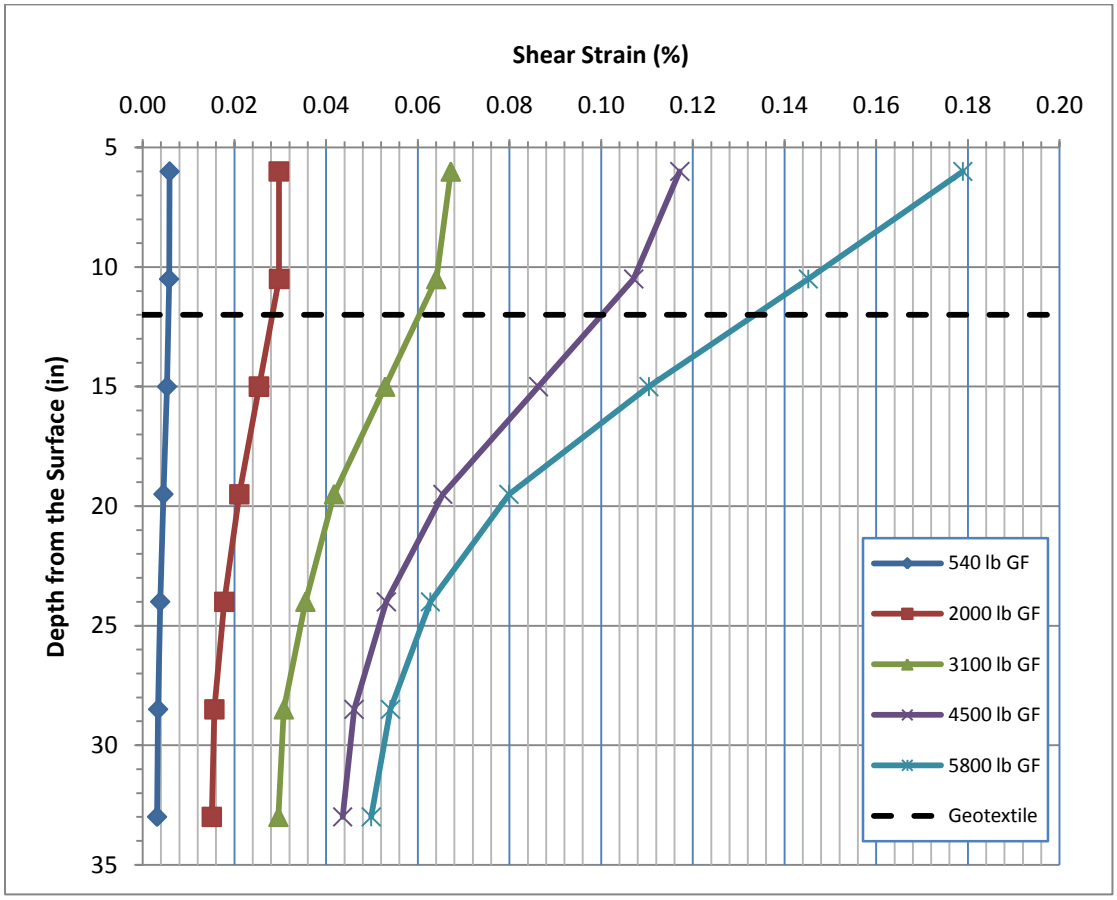

Figure 3.34: Shear strain versus depth for the geotextile test section at each staged load.

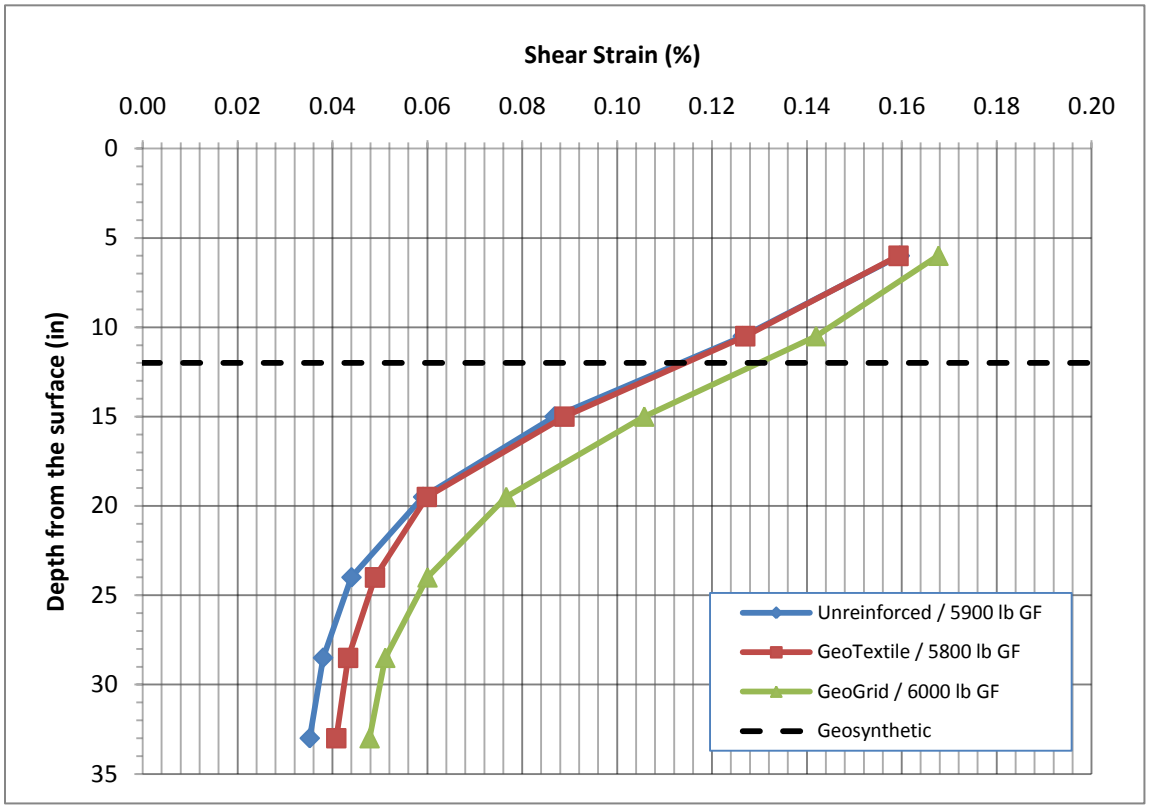

Figure 3.35: Comparison of shear strain versus depth at the highest applied GF to each test section.

the geogrid-reinforced section when compared to the other two sections. However, the force applied to the geotextile section was approximately 100 lbs (1.7%) less than the force applied to the unreinforced section and the shear strains in the geotextile section were actually greater at depth.

In order to compare the results for all three test sections, the shear strains in the geogrid and geotextile reinforced test sections were adjusted to the strains expected at an equivalent reference ground force (RGF) of 5900 lbs (i.e. the force applied to the unreinforced test section). Table 3.9 tabulates the in-situ shear strains for the maximum applied load for each test section along with the shear strains adjusted to the RGF of 5900 lbs. The strains from the geogrid section were adjusted down by approximately 1.7%, while the strains from the geotextile section

Table 3.9: Shear strains from the highest applied ground force (GF) for each test section along with the shear strains adjusted to the reference ground force (RGF) of 5900 lbs

	Shear Strain (%)				
	Unreinforced	Geogrid		Geotextile	
Depth (in)	GF=5900 lb	GF=6000 lb	RGF=5900 lb	GF=5800 lb	RGF=5900 lb
6	0.1596	0.1677	0.1649	0.1593	0.1620
10.5	0.1265	0.1419	0.1395	0.127	0.1292
15	0.0868	0.1057	0.1039	0.0889	0.0904
19.5	0.0591	0.0766	0.0753	0.0599	0.0609
24	0.044	0.06	0.0590	0.04895	0.0498
28.5	0.038	0.0511	0.0502	0.0433	0.0440
33	0.0352	0.0478	0.0470	0.0408	0.0415

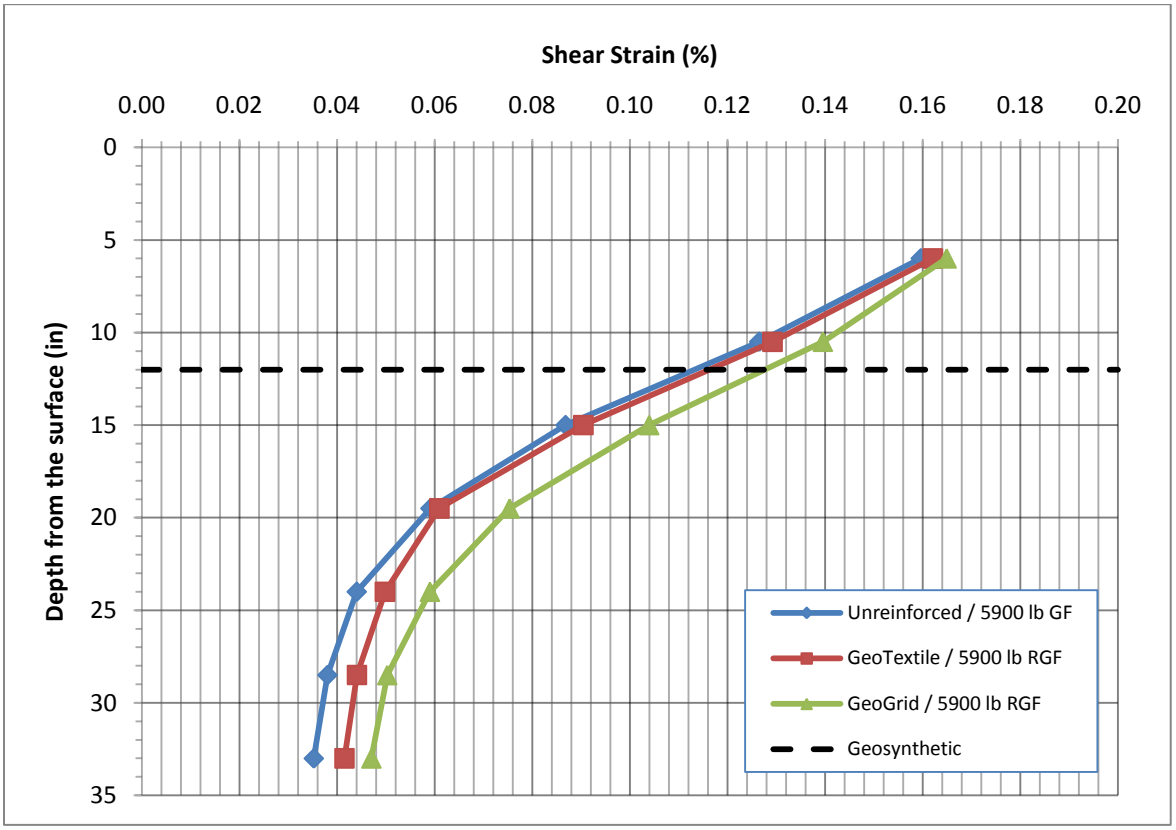

Figure 3.36: Comparison of shear strain versus depth in each test section after adjusting all strains to a reference ground force (RGF) of 5900 lbs.

were adjusted up by approximately 1.7%. The adjusted shear strain versus depth information for the 5900 lbs force level is shown Figure 3.36. The strain adjustment to account for differences in applied force level did not significantly change the curves or the overall trends. The trend shown in Figure 3.36 is that the geosynthetic reinforced test sections have equal or higher strains at all depths relative to the unreinforced section. However, these differences are minimal and may be assumed to be approximately equal in all test sections. At these strain levels, ranging from linear elastic to nonlinear inelastic, the introduction of geosynthetic reinforcement does not alter the shear strain distribution within the test section during dynamic. However, at less than one percent shear strain, it is likely that the geosynthetic reinforcement was not mobilized during testing. Still, these low strain levels likely represent the "working" strain levels one might expect under typical low-volume traffic loads.

It should be noted that some of the minor differences in measured shear strain between tests sections may be attributed to small variations in the dry unit weight and moisture content (negative pore water pressures) of each test section (refer to Table 3.5). While the geogrid test section had the highest level of induced shear strain, it also had the lowest dry unit weight (107.8 pcf) compared to that of the unreinforced section (109.6 pcf). However, at depths great than 20 inches, the geotextile reinforced section had greater strains than the unreinforced section despite having a higher dry unit weight (110.7 pcf). A pattern does not develop relative to these small, and presumably minor, variations in dry unit weight. Furthermore, the water contents inferred from the nuclear gauge in each section varied by less than 1%. It is believed that these small variations likely had some affect on the measured shear strains but certainly not a large enough affect to mask out the contribution of the geosynthetic reinforcement had one existed.

3.6.2 Normal Strain Response

Vertical normal strains during vertical (compression) loading were calculated at the same depths that shear strains were calculated (refer to Figure 3.31). The tabulated vertical normal strains versus depth for each staged load on the unreinforced test section, geogrid reinforced test section, and geotextile reinforced test section are provided in Table 3.10, Table 3.11, and Table 3.12, respectively. The unreinforced, geogrid reinforced, and geotextile reinforced test section curves for vertical normal strains versus depth for each staged load are shown in Figure 3.37, Figure 3.38, and Figure 3.39, respectively. The scales on the x- and y-axes are the same for the vertical normal strain versus depth plots as for the shear strain versus depth plots in Section 3.6.1. This was done in order to keep from exaggerating the vertical normal strain versus depth results relative to the shear strain versus depth results. For a given magnitude of applied surface load, an equivalent shear load will induce much larger shear strains with depth than an equivalent vertical load will induce vertical normal strains with depth.

The vertical strain versus depth calculated for the compressive loading stages with a magnitude of approximately 6300 lbs in each section is compared in Figure 3.40. A magnitude of 6300 lbs was chosen for comparison because force levels higher than 6300 lbs were not generated while testing the geogrid section, and therefore this represents the highest common force level shared by all three test sections. As noted in the comparisons discussed above, the largest strain magnitudes were measured in the geogrid reinforced section, while similar strains were measured in the unreinforced and geotextile reinforced sections. However, the differences in the measured vertical strains are very small, considering that the maximum strain is less than 0.05%. As mentioned in Section 3.4.2, the loads on each test section varied somewhat due to the inability to operate the Vibroseis with a force feedback loop under such short loading bursts.

Table 3.10: Vertical normal strain versus depth measurements for each staged load applied to the unreinforced test section

	Unreinforced Test Section				
	Vertical Normal Strain (%)				
Depth from Surface (in)	GF=600 lb	GF=2700 lb	GF=4700 lb	GF=5800 lb	GF=6300 lb
6	0.0016	0.0094	0.0223	0.0367	0.0419
10.5	0.0016	0.0094	0.0223	0.0367	0.0419
15	0.0015	0.0086	0.02015	0.03315	0.03825
19.5	0.0014	0.0078	0.018	0.0296	0.0346
24	0.001172	0.0065	0.015	0.0239	0.0281
28.5	0.000945	0.0052	0.012	0.0182	0.0216
33	0.000945	0.0052	0.012	0.0182	0.0216

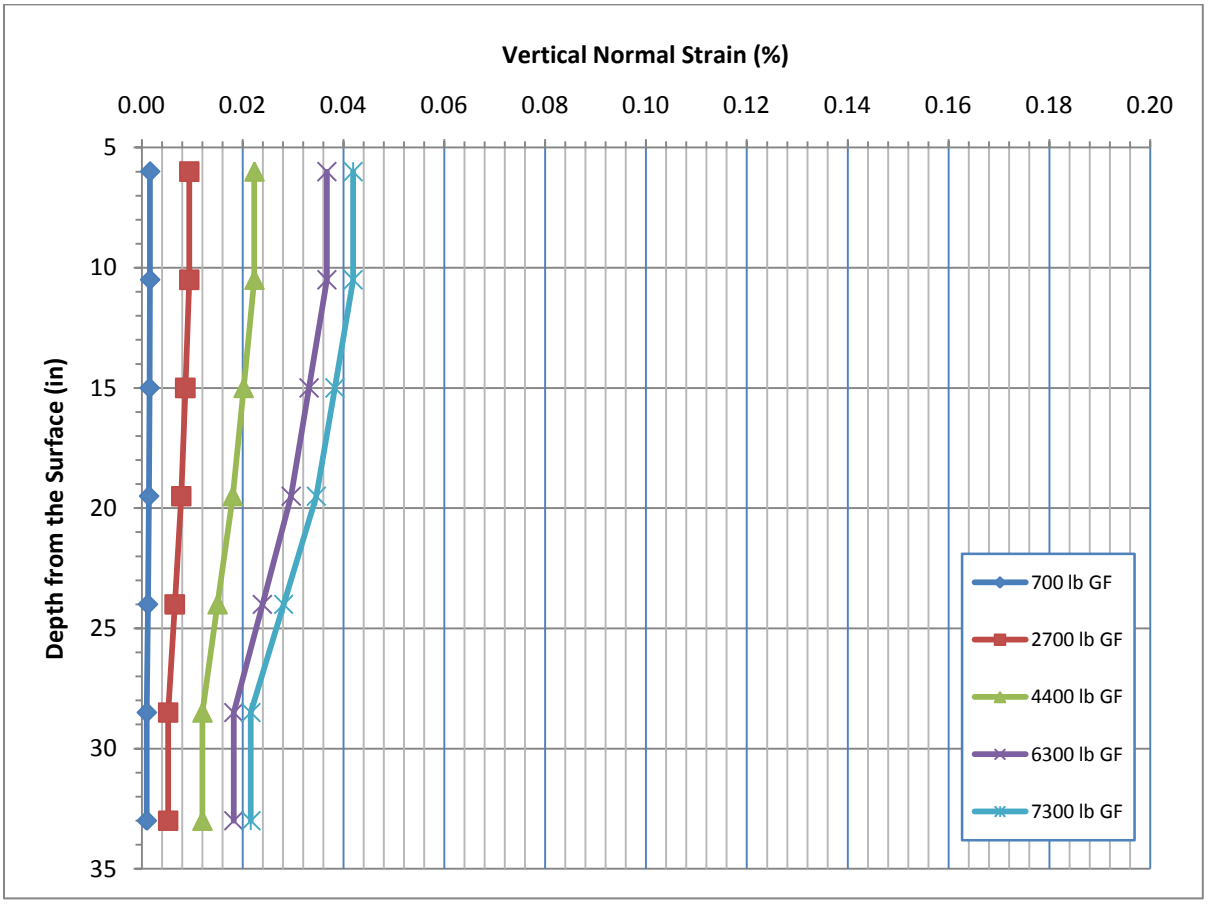

Figure 3.37: Vertical normal strain versus depth for the unreinforced test section at each staged load.

Table 3.11: Vertical normal strain versus depth measurements for each staged load applied to the geogrid reinforced test section

	Geogrid Reinforced Test Section				
	Vertical Normal Strain (%)				
Depth from Surface (in)	GF=600 lb	GF=2700 lb	GF=4700 lb	GF=5800 lb	GF=6300 lb
6	0.0015	0.0091	0.022	0.0349	0.0418
10.5	0.0015	0.0091	0.022	0.0349	0.0418
15	0.0014	0.00815	0.01945	0.03105	0.0374
19.5	0.0013	0.0072	0.0169	0.0272	0.033
24	0.001085	0.00595	0.0138	0.02215	0.027
28.5	0.00087	0.0047	0.0107	0.0171	0.021
33	0.00087	0.0047	0.0107	0.0171	0.021

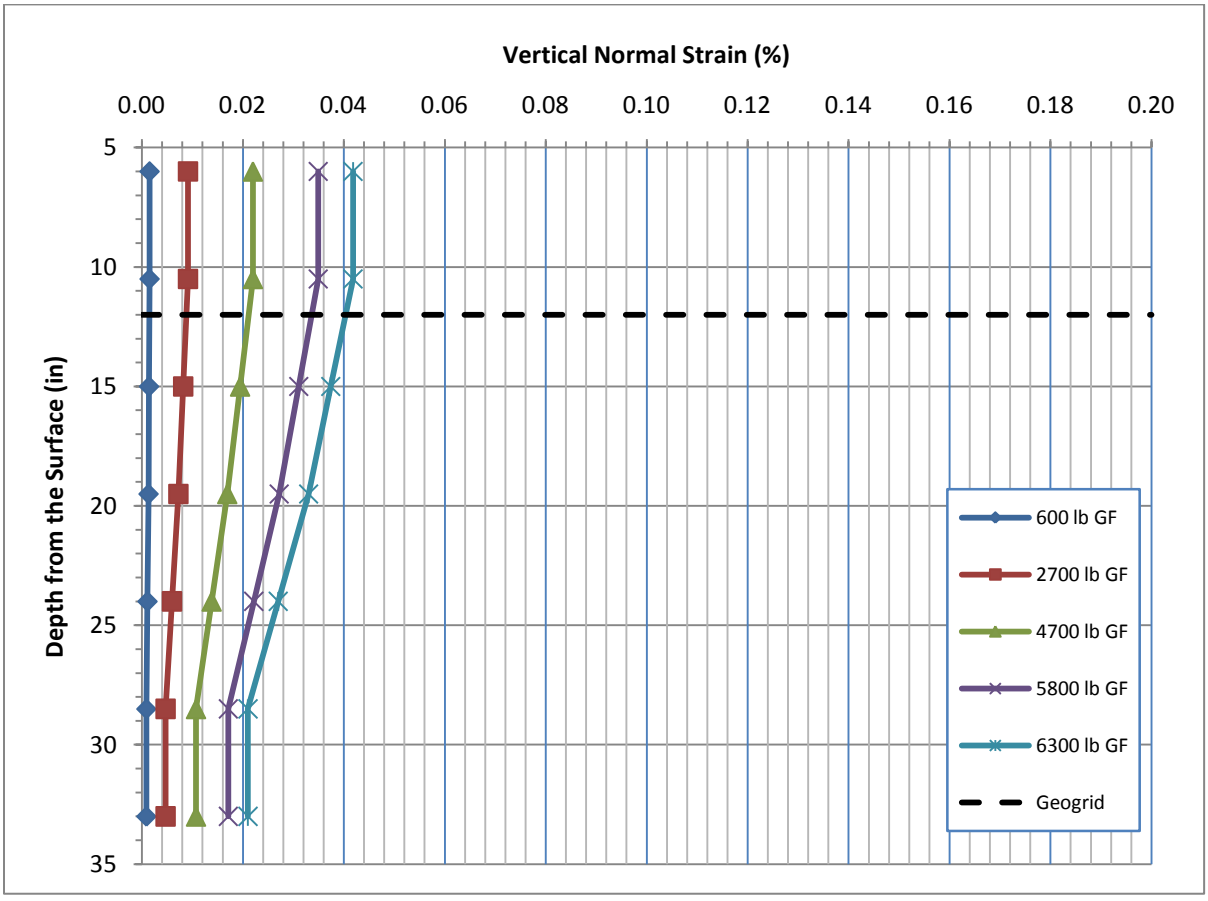

Figure 3.38: Vertical normal strain versus depth for the geogrid test section at each staged load.

Table 3.12: Vertical normal strain versus depth measurements for each staged load applied to the geotextile reinforced test section

	Geotextile Reinforced Test Section				
	Vertical Normal Strain (%)				
Depth from Surface (in)	GF=600 lb	GF=2700 lb	GF=4700 lb	GF=5800 lb	GF=6300 lb
6	0.0016	0.0105	0.0247	0.0402	0.0489
10.5	0.0016	0.0105	0.0247	0.0402	0.0489
15	0.00135	0.0084	0.01955	0.0324	0.0399
19.5	0.0011	0.0063	0.0144	0.0246	0.0309
24	0.000893	0.00505	0.0117	0.01985	0.0251
28.5	0.000685	0.0038	0.009	0.0151	0.0193
33	0.000685	0.0038	0.009	0.0151	0.0193

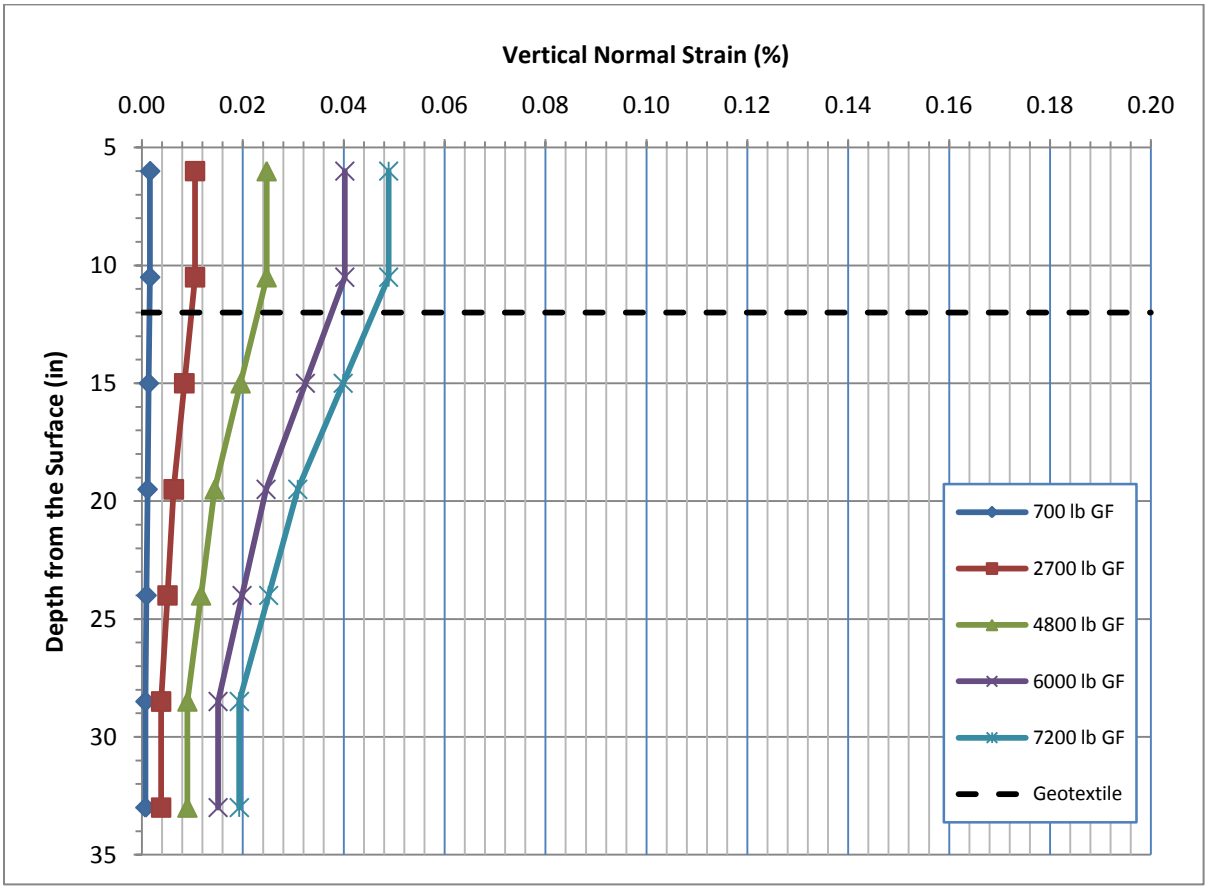

Figure 3.39: Vertical normal strain versus depth for the geotextile test section at each staged load.

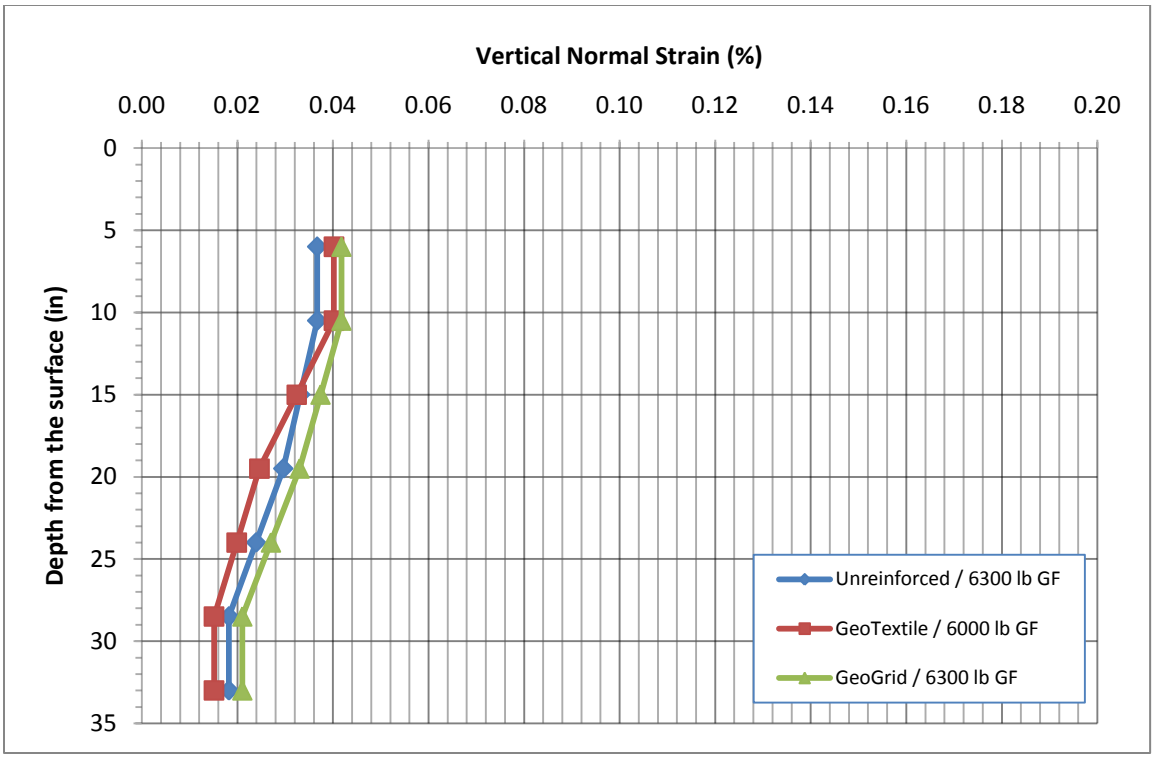

Figure 3.40: Comparison of vertical normal strain versus depth at the ground force nearest to 6300 lbs in each test section.

The maximum forces applied to the unreinforced, geogrid reinforced, and geotextile reinforced test sections were 6300 lbs, 6300 lbs, and 6000 lbs, respectively. So, the compressive force applied to the geotextile section was approximately 300 lbs (5%) less than the force applied to the unreinforced and geogrid sections.

In order to compare the relative results for all three test sections, the vertical strains in the geotextile reinforced test sections were normalized to the strains expected at an equivalent reference ground force (RGF) of 6300 lbs (i.e. the force applied to the unreinforced and geogrid reinforced test sections). Table 3.13 tabulates the in-situ vertical strains for the applied ground force nearest 6300 lbs along with the vertical strains adjusted to an equivalent reference ground force of 6300 lbs. This adjustment only affected the strains from the geotextile section as the

Table 3.13: Vertical normal strains from the applied ground force (GF) nearest to 6300 lbs for each test section along with the vertical normal strains adjusted to the reference ground force (RGF) of 6300 lbs

	Vertical Normal Strain (%)			
	Unreinforced	Geogrid	Geotextile	
Depth (in)	GF=6300 lb	GF=6300 lb	GF=6000 lb	RGF=6300 lb
6	0.0367	0.0418	0.0402	0.0422
10.5	0.0367	0.0418	0.0402	0.0422
15	0.03315	0.0374	0.0324	0.0340
19.5	0.0296	0.033	0.0246	0.0258
24	0.0239	0.027	0.01985	0.0208
28.5	0.0182	0.021	0.0151	0.0159
33	0.0182	0.021	0.0151	0.0159

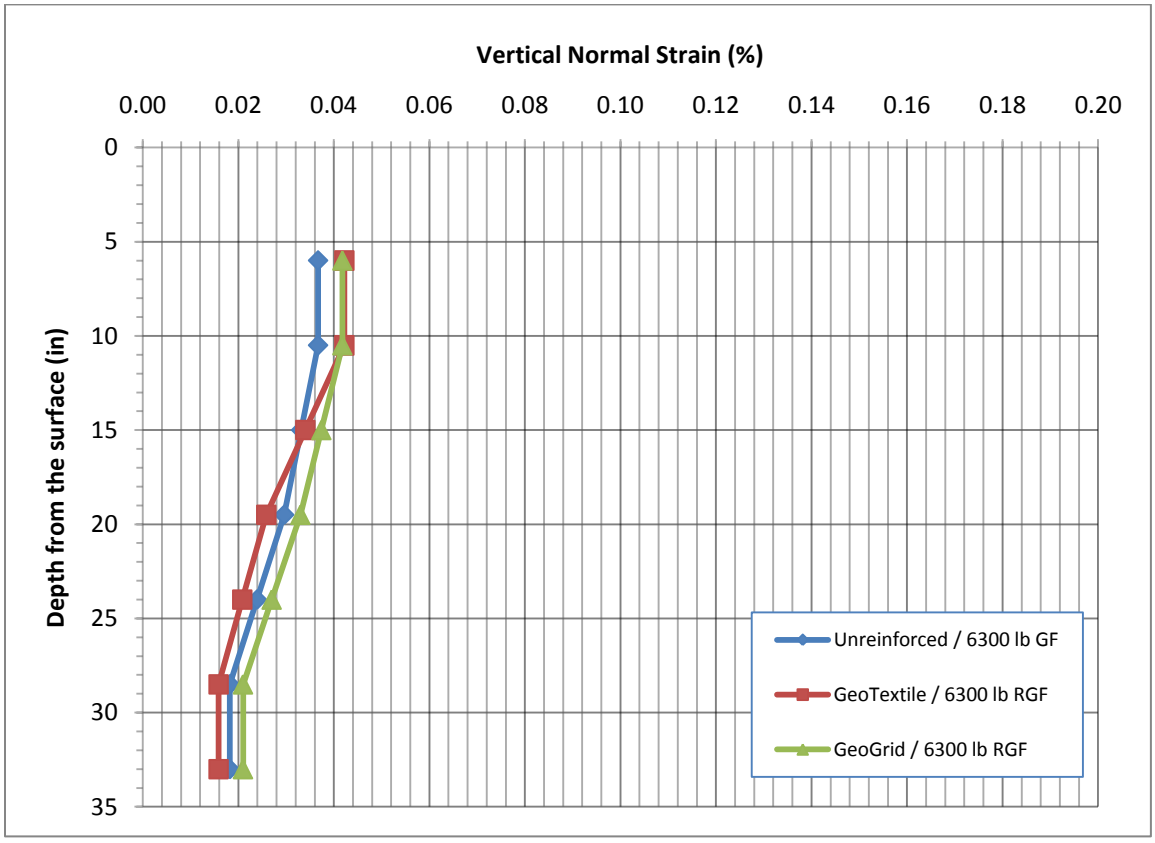

Figure 3.41: Comparison of vertical normal stain versus depth in each test section after adjusting all strains to a reference ground force (RGF) of 6300 lbs.

other two sections had a ground force equal to 6300 lbs. The vertical strain versus depth information for the RGF of 6300 lb is shown Figure 3.41. The strain adjustment to account for differences in applied force level did not significantly change the curves or the overall trends. The trend observed in Figure 3.41 for vertical normal strain versus depth is slightly different than that of shear strain versus depth. Figure 3.41 shows that the geogrid test section still has slightly higher vertical normal strains than the unreinforced test section at all depths; however, the geotextile test section has slightly higher vertical normal strains near the surface, but at the depth of the geotextile the vertical normal strain becomes less than that of the unreinforced section. However, these differences are minimal and for all intents and purposes might reasonably be assumed to be equal. Therefore, at these strain levels, the introduction of geosynthetic reinforcement does not alter the vertical strain distribution within the test section during dynamic loading. However, as mentioned above in regards to shear strain distribution, it is likely that the geosynthetic reinforcement was not mobilized during testing. The magnitudes of shear and vertical normal strain needed to mobilize a contribution from the geotextile reinforcement was not determined from this particular set of tests, but is believe to be quite high. This is consistent with observations from the literature by Giroud and Noiray (1980) and Gabr and Hart (1996).

3.7 Conclusions

A procedure for measurement of in-situ dynamic shear and vertical normal strains as a function of depth during dynamic surface loading was presented in this chapter. The ability to measure dynamic strains induced in geosynthetic-soil systems is critical to understanding the strain distribution as a function of depth within these systems. The results from the small-strain dynamic load tests performed in this study indicate that the presence of geosynthetic

reinforcement (either geogrid or geotextile) does not significantly impact the shear strain or vertical normal strain distribution relative to an unreinforced control section for the magnitudes of surface shear and compressive loads applied to the soil surface. However, the shear and vertical normal strains induced in these tests were sufficiently small (less than 0.2% and 0.05%, respectively) that the contribution from the geosynthetic reinforcement was likely not mobilized. Although this observation was not entirely unexpected, as previous studies indicate that significant displacements are required to mobilize tension in the geogrid, it was surprising that a load spreading mechanism or a lateral constrain mechanism was not revealed in the strain distribution data.

Chapter 4

4.0 Accelerated Dynamic Deflectometer (ADD) Test

4.1 Overview

This chapter presents a description of the testing approach and results from large-strain surface loading tests conducted on a new set of geosynthetic reinforced test sections constructed at the Engineering Research Center (ERC) at the University of Arkansas. This test is referred to as the "Accelerated Dynamic Deflectometer (ADD)" test. In essence, the ADD test is a cyclic plate load test in which dynamic measurements of surface deformations are made at different distances from the loading footprint. The test is "accelerated" because it applies several thousand cycles of load in a short period of time due to the higher frequency of loading. The test is "dynamic" because the dynamic response of the surface deformation is recorded after various cycles of load are applied. Finally the test is a "deflectometer" because the surface deflections are measured with distance away from the loading footprint, similar to the Falling Weight Deflectometer (FWD).

ADD tests were performed on unreinforced, geotextile reinforced, and geogrid reinforced test sections as a means to evaluate the structural performance (i.e., surface deflection) of soil layers subject to several thousand cycles of load. Permanent deformations at the soil surface and within the soil mass are expected when the magnitude of the cyclic load leads to strain values greater than the cyclic threshold strain. Accordingly, in-situ strain measurements such as those described in Chapter 3 were not possible when performing ADD tests because the locations of the sensors could not be verified as a function of number of loading cycles due to permanent displacements. This chapter describes the material properties, test section construction, experimental setup, data collection, and data analysis of the ADD tests.

4.2 Material Properties

4.2.1 Sand

The same type of poorly-graded and (SP) used for the test sections described in Chapter 3 was also used for ADD testing. However, different from the test sections described in Chapter 3, the SP was used as a sub-base material, and was overlain by a compacted base course aggregate layer.

4.2.2 Class 7 Base Course Aggregate (SB2)

The base course aggregate used in the test sections described in this chapter is a Class 7 base course aggregate typically used by the Arkansas State Highway and Transportation Department (AHTD). It is locally referred to as SB2 (special base 2). The sieve analysis results for SB2 are provided in Table 4.1 and the grain-size distribution curve is shown in Figure 4.1. According to the American Association of State Highway and Transportation Officials (AASHTO), the Class 7 base course aggregate is classified as an A-1-a soil. The Unified Soil Classification System (USCS) classifies it as well-graded gravel (GW). Modified Proctor tests performed according to ASTM T-180 (Method D) yield a maximum dry unit weight of approximately 140 pcf at an optimum water content of 5.5%.

4.2.3 Geosynthetics

The same geosynthetic materials used the in-situ strain tests discussed in Chapter 3, Mirafi® BXG12 (geogrid) and Mirafi® HP570 (geotextile), were also used in the test sections constructed for ADD testing.

Table 4.1: Sieve analysis data for the Class 7 base course aggregate used in this project

Sieve No.	Sieve Size (mm)	Percent Passed (%)
1.5"	38.1	100
1"	25.4	95
.75"	19.95	85
.5"	12.7	67
.375"	9.525	57
#4	4.750	40
#10	2.000	27
#40	0.425	15
#200	0.075	9.4

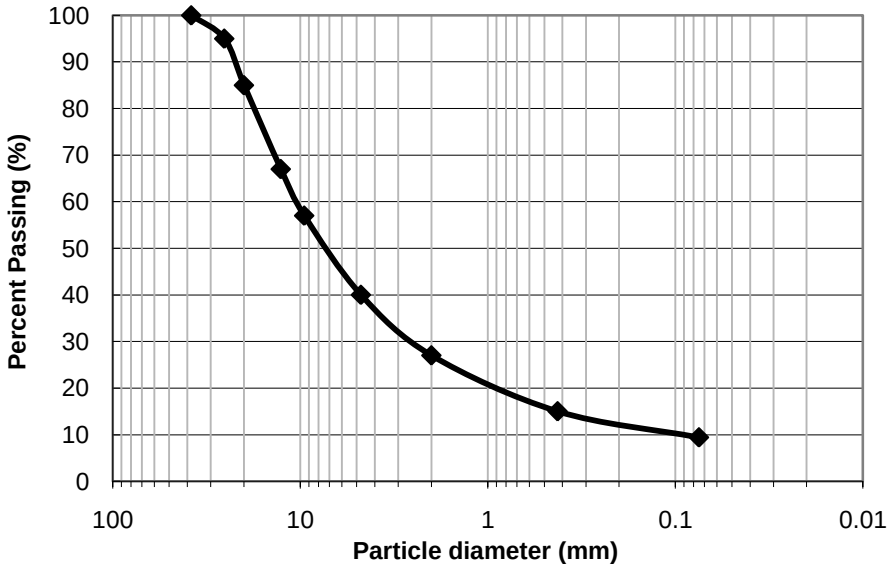

Figure 4.1: Grain-size distribution curve for the Class 7 base course aggregate used in this project.

4.3 Test Section Construction

The same geosynthetic-lined test pit at the University of Arkansas' Engineering Research Center (ERC) used for the in-situ strain tests described in Chapter 3 was also used for the ADD tests. The geotextile liner, sump pump, and 8 inch pea gravel layer were left in place from the in-situ strain testing. All three test sections were built identical to one another, except for the placement of the geosynthetic reinforcement. A schematic of the unreinforced test section is

shown in Figure 4.2. After re-compaction of the gravel layer, five sand layers were placed and compacted with the vibratory plate compactor to achieve 6-inch lifts, as shown in Figure 4.3.

Quality control was performed during construction to ensure that each test section was constructed in a similar manner. A Troxler® nuclear density gauge was used to measure the unit weight and water content of the fifth sand layer and the Class 7 base course layer in each test section (refer to Figure 4.4 and Figure 4.6). The nuclear density gage readings for dry unit weight and water content for each test section are tabulated in Table 4.2. The average dry unit weight of the sand for all three sections was 105.4 pcf with a standard deviation of 0.6 pcf, and the average water content for the sand was 3.2 % with a standard deviation of 0.4 %.

A total of 10 inches of compacted Class 7 base course aggregate was placed on top of the sand. A four-inch lift was placed first, and then an additional six-inch lift was added. Each base course lift was compacted with a Whacker Packer compactor, as shown in Figure 4.5. The reason for placing the base course in a four-, and then a six-inch lift, had to do with the placement of the geosynthetic reinforcement and will be discussed in Section 4.3.1. Similar to the compacted sand layers, the nuclear gauge was used to measure the dry unit weight and water content of the compacted base course layer. The dry unit weights of the compacted base course in each test section varied from 125.3 pcf for the geogrid reinforced section to 131.7 pcf for the unreinforced section (a total maximum difference of less than 5%). Given the Modified Proctor maximum dry unit weight of approximately 140 pcf for this material, the dry unit weights for all sections fell within 90 – 94% relative compaction as it was difficult to achieve 95% compaction with the Whacker Packer. The water content measurements for the base were all very similar and averaged 5% (very near optimum) with a standard deviation of 0.2 %.

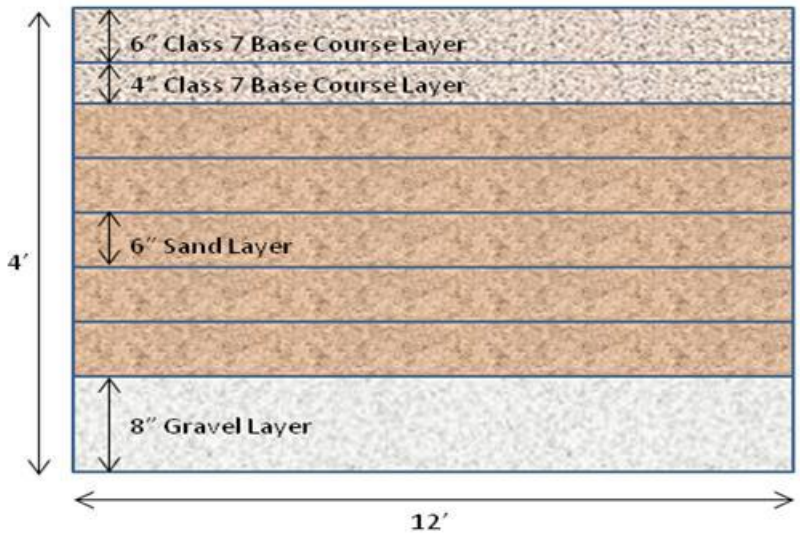

Figure 4.2: Schematic of the unreinforced test section.

Figure 4.3: Compacting 6” sand lifts with the vibratory plate compactor.

Figure 4.4: Nuclear density reading on the sand layer.

Figure 4.5: Compacting Class 7 base course layer with the whacker packer.

Figure 4.6: Nuclear density reading on the Class 7 base course layer.

Table 4.2: Nuclear density reading for the sand and Class 7 base course in each test section

	Sand (SP)		Class 7 Base Course	
	Dry Density(pcf)	Water Content(%)	Dry Density(pcf)	Water Content(%)
Geogrid	105	3.2	125.3	5.2
Geotextile	105.2	3.6	130.5	5
Unreinforced	106.1	2.8	131.7	4.8
Average	105.4	3.2	129.2	5.0
Standard Deviation	0.6	0.4	3.4	0.2

4.3.1 Geosynthetic Placement

The geosynthetic reinforcement was placed at different locations depending on the geosynthetic type. In the geogrid reinforced test section, the geogrid was placed six inches from the top of the test section within the Class 7 base course aggregate layer, as shown in Figure 4.7. In the geotextile reinforced test section, the geotextile was placed at the interface between the Class 7 base course aggregate layer and the sand layer, as shown in Figure 4.8. The actual placement of the geogrid within the test section is shown in Figure 4.9, while the actual placement of the geotextile within the test section is shown in Figure 4.10. The location for each geosynthetic type was chosen based on previous research that concludes that the performance of the geotextile reinforcement is best when placed at the interface between the base and sub-base layer and that the performance of the geogrid reinforcement is best when placed in the base course layer (Perkins 1999, Barksdale et al 1989, Haas et al 1988). During installation, care was taken to guarantee that the geosynthetic material was pulled tight and no wrinkles were present.

4.4 Experimental Setup

A schematic of the ADD test setup is shown in Figure 4.11. Additional background information regarding the experimental ADD test setup may be found in Cox et al. (2010).

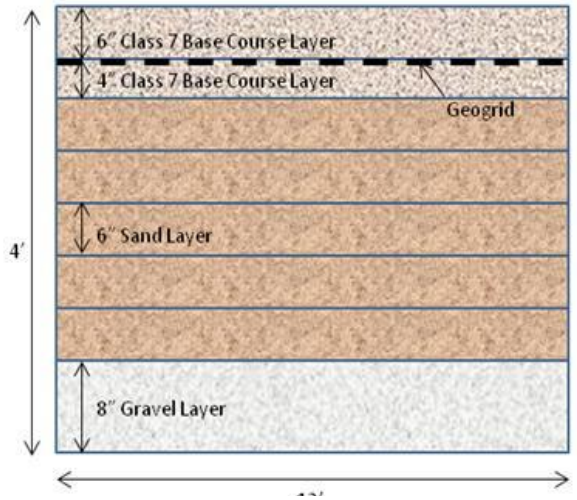

Figure 4.7: Location of geogrid reinforcement.

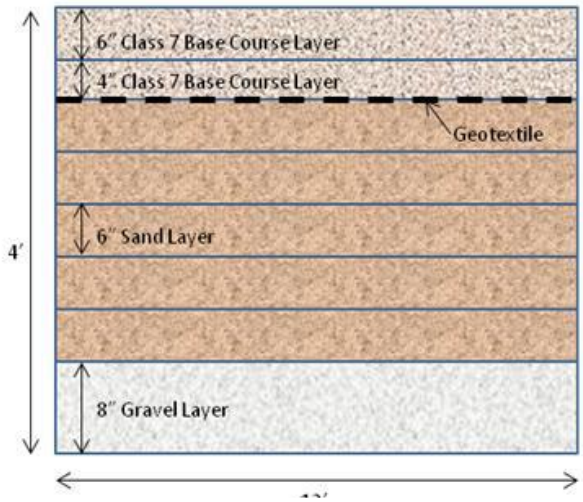

Figure 4.8: Location of geotextile reinforcement.

Figure 4.9: Placement of the geogrid in the test section.

Figure 4.10: Placement of the geotextile in the test section.

During ADD tests, the oscillating mass of the Vibroseis truck was oriented in the vertical direction in order to apply cyclic vertical loads to the test sections. The loads were applied to the surface of the test section through a wooden rectangular footing measuring 10 inches wide by 20 inches long. This loading footprint was chosen to simulate a standard dual-tire area of 200 square inches, as recommended in the AASHTO LRFD Bridge Design Specifications (2007). A load cell was placed between the footing and the base plate of the Vibroseis truck to monitor the static and dynamic loads during testing, and to maintain a constant force level using a force-feedback

loop. A 14 ft-long aluminum support frame was used to suspend nine linear variable deformation transformers (LVDTs) above the test section. The support feet for the aluminum frame were placed beyond the zone of influence created by dynamic loading on the test section. The LVDTs were used to measure the dynamic and permanent surface deflection basins as a function of number of loading cycles applied to the test section. The LVDTs were placed at the following distances from the center of the applied load: 0, 8, 12, 18, 24, 36, 48, 60, and 72 inches, as shown in Figure 4.11. A hole slightly larger than the diameter of the LVDT was cut into the center of the footing in order to measure deformation at the location of the applied load (i.e. 0 inches). Once the LVDTs were in place, and before any applied load, an initial reading for each LVDT was obtained to establish the baseline. This was done because the stroke on each LVDT was set independently, depending on its location relative to the footprint. For example, the LVDT at the center of the applied load was set so that it could record a significant amount of deflection; however, the LVDT's placed at 18 and 24 inches from the applied load were set to record heave.

4.4.1 Test Section Loading

The base plate of the Vibroseis truck was lowered onto the load cell until reaching a static hold-down force of approximately 5,000 lbs. Then, an average peak dynamic compressive force of 5,000 lbs was applied to the test section at a frequency of 50 Hz. This total static and dynamic downward force applied to the surface (i.e. approximately 10,000 lbs) is similar to half an ESAL applied to a dual-tire footprint. A frequency of 50 Hz was used in order to determine the deflection behavior of the test section after 100,000 loading cycles in approximately 34 minutes. The load cell between the footing and the base plate of the Vibroseis truck monitored the average static and dynamic loads applied to the test section during testing. A typical load pattern as a function of number of loading cycles is shown in Figure 4.12. There is some variation in the

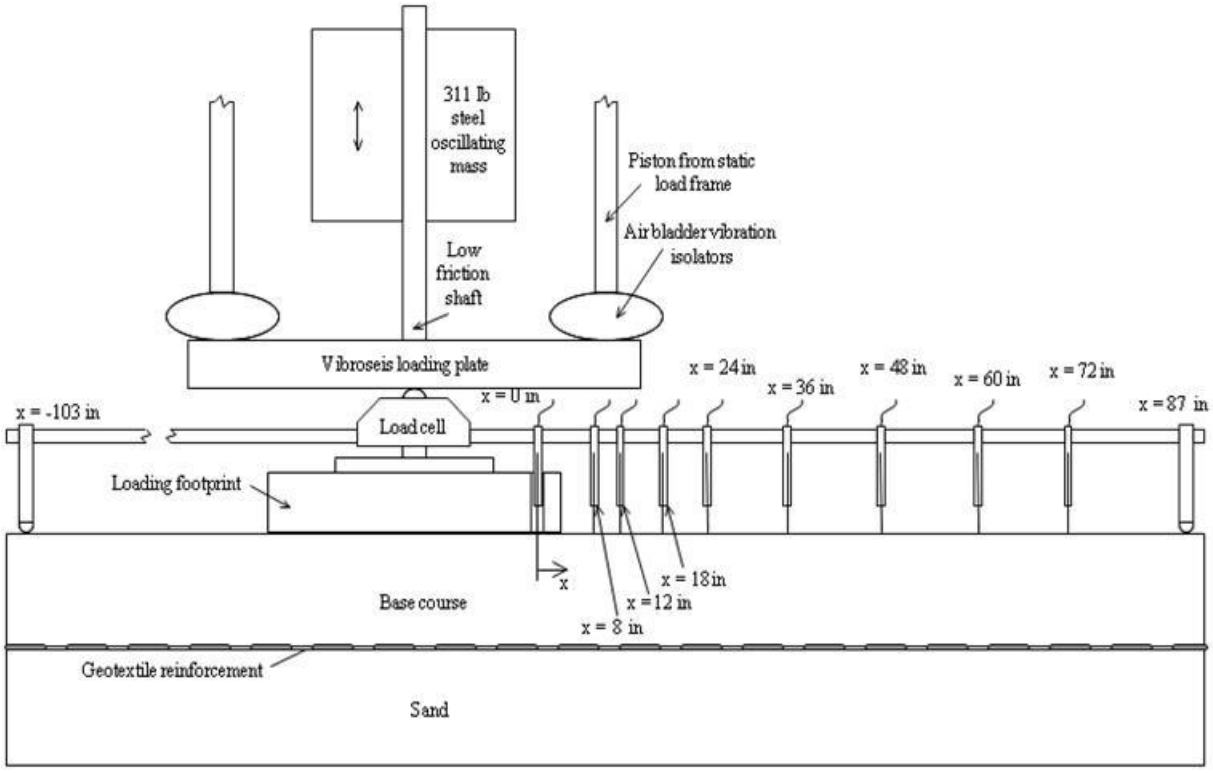

Figure 4.11: Schematic of the ADD test setup with surface deflection measurements (Cox et al. 2010).

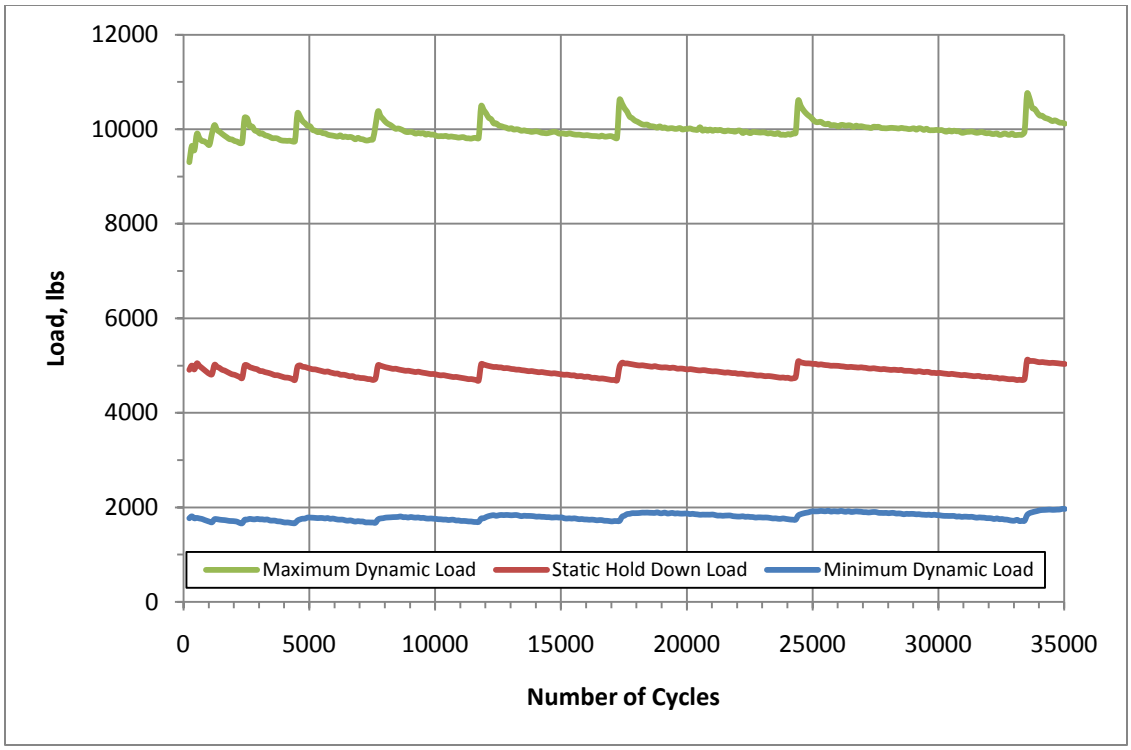

Figure 4.12: Load as a function of number of cycles applied to the geogrid reinforced test section.

force levels, but the maximum dynamic force is essentially 10,000 lbs throughout the duration of the test. The minimum dynamic force is slightly less than 2,000 lbs (upward dynamic force added to static hold-down force), and the average (static hold-down) force remained approximately 5,000 lbs throughout the test. Each test section was monitored closely during testing, as shown in Figure 4.13, to make sure that the LVDTs were not touching the footing or deflecting outside of their linear range of deformation. The output signal of each LVDT was also monitored, using the same 32-channel data acquisition system explained in Section 3.4.3, in order to verify that none of the LVDTs were out of their linear range and that no problems were encountered during testing, as shown in Figure 4.14. Although the intention was to load each test section for 34 minutes, or 100,000 cycles, each test section was stopped after different numbers of loading cycles because some of the LVDTs were reaching the end of their linear range. Specifically, the dynamic loading cycles of the unreinforced, geotextile reinforced, and geogrid reinforced test sections were stopped at 75,000 cycles, 50,000 cycles, and 35,000 cycles, respectively. Therefore, the relative surface deflection of each test section will be compared only up to 30,000 cycles of dynamic load.

4.5 Results

During dynamic loading of each test section, nearly an inch of permanent deformation was measured at the LVDT placed directly under the dual-tire loading footprint. The permanent surface deformations of the geogrid reinforced test section are shown as a function of number of loading cycles for all nine LVDTs in Figure 4.15. The LVDT placed directly under the applied load (i.e. LVDT at 0 in) has the most deflection (i.e., negative deformation) as indicated in Figure 4.15. The LVDTs placed 8 and 12 inches from the applied load have the next greatest amounts of deflection. The remaining LVDTs placed at distances greater than 12 inches all

Figure 4.13: Monitoring the deformation of the test section during loading.

Figure 4.14: Monitoring the LVDTs output signals during loading.

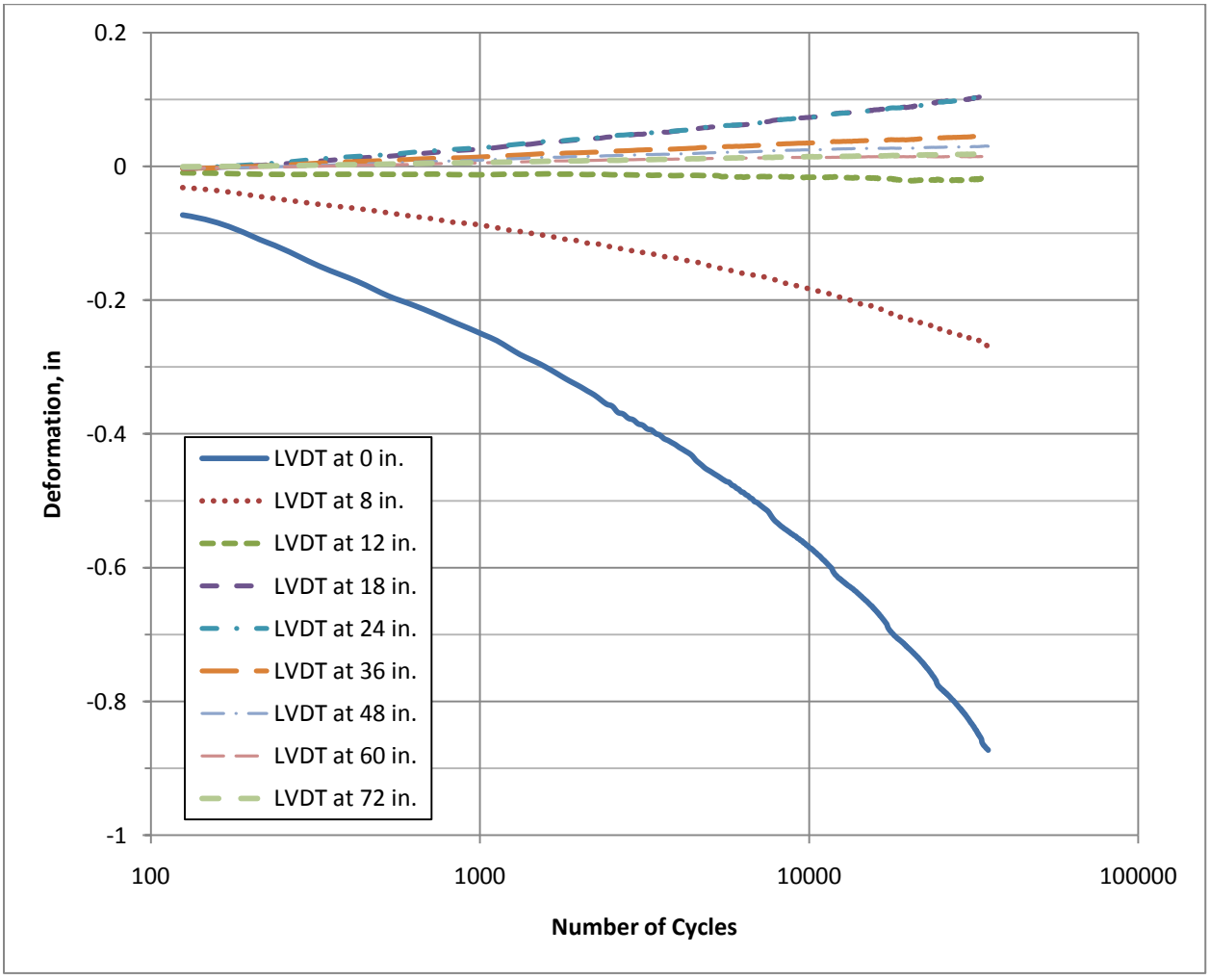

Figure 4.15: Surface deflection as a function of number of loading cycles applied to the geogrid reinforced test section.

measured slight heave (i.e. positive deformation) rather than settlement. Figures 4.16, 4.17, and 4.18 show the unreinforced, geotextile reinforced, and geogrid reinforced test section surface deflection basins for the static hold down load and 1,000 cycles, 5,000 cycles, 10,000 cycles,20,000 cycles, and 30,000 cycles of dynamic loading. These three figures show that surface deflections only occur up to distances of approximately 12 inches from the center of the applied load. At distances greater than 12 inches, the test sections all tended to heave until a distance of approximately 48 inches from the center of the applied load. The LVDTs placed greater than 48 inches from the center of the applied load showed very little deformation (either settlement or heave) during the first 5,000 cycles applied to the test section and then no additional changes in deformation after 5,000 cycles. This same pattern is observed for all three test sections in Figures 4.16, 4.17, and 4.18. The deflections measured at each LVDT as a function of the number of loading cycles applied to each test section can be found in Tables 4.3, 4.4, and 4.5 for the unreinforced, geotextile reinforced, and geogrid reinforced test sections, respectively.

In order to directly compare the deflection measurements for each test section, the surface deflection basins are plotted together for the static hold-down load and 1,000 cycles, 5,000 cycles, 10,000 cycles, 20,000 cycles, and 30,000 cycles of dynamic loading in Figures 4.19 - 4.24, respectively. As shown in Figure 4.19, all three test sections essentially deflected the same amount under the static hold-down force of 5,000 lbs. At 1,000 cycles of dynamic load (Figure 4.20), all three test sections are once again nearly identical having a maximum deflection of 0.25 inches at the location of the applied load and a small amount of heave beginning to develop between 12 and 24 inches. At 5,000 cycles of dynamic load (Figure 4.21), the deflections in the three test sections remain very similar with a maximum deflection near 0.50 inches at the

Table 4.3: Deflection of the unreinforced test section at specified distances from the loading footprint up to 30,000 cycles of dynamic load

	Deflection (in)								
Distance from Loading Footprint (in)	**0**	**8**	**12**	**18**	**24**	**36**	**48**	**60**	**72**
Static Load	-0.0235	-0.0051	-0.0004	-0.0006	-0.0011	-0.0007	-0.0003	-0.0001	-0.0001
1000 Cycles	-0.2566	-0.0490	0.0172	0.0448	0.0326	0.0083	0.0003	-0.0047	-0.0019
5000 Cycles	-0.4246	-0.0806	0.0346	0.0914	0.0717	0.0216	0.0086	-0.0034	-0.0004
10000 Cycles	-0.5564	-0.1080	0.0420	0.1234	0.1002	0.0327	0.0146	-0.0016	0.0008
20000 Cycles	-0.7288	-0.1461	0.0494	0.1586	0.1331	0.0434	0.0202	0.0011	0.0018
30000 Cycles	-0.8246	-0.1676	0.0526	0.1731	0.1470	0.0463	0.0210	0.0016	0.0023

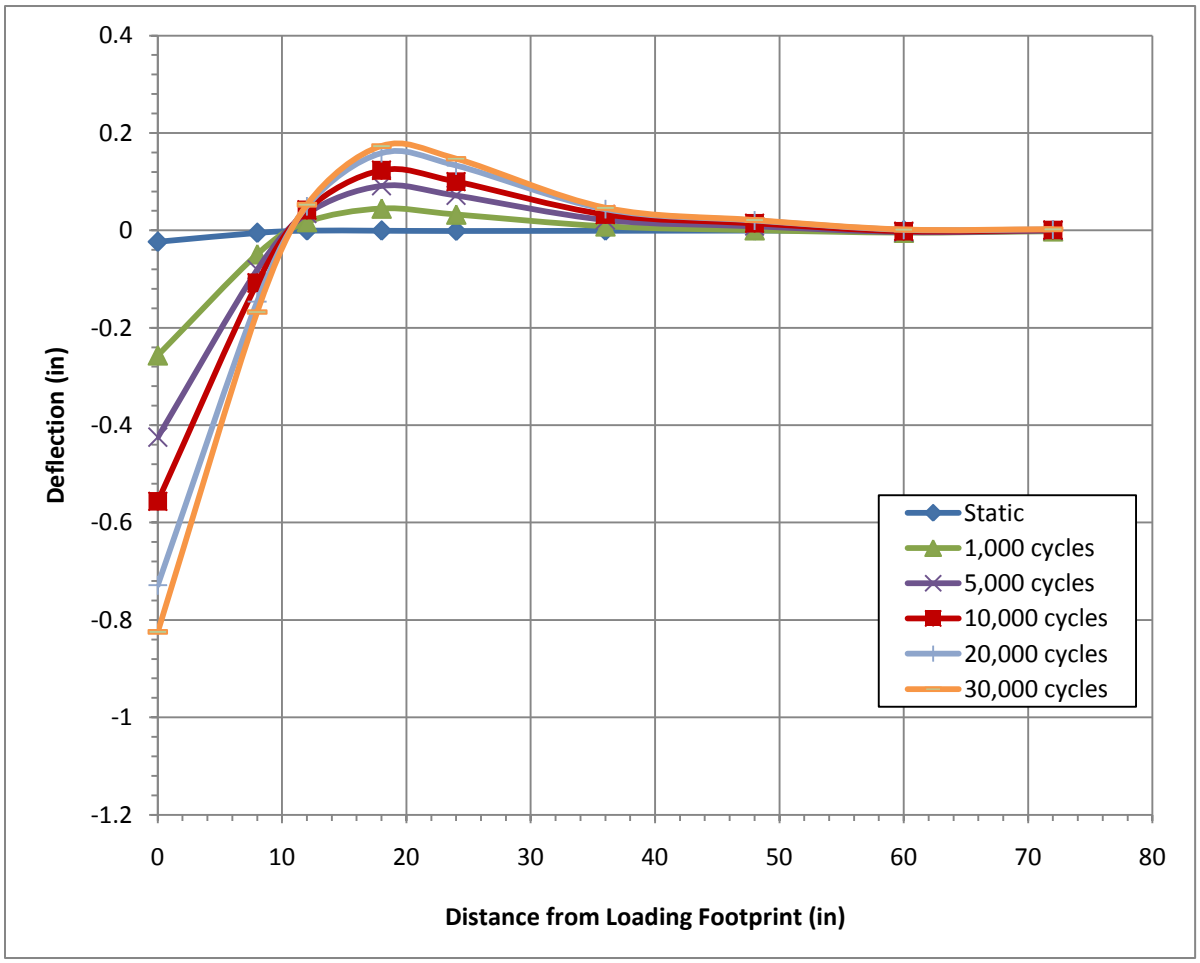

Figure 4.16: Unreinforced test section permanent deflection basins as a function of number of cycles.

Table 4.4: Deflection of the geotextile reinforced test section at specified distances from the loading footprint up to 30,000 cycles of dynamic load

	Deflection (in)								
Distance from Loading Footprint (in)	**0**	**8**	**12**	**18**	**24**	**36**	**48**	**60**	**72**
Static Load	-0.0410	-0.0102	-0.0064	-0.0049	-0.0045	-0.0038	-0.0030	-0.0021	-0.0009
1000 Cycles	-0.2434	-0.0493	0.0002	0.0306	0.0181	0.0041	0.0126	0.0071	0.0189
5000 Cycles	-0.4793	-0.1137	0.0271	0.0763	0.0470	0.0244	0.0297	0.0198	0.0340
10000 Cycles	-0.6745	-0.1993	0.0395	0.0977	0.0607	0.0321	0.0328	0.0235	0.0365
20000 Cycles	-0.8844	-0.3045	0.0425	0.1089	0.0656	0.0323	0.0319	0.0235	0.0362
30000 Cycles	-1.0316	-0.4105	0.0453	0.1187	0.0730	0.0337	0.0319	0.0235	0.0363

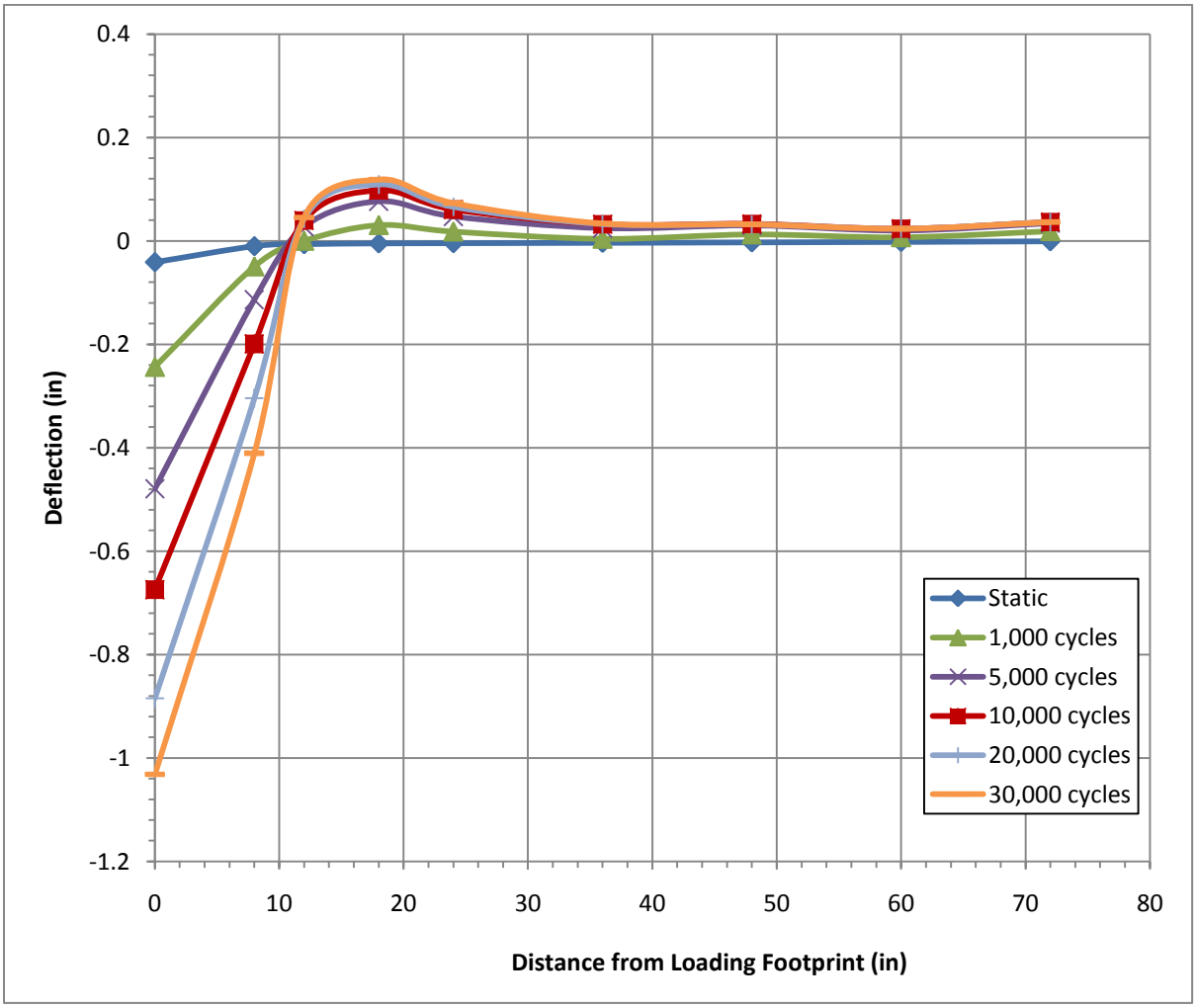

Figure 4.17: Geotextile test section permanent deflection basins as a function of number of cycles.

Table 4.5: Deflection of the geogrid reinforced test section at specified distances from the loading footprint up to 30,000 cycles of dynamic load

	Deflection (in)								
Distance from Loading Footprint (in)	**0**	**8**	**12**	**18**	**24**	**36**	**48**	**60**	**72**
Static Load	-0.0223	-0.0067	0.0002	0.0005	-0.0001	-0.0004	-0.0002	-0.0001	0.0000
1000 Cycles	-0.2420	-0.0793	-0.0047	0.0332	0.0330	0.0157	0.0112	0.0069	0.0070
5000 Cycles	-0.4473	-0.1393	-0.0067	0.0658	0.0644	0.0303	0.0216	0.0133	0.0134
10000 Cycles	-0.5612	-0.1739	-0.0095	0.0804	0.0787	0.0366	0.0257	0.0146	0.0160
20000 Cycles	-0.7118	-0.2207	-0.0146	0.0955	0.0936	0.0415	0.0280	0.0155	0.0178
30000 Cycles	-0.8138	-0.2458	-0.0132	0.1073	0.1054	0.0456	0.0299	0.0157	0.0192

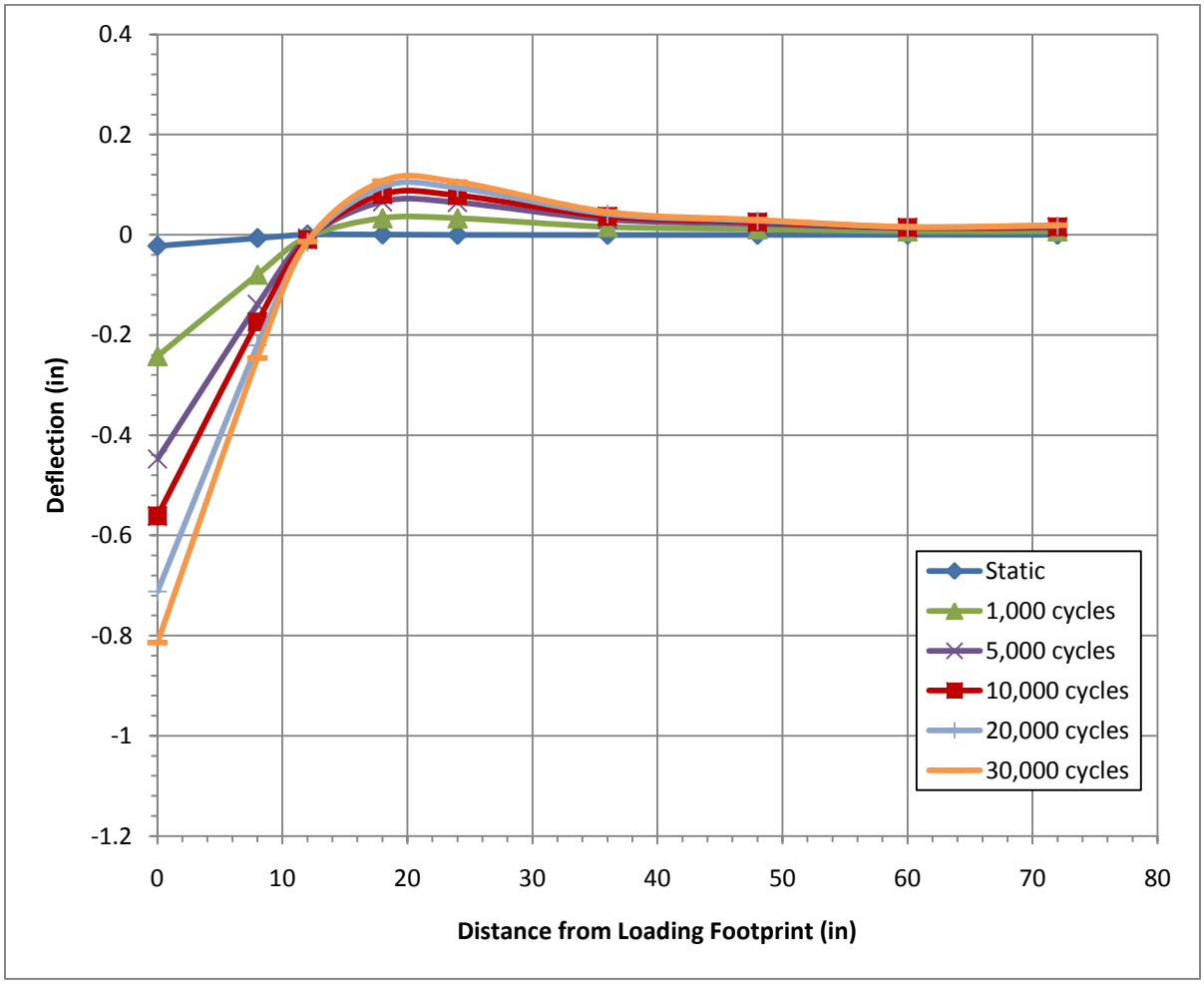

Figure 4.18: Geogrid test section permanent deflection basins as a function of number of cycles.

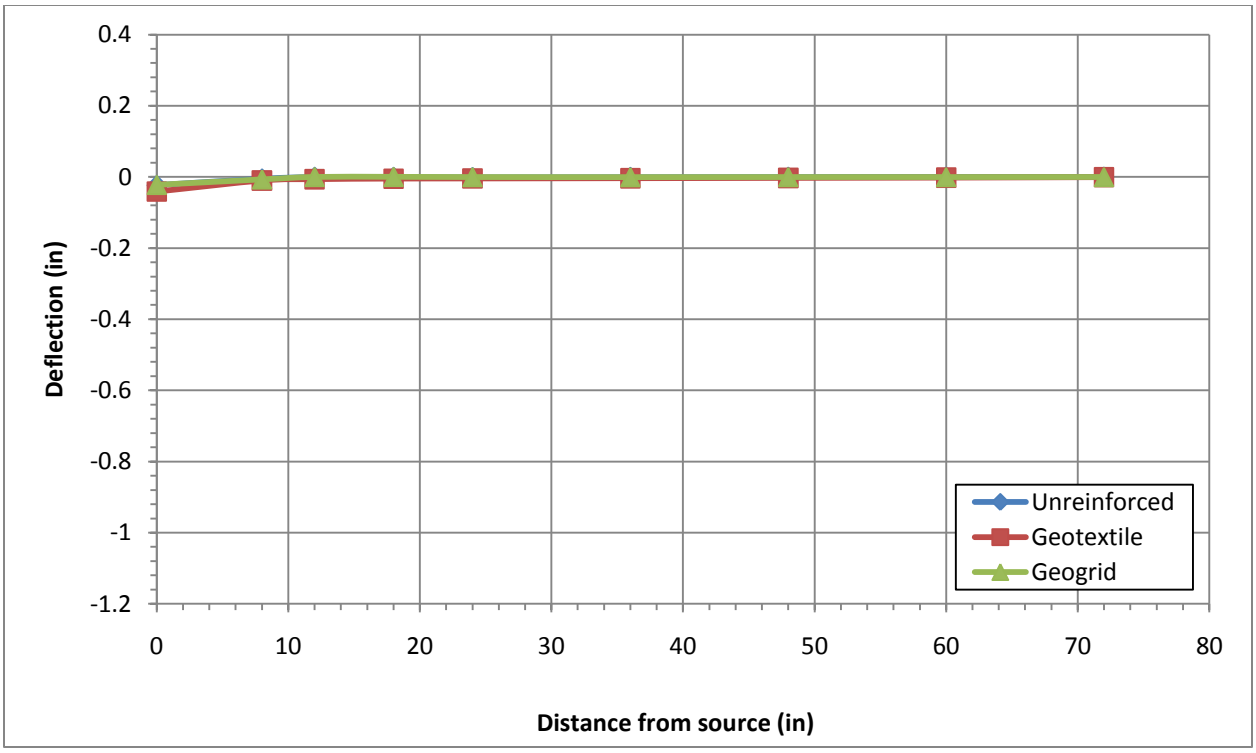

Figure 4.19: Initial permanent surface deflection basin for each test section after the static hold-down force was applied.

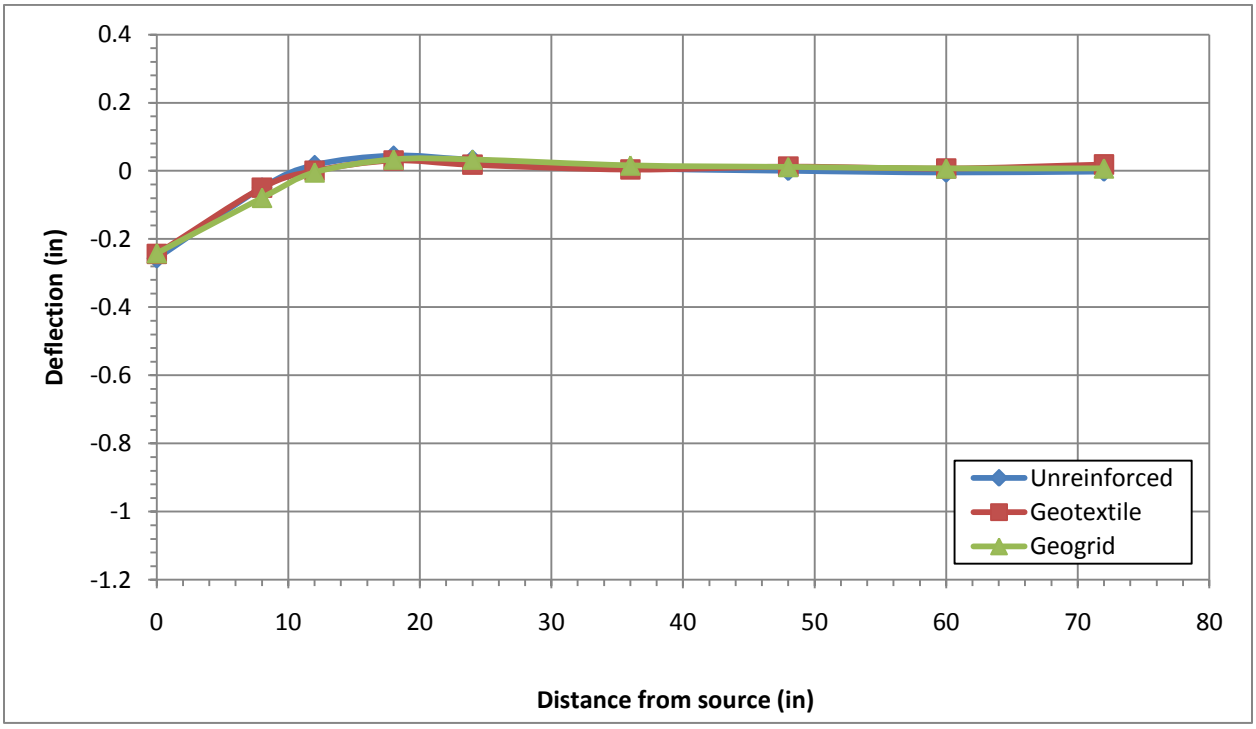

Figure 4.20: Final permanent surface deflection basin for each test section after 1,000 cycles of dynamic load.

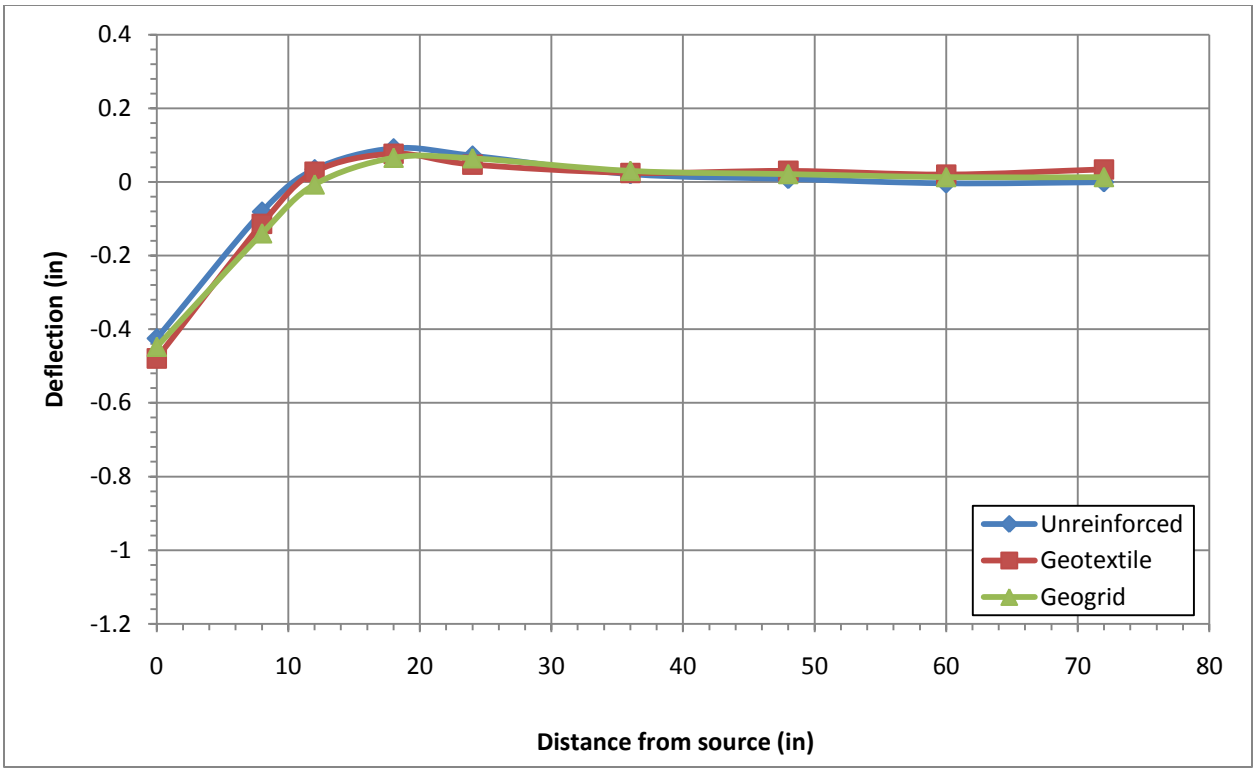

Figure 4.21: Permanent surface deflection basin for each test section after 5,000 cycles of dynamic load.

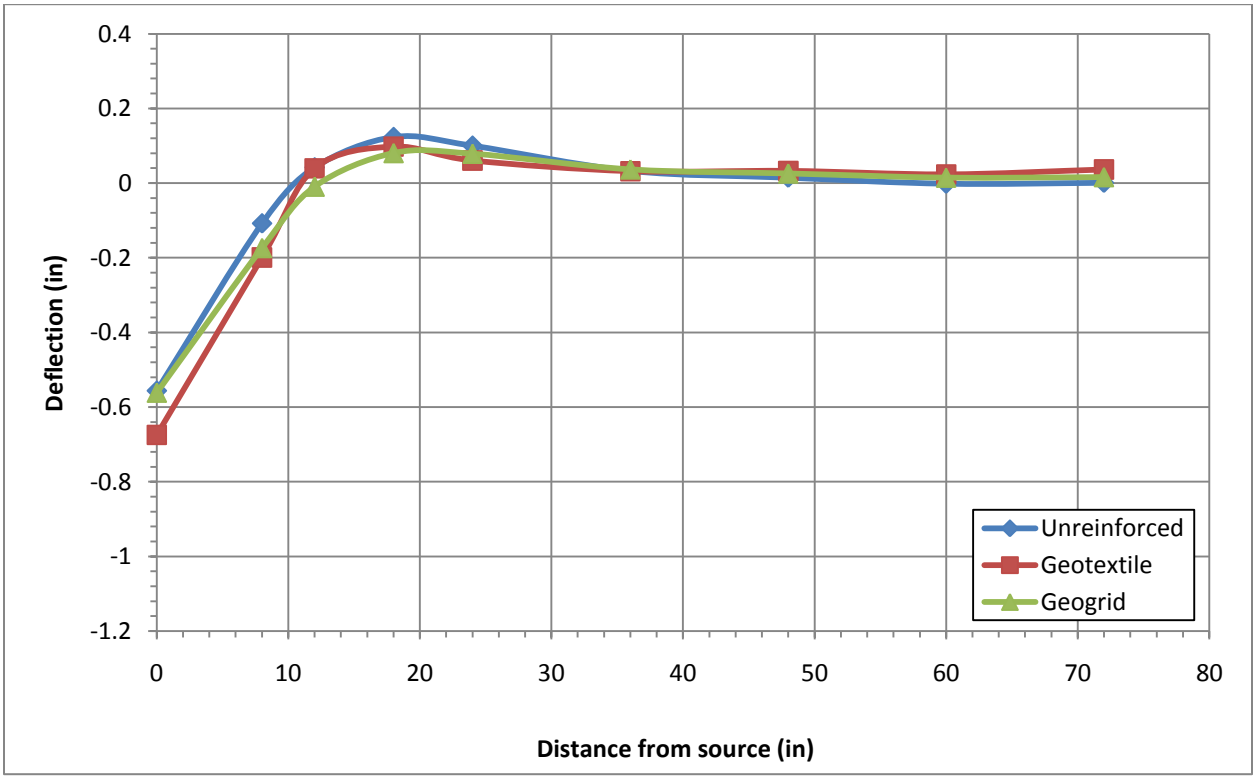

Figure 4.22: Permanent surface deflection basin for each test section after 10,000 cycles of dynamic load.

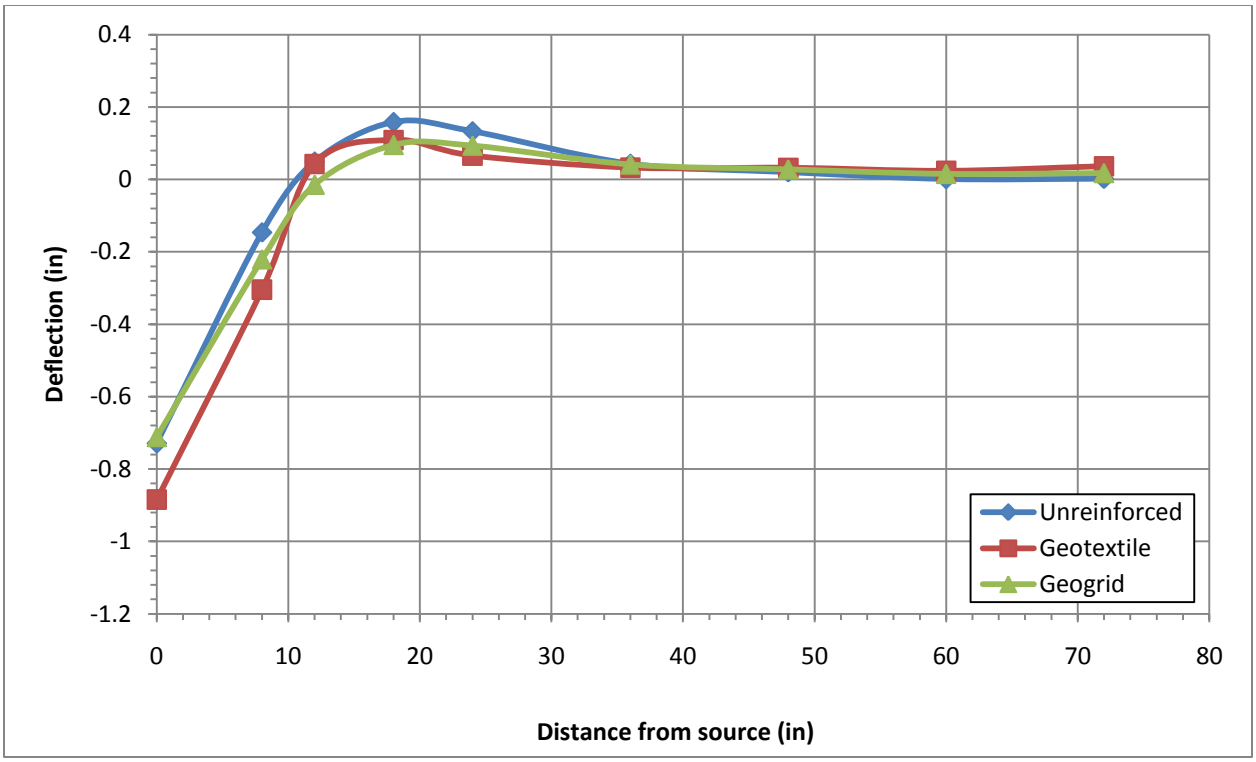

Figure 4.23: Permanent surface deflection basin for each test section after 20,000 cycles of dynamic load.

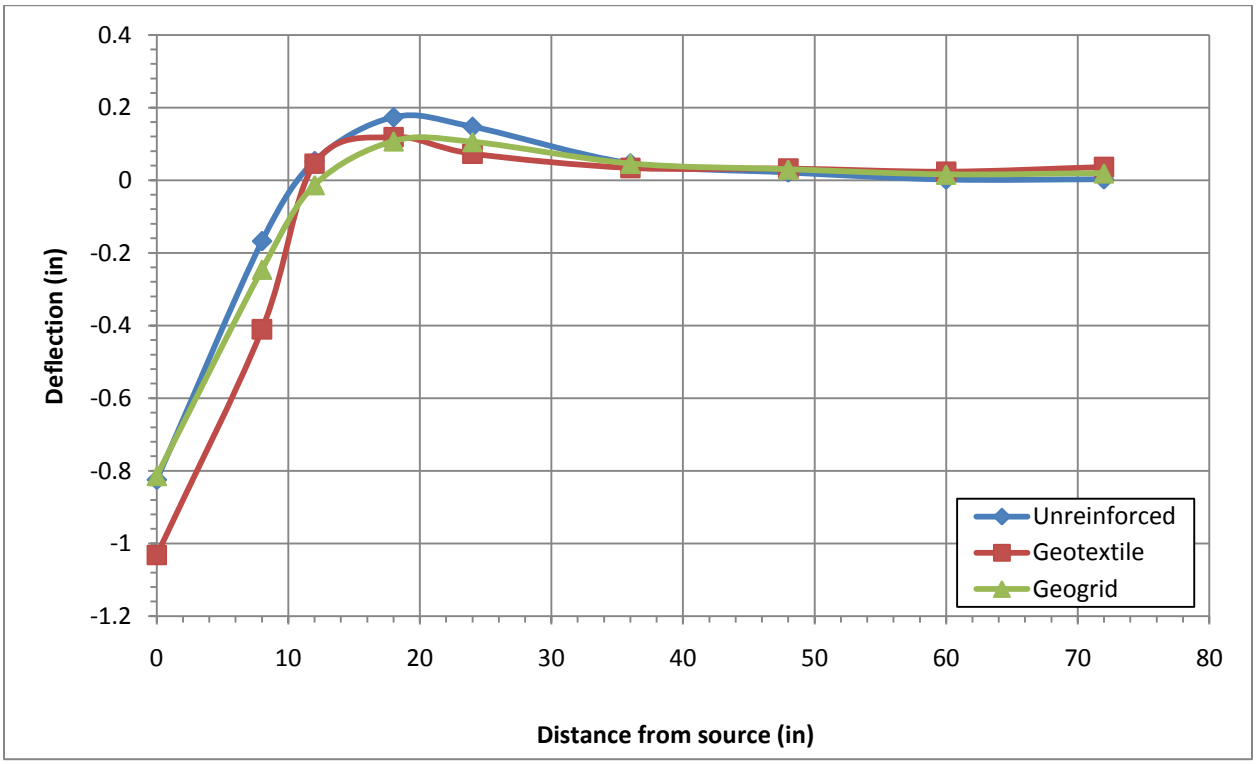

Figure 4.24: Permanent surface deflection basin for each test section after 30,000 cycles of dynamic load.

location of the applied load and additional heave between 12 to 36 inches from the center of the applied load. A more noticeable, but unexpected, difference in the three test sections was apparent at the location of the applied load at 10,000 cycles of dynamic loading (Figure 4.22). The maximum deflection of the geotextile reinforced test section was 0.68 inches, whereas the maximum deflections of the geogrid and unreinforced test sections were 0.55 inches. At 20,000 cycles of loading (Figure 4.23) the geotextile reinforced test section continued to experience more deflection at the location of the applied load, while the unreinforced test section began to show slightly higher amounts of heave than the two geosynthetic test sections. At 30,000 cycles of dynamic load (Figure 4.24), the maximum deflection at the location of the applied load reached 0.83 inches, 0.82 inches, and 1.02 inches for the unreinforced, geogrid reinforced, and geotextile reinforced test sections, respectively. The geogrid and the unreinforced test sections performed almost identical at the location of the applied load, but the unreinforced test section had higher amounts of heave at distances between 12 to 36 inches from the applied load. The geotextile section experienced the most surface settlement, while the geogrid section essentially performed similar to the unreinforced section, albeit with slightly less heave. This is contrary to the expected trends. It was expected that the contribution of geosynthetic reinforcement would be visible after surface deflections in the range of 1 inch had been generated.

In order to rule out the possibility that variability in test section construction was partially the cause of these counter-intuitive results, the dry unit weight and water content of each test section was further reviewed (refer to Table 4.2). The unreinforced test section does have the highest dry density of the Class 7 base course aggregate layer of the three test sections, but it is only 1.2 pcf greater than the geotextile reinforced test section and 6.4 pcf greater than the geogrid reinforced test section. These slight differences in dry density of each of the three test

sections are likely insignificant, especially considering all of them are within 90 – 94% Modified Proctor relative compaction (refer to Section 4.3). Furthermore, the greatest difference in dry unit weight is between the unreinforced test section and the geogrid test section; however, the greatest difference in surface deflection is between the unreinforced test section and the geotextile section. Additionally, the water content values of all three test sections are within 0.2% of one another.

After ruling out test section construction bias, the results show that a reduction in surface deflection in the geosynthetic reinforced test sections were not observed during ADD testing. Furthermore, the ADD tests ultimately achieved surface deflections in the range of 1 inch (commonly accepted as failure deformations in pavements). If the contribution of the geosynthetic is not mobilized after a surface deflection of 1.0 inch, the pavement will have already "failed" from a serviceability limit state.

It is possible that the geosynthetic reinforcement may have contributed more to a "weaker" (i.e. less compaction energy or saturated conditions) or a thinner base course layer. However, additional research is needed to quantify the geosynthetic contributions in these situations. Another hypothesis for this lack of geosynthetic contribution in the results could be the manner in which the loads were applied to the test section. Perhaps compressive surface loading does not lead to a state of stress at the depth of the geosynthetic in which the tensile or lateral restraint mechanisms are activated. It is possible that dynamic shear or a rolling/rocking loading could reveal a geosynthetic reinforcement contribution.

4.6 Conclusions

ADD tests were conducted on three different geosynthetic reinforced test sections; namely, an unreinforced test section, a geotextile reinforced test section, and a geogrid reinforced

test section. All three test sections were constructed in a similar manner and consisted of 10 inches of Class 7 base course overlying approximately 30 inches of poorly-graded sand. Surface deflections commonly accepted as indicative of failure (i.e. approximately 1 inch) were developed in each test section after approximately 30,000 cycles of 10,000 lbs peak dynamic load. A reduction in surface deflection due to the presence of geosynthetic reinforcement was not measured during the ADD tests conducted in this research. In conclusion, the geosynthetic reinforcement did not significantly influence the surface deflection performance of test sections at the levels of strain associated with the cyclic load applied to the sections.

Additional studies are necessary to quantify the impact of weaker base course material (i.e., wet conditions) and thinner base course sections. Furthermore, additional studies are required to understand the impact of the type of dynamic loading (compressive, shear, rolling/rocking) and if this influences the results.

Chapter 5

5.0 Conclusions

The research objective of this study was to develop and validate new accelerated testing approaches to characterize large-scale, geosynthetic reinforced pavement models. This report includes a description of the methodology and results from two different types of dynamic tests using a Vibroseis truck as the loading mechanism: (1) relatively small-strain tests (shear strains less than 0.2%) where embedded geophones allowed for measurement of shear and normal strain distribution within the geosynthetic reinforced test sections as a function of depth, and (2) relatively large-strain tests (surface deflections on the order of 1 inch) where significant numbers (30,000 plus) of ESAL's were applied to the geosynthetic reinforced test sections while permanent surface deflection basins were monitored with LVDT's as a function of number of loading cycles.

These two dynamic tests were conducted on large-scale unreinforced, geogrid reinforced, and geotextile reinforced test sections constructed in a 4-ft deep by 12-ft wide by 12-ft long pit at the Engineering Research Center (ERC) of the University of Arkansas. The small-strain tests were performed on test sections constructed completely out of poorly-graded sand. This simple, uniform material was chosen so as to evaluate how geosynthetic reinforcement influenced subsurface strain distribution without interference from other complicating factors that would make relative comparison of strain distribution difficult (i.e. different soil layer interfaces, varying negative pore water pressures in soils with significant fines content, etc.) The large-strain tests were performed on test sections constructed out of 10 inches of Class 7 base course overlying 30-plus inches of poorly-graded sand. Both sets of tests were performed so as to determine the contribution of geosynthetic reinforcement to structural pavement performance

(i.e. relative strain distribution and surface deflection only). No attempts were made to evaluate the other potentially beneficial mechanisms of geosynthetic reinforcement.

5.1 In-Situ Strain Test Results

The in-situ strain tests (discussed in Chapter 3) were performed to reveal the influence of the geosynthetic reinforcement on the stress/strain distribution in the soil during cyclic loading. These tests were successful at measuring the subsurface strain distribution within the soil as a function of depth and certainly show promise for additional future studies. The results from the small-strain dynamic load tests performed in this study indicate that the presence of geosynthetic reinforcement (either geogrid or geotextile) does not significantly impact the shear strain or vertical normal strain distribution relative to an unreinforced control section for the magnitudes of surface shear and compressive loads applied to the soil surface. However, the shear and vertical normal strains induced in these tests were sufficiently small (less than 0.2% and 0.05%, respectively) that the contribution from the geosynthetic reinforcement may not have been mobilized. That being said, these relatively low dynamic strain levels were the result of fairly significant loads (9000 lbs static hold-down force plus up to an additional 6000 lbs dynamic force) applied directly to the surface of a weak soil (i.e. without an asphalt surface to help redistribute stresses). Although this observation was not entirely unexpected, as previous studies indicate that significant displacements are required to mobilize tension in the geogrid, it was surprising that a load spreading mechanism or a lateral constraint mechanism was not revealed in the strain distribution data. This lack of an observable trend indicates that this mechanism needs further research to be considered a relevant contributor to base reinforcement.

5.2 Accelerated Dynamic Deflectometer (ADD) Test Results

ADD tests (discussed in Chapter 4) were performed as a means to evaluate the structural performance (i.e. surface deflection) of soil layers subject to many thousands of load cycles. These tests were performed on tests sections (unreinforced, geogrid-reinforced, and geotextile reinforced) consisting of a 10-inch layer of base course compacted atop a sand layer. Cycles of load were applied to the soil layers through a dual-wheel sized footprint until surface deflections commonly accepted as indicative of failure (i.e. approximately 1 inch) were developed. Data is presented herein for a peak load of 10,000 lbs (just greater than ½ and ESAL) applied up to 30,000 cycles. A change in surface deflection due to the presence of geogrid or geotextile reinforcement was not observed during the ADD tests conducted in this research. Similar to the small strain tests, the geosynthetic reinforcement was observed not to significantly influence the structural behavior of the test sections at the levels of strain associated with the cyclic loads applied to the sections.

The lack of an observed benefit in geosynthetic reinforcement in the compacted soil test sections may also be due to the fact that the test sections were already relatively stiff, so the impact of geosynthetic reinforcement was minor compared to the strength of the compacted base course layer. Additional studies are necessary to quantify the impact of weaker base course material (i.e., wet conditions), thinner base course sections, and weaker subbase. Furthermore, additional studies are required to understand the impact of the type of dynamic loading (compressive, shear, rolling/rocking) and if this influences the results.

References

Al-Qadi, I. L., Brandon, T. L. Smith, T. A., and Lacina, B. A. (1994) "How Do Geosynthetics Improve Pavements's Performance," Proceedings of Material Engineering Conference, San Diego, CA, USA, pp. 606-616.

Al-Qadi, I.L., Brandon, T.L., Valentine, R.J., Lacina, B.A. and Smith, T.E. (1994). "Laboratory Evaluation of Geosynthetic Reinforced Pavement Sections," In Transportation Research Record 1439, TRB, National Research Council, Washington DC., pp. 25-31.

Barenberg, E.J., Dowland, J.H., and Hales, J. II (1975). "Evaluation of soil-aggregate systems with Mirafi fabric." Department of Civil Engineering, University of Illinois.

Barker, W.R. (1987). "Open-graded bases for airfield pavements." USAE Waterways Experiment Station, Vicksburg, Mississippi, USA. Technical Report GL-87-16.

Barksdale, R. D., Brown, S. F. and Chan, F. (1989). "Potential Benefits of Geosynthetics in Flexible Pavement Systems." National Cooperative Highway Research Program Report No. 315, Transportation Research Board, National Research Council, Washington, DC.

Berg R., Christopher, B., and Perkins, S. (2000). "Geosynthetic Reinforcement of the Aggregate Base Course of Flexible Pavement Structures." GMA White Paper II, Geosynthetic Materials Association, Roseville, MN, USA, 130p.

Brown, S.F., Jones, C.P.D, and Brodrick, B.V. (1982). "Use of Non-woven Fabrics in permanent road pavements." Proceedings of the Institution of Civil Engineers. London, Part 2, Vol. 73, pp. 541-563.

Cancelli, A., Montanelli, F., Rimoldi, P., and Zhao, A. (1996). "Full Scale Laboratory Testing on Geosynthetics Reinforced Paved Roads." Proceedings of the International Symposium on Earth Reinforcement. Fukuoka/Kyushu, Japan, November, Balkema, pp. 573-578.

Chen, C., Ge, L., and Zhang, J. (2009). "Modeling permanent deformation and resilient modulus of unbound granular materials under repeated loading", International Journal of Geomechanics.

Chen, C., and Ge, L. (2009). “Modeling resilient modulus of unbound granular materials under repeated loading.” GeoHunan, International Conference: Challenges and Recent Advances in Pavement Technologies and Transportation Geotechnics, Hunan, China, in Review.

Collin, J. G., Kinney, T. C. and Fu, X. (1996). "Full Scale Highway Load Test of Flexible Pavement Systems with Geogrid Reinforced Base Courses," Geosynthetics Intentional, Industrial Fabrics Association International, Roseville, MN, Vol. 3, No. 4, pp. 537-549.

Cook, R.D., Malkus, D.S., and Plesha, M.E. (1989). Concepts and Applications of Finite Element Analysis. 3rd Edition. John Wiley and Sons, New York, NY.

Cox, B.R., Stokoe, K.H., II, and Rathje, E.M. (2009a). “An In-Situ Test Method for Evaluating the Coupled Pore Pressure Generation and Non-linear Shear Modulus Behavior of Liquefiable Soils.” ASTM Geotechnical Testing Journal, V. 32, No. 1, pp. 11-21.

Cox, B.R., McCartney, J.S., Curry, B., Wood, C.M., Young, C. (2009b). “In-Situ Strain Measurements During Dynamic Shear Loading of An Unbound Geogrid Reinforced Flexible Pavement Section,” Eighth International Conference on the Bearing Capacity of Roads, Railways, and Airfields, Urbana-Champaign, Illinois, 29 June – 2 July 2009.

Cox, B.R., McCartney, J.S., Wood, C.M., Curry, B. (2010). “Performance Evaluation of Full-Scale Geosynthetic-Reinforced Flexible Pavements Using Field Cyclic Plate Load Tests,” The Transportation Research Board 89th Annual Meeting, Washington, D.C., pp. 10-14.

Cuelho, E., Perkins, S. (2009). “Field Investigation of Geosynthetic Used for Subgrade Stabilization.” Performed for the State of Montana, Department of Transportation, NAUE GmbH & Co. KG, in cooperation with the U.S. Department of Transportation, Federal Highway Administration.

Fannin, R.J. and Sigurdsson, O. (1996). “Field Observations on Stabilization of unpaved roads with geosynthetics.” Journal of Geotechnical Engineering, ASCE, 122, No. 7, pp. 544-553.

Giroud, J.P. and Noiray, L. (1981). “Geotextile Reinforced Unpaved Road Design.” Journal of the Geotechnical Engineering Division. ASCE, Vol. 107, No GT9, pp. 1233-1254.

Haas R., Wall, J., and Carroll, R.G. (1988). "Geogrid Reinforcement of Granular Bases in Flexible Pavements," In Transportation Research Record 1188, TRB, National Research Council, Washington, DC, USA, pp. 19-27.

Haliburton, Lawmaster and King. (1970). “Potential Use of Geotextile Fabric in Airfield Runway Design.” Air Force Office of Scientific Research, AFOSR Report 79-00871.

Halliday, A.R. and Potter, J.F. (1984). "The Performance of a Flexible Pavement Constructed on a Strong Fabric," Transport and Road Research Laboratory, Report 1123, Crowthorne, Berkshire, 15 p.

Henwood, Justin T. and K.Y Haramy. (2002). “Vibrations Induced by Construction Traffic: A Historic Case Study.” Prepared for the Federal Highway Administration, Denver, Colorado.

Hufenus, R., Ruegger, R., Banjac, R., Mayor, P., Springman, S.M., Bronnimann, R., (2006). Full-scale field tests on geosynthetics reinforced unpaved roads on soft subgrade. Geotextiles and Geomembranes 24/1, pp. 21–37.

Leng, J. and Gabr, M. (2002). “Characteristics of geogrid-reinforced aggregate under cyclic load.” Journal of Transportation Research Board No. 1786. National Research Council. Washington D.C. pp. 29-35.

Ling, H. and Liu, Z. (2001). “Performance of geosynthetic reinforced asphalt pavements.” Journal of Geotechnical and Geoenvironmental Engineering. 127(2), pp. 177-184.

Montanelli, F., Zhao, A. and Rimoldi, P. (1997). "Geosynthetic-Reinforced Pavement System: Testing and Design," Proceedings of the Conference Geosynthetics ’97, Long Beach, CA, USA, Vol. 2, pp. 619-632.

Perkins, S.W., and Cortez, E. (2005). “Evaluation of base-reinforced pavements using a heavy vehicle simulator.” Geosynthetics International. 12(2), pp. 87-98.

Perkins, S.W., Ismeik, M. and Fogelsong, M.L. (1999). "Influence of Geosynthetic Placement Position on the Performance of Reinforced Flexible Pavement Systems," Proceedings of the Conference Geosynthetics '99, Boston, MA, USA, Vol. 1, pp. 253-264.

Perkins, S.W., Ismeik, M. and Fogelsong, M.L. (1998). "Mechanical Response of a Geosynthetic-Reinforced Pavement System to Cyclic Loading," Proceedings of the Fifth International Conference on the Bearing Capacity of Roads and Airfields, Trondheim, Norway, Vol. 3, pp. 1503-1512.

Steward, J., Williamson, R., and Mohney, J. (1977). "Guidelines for Use of Fabrics in Construction and Maintenance of Low-Volume Roads." Forest Service Report PB-276 972.

Tingle, J. and Jersey, S. (2005). "Cyclic Plate Load Testing of Geosynthetic-Reinforced Unbound Aggregate Roads." Transportation Research Record: Journal of the Transportation Research Board, No. 1936, Transportation Research Board of the National Academies, Washington, D.C., 2005, pp. 60–69.

Webster, S.L. (1993). "Geogrid reinforced base courses for flexible pavements for light aircraft, test section construction, behavior under traffic, laboratory tests and design criteria. Technical Report GL-93-6, USAE Waterways Experiment Station,Vicksberg, MS, USA, 86p.

Yetimoglu, T., Wu, J.T.H., & Saglamer, A. (1994). "Bearing capacity of rectangular footings on geogrid-reinforced sand."Journal of Geotechnical Engineering, 120 (12), pp. 2083-2099.

Zhang, L. (1996). "Vibration at the ESRF." EPAC96